TECHNISCHE UNIVERSITÄT MÜNCHEN

FAKULTÄT CHEMIE

LEHRSTUHL ORGANISCHE CHEMIE II

PROTEOMIC TARGET SPECTRUM AND MODE OF ACTION ANALYSIS OF ANTIBACTERIAL SMALL MOLECULES

DISSERTATION ZUR ERLANGUNG DES AKADEMISCHEN GRADES EINES
DOKTORS DER NATURWISSENSCHAFTEN VON

JAN DOMINIK VOMACKA

MÜNCHEN 2016

TECHNISCHE UNIVERSITÄT MÜNCHEN

FAKULTÄT CHEMIE

LEHRSTUHL ORGANISCHE CHEMIE II

PROTEOMIC TARGET SPECTRUM AND MODE OF ACTION ANALYSIS OF ANTIBACTERIAL SMALL MOLECULES

JAN DOMINIK VOMACKA

Vollständiger Abdruck der von der Fakultät für Chemie der Technischen Universität München

zur Erlangung des akademischen Grades eines

DOKTORS DER NATURWISSENSCHAFTEN

genehmigten Dissertation.

Vorsitzender:		Prof. Dr. Kathrin Lang
Prüfer der Dissertation:	1.	Prof. Dr. Stephan A. Sieber
	2.	Prof. Dr. Tobias A. M. Gulder

Die Dissertation wurde am 7.10.2016 bei der bei der Technischen Universität München eingereicht und durch die Fakultät für Chemie am 16.11.2016 angenommen.

Remembering you are going to die is the best way I know
to avoid the trap of thinking you have something to lose.
– Steve Jobs

ACKNOWLEDGEMENT

I thank Prof. Dr. Stephan A. Sieber and Dr. Katrin Lorenz-Baath for the opportunity to contribute to the exciting field of anti-virulence agents. The positive environment and the frequent possibility for presenting and discussing current issues in the Sieber research group and the AVIRU GmbH laboratories enabled focused and target-oriented work. I especially value the exceptional experience of being part of the AVIRU start-up team: Dr. Katrin Lorenz-Baath, Prof. Dr. Stephan A. Sieber, Dr. Oliver Baron, Dr. Vadim Korotkov, Dr. Bianca Bauer, Dr. Axel Pahl, Dr. Franziska Weinandy, Christian Fetzer, Ernst Bernges and Heike Hofmann. We were very close to save the world.

I acknowledge internal and external collaborators on a rich variety of projects in the fields of anti-microbial (*Staphylococcus aureus* and *Mycobacterium tuberculosis*) agents, mass spectrometry and chemical biology (affinity based protein profiling, cellular thermal shift): Matthias Stahl, Christian Fetzer, Wolfgang Heydenreuter, Barbara Hofbauer, Markus Lakemeyer, Johannes Lehmann, Dr. Joanna Krysiak, Mathias Hackl, Weining Zhao, Franziska Mandl, Dr. Martin Kunzmann, Dr. Knud Esser (Helmholtz Zentrum, München), Katharina Kolbe (Leibniz-Zentrum für Medizin und Biowissenschaften, Forschungszentrum Borstel), Megan Jennings (Wuest Group, Temple University, Philadelphia), Svenja Petzoldt (OmicScouts GmbH, Freising), Fabian Bischoff (Pharmaceutical Biology, Ludwig-Maximilians-Universität, München). I thank Elena Kunold, Philipp Kleiner, Dr. Maria Dahmen and Dr. Malte Gersch for assistance, ideas and support during the work in the laboratory. Furthermore, I acknowledge the outstanding contribution of my interns: Ruben Weiß, Tamara Heermann, Anja Bufe, Celina Eckfeld, Barbara Tremmel, Moritz Mühlhofer, Frank Braun and Barbara Teufelhart. Equally, I would like to thank Katja Bäuml, Mona Wolff, Ernst Bernges and Heike Hofmann for providing a reliable working environment. Finally, I would like to thank Prof. Dr. Stephan A. Sieber for the revision of the Thesis.

TABLE OF CONTENTS

TABLE OF CONTENTS 9

INTRODUCTORY REMARKS 11

SUMMARY 13

ZUSAMMENFASSUNG 15

INTRODUCTION 17

STAPHYLOCOCCUS AUREUS 18

MYCOBACTERIUM TUBERCULOSIS 21

PHENOTYPE BASED ANTI-BACTERIAL DRUG DEVELOPMENT 23

ACTIVITY / AFFINITY BASED PROTEIN PROFILING 25

REFERENCES 31

AN AROMATIC HYDROXYAMIDE ATTENUATES MULTIRESISTANT STAPHYLOCOCCUS TOXIN EXPRESSION 33

SUMMARY 35

AUTHOR CONTRIBUTIONS 35

HUMAN LYSOSOMAL ACID LIPASE INHIBITOR LALISTAT IMPAIRS MYCOBACTERIUM TUBERCULOSIS GROWTH BY TARGETING BACTERIAL HYDROLASES 37

SUMMARY 91

AUTHOR CONTRIBUTIONS 91

POSTER CONTRIBUTIONS 105

STAPHYLOCOCCUS AUREUS VIRULENCE IS REDUCED BY INHIBITION OF THE MANGANESE UPTAKE PROTEIN MNTC 107

STAPHYLOCOCCUS AUREUS AND LISTERIA MONOCYTOGENES VIRULENCE IS REDUCED BY THE SMALL MOLECULE INHIBITOR AV73 113

INTRODUCTORY REMARKS

The present doctoral dissertation was accomplished between June 2013 and Mai 2016 under the supervision of Prof. Dr. Stephan A. Sieber at the Chair of Organic Chemistry II of the Technische Universität München.

PARTS OF THIS THESIS HAVE BEEN PUBLISHED IN:

Johannes Lehmann,* Jan Vomacka,* Knud Esser,* Matthew Nodwell, Katharina Kolbe, Patrick Rämer, Ulrike Protzer, Norbert Reiling and Stephan A. Sieber: *Human lysosomal acid lipase inhibitor lalistat impairs Mycobacterium tuberculosis growth by targeting bacterial hydrolases*, Medicinal Chemical Communications **2016**.

*contributed equally

Jan Vomacka, Vadim S. Korotkov, Bianca Bauer, Franziska Weinandy, Martin H. Kunzmann, Joanna Krysiak, Oliver Baron, Thomas Böttcher, Katrin Lorenz-Baath and Stephan A. Sieber: *An aromatic hydroxyamide attenuates multiresistant Staphylococcus aureus toxin expression*, Chemistry - A European Journal **2016**, *22* (5), 1622 - 1630.

PUBLICATIONS NOT HIGHLIGHTED IN THIS THESIS:

Joanna Krysiak,* Jan Vomacka,* Matthias Stahl,* Christian Fetzer, Markus Lakemeyer, Anja Fux and Stephan A. Sieber: *A quantitative map of beta-lactone induced virulence regulation*, manuscript in preparation.

*contributed equally

Franziska Mandl, Volker Kirsch, Ilke Ugur, Elena Kunold, Jan Vomacka, Christian Fetzer, Sabine Schneider, Klaus Richter Thilo Fuchs and Iris Antes: *Natural product inspired amino-epoxybenzoquinones kill members of the gram-negative pathogen Salmonella by attenuating cellular stress response*, Angewandte Chemie International Edition **2016**.

Axel Pahl,* Markus Lakemeyer,* Marie-Theres Vielberg,* Mathias W. Hackl, Jan Vomacka, Vadim S. Korotkov, Martin L. Stein, Christian Fetzer, Katrin Lorenz-Baath, Klaus Richter, Herbert Waldmann, Michael Groll,* and Stephan A. Sieber: *Reversible inhibitors arrest ClpP in a defined conformational state that can be revoked by ClpX association*, Angewandte Chemie International Edition **2015**, *54* (52), 15892 - 15896.

*contributed equally

PATENT APPLICATION:

Jan Vomacka, Johannes Lehmann, Knud Esser, Matthew Nodwell, Katharina Kolbe, Patrick Rämer, Ulrike Protzer, Norbert Reiling, Stephan A. Sieber: *Means and methods for treating mycobacterial diseases*, European Patent Application **2016**, EP 16 169 499.7.

CONFERENCES AND WORKSHOPS:

26th Congress of the European Society of Clinical Microbiology and Infectious Diseases, Amsterdam (the Netherlands) **2016**, *poster presentation*.

Max-Planck-Institut für Biochemie - MaxQuant Summer School, Munich (Germany) **2015**.

Gordon Research Conference - Bioorganic Chemistry, Boston (USA) **2015**, *poster presentation*.

24th Congress of the European Society of Clinical Microbiology and Infectious Diseases, Barcelona (Spain) **2014**.

SUMMARY

Staphylococcus aureus and *Mycobacterium tuberculosis* are both lethal pathogenic bacteria that maintain a large number of hosts with no active infection. Individuals colonized with *S. aureus* or latently infected with *M. tuberculosis* have no symptoms until the outbreak of an active infection. Antibiotic treatment is facing the challenge of resistance development in both cases: methicillin-resistant *S. aureus* (MRSA) and extensively drug-resistant tuberculosis (XDR-TB).

In two publications a phenotype based strategy using chemical proteomics is employed to identify new cellular targets and mechanisms. A phenotypically active compound in a cell culture assay is converted into a chemical probe. ABPP (activity based protein profiling) experiments followed by target validation reveal new protein targets. These findings are a starting point for the development of sophisticated treatment options with a potential to address the burden of resistance development.

(1) An aromatic hydroxyamide attenuates multiresistant *Staphylococcus aureus* toxin expression

Hydroxyamide (*R**,*R**)-3 broadly inhibited a set of *S. aureus* virulence factors: hemolysins, toxic shock syndrome toxins, enterotoxins. The effect could be observed with laboratory strains as well as with various clinical isolates. Anti-virulence activity was confirmed by transcriptome analysis. ABPP experiments revealed a set of protein targets. After validation experiments with transposon mutant strains manganese transporter subunit C (MntC) was identified as a virulence related target protein. Hydroxyamide (*R**,*R**)-3 showed no resistance development *in vitro* and was effective in a systemic mouse infection model.

(2) Human lysosomal acid lipase inhibitor lalistat impairs *Mycobacterium tuberculosis* growth by targeting bacterial hydrolases.

Mammalian lipase inhibitor lalistat showed antibiotic activity against *M. tuberculosis* in cell culture and in a macrophage infection model. In addition synergistic effects with vancomycin were measured. ABPP experiments including a competition control with unmodified lalistat revealed a distinct set of hydrolases including seven proteins from the lipase family.

ZUSAMMENFASSUNG

Staphylococcus aureus und *Mycobacterium tuberculosis* sind pathogene Bakterien mit einer Vielzahl an Wirten ohne aktive Infektion. Menschen, die mit *S. aureus* kolonisiert sind oder eine latente *M. tubeculosis* Infektion haben, zeigen keine Symptome bis zum Ausbruch der aktiven Erkrankung. Die Behandlung mit Antibiotika wird in beiden Fällen durch die Entwicklung von Resistenzen erschwert: MRSA (methicillin-resistant *S. aureus*) und XDR-TB (extensively drug-resistant tuberculosis).

In zwei Publikationen wird eine Phänotyp-basierte Strategie unter Verwendung von chemischer Proteomik verfolgt. Das Ziel ist die Identifizierung von neuen zellulären Angriffszielen und Mechanismen. Eine in Zellkultur aktive Substanz wird zu einer chemischen Sonde derivatisiert. ABPP (activity based protein profiling) Experimente und Angriffsziel-Validierung führen zur Entdeckung von neuen Protein Angriffszielen. Diese Ergebnisse sind ein Startpunkt für die Entwicklung von durchdachten Behandlungsoptionen auch mit dem Potential die Herausforderung von Resistenzbildung zu adressieren.

(1) Ein aromatisches Hydroxyamid verringert die Expression von Toxinen durch multiresistenten *Staphylococcus aureus*.

Das Hydroxyamid (*R**,*R**)-3 inhibiert ein breites Spektrum an Virulenzfaktoren: Hämolysine, Toxic Shock Syndrom Toxine, Enterotoxine. Der Effekt konnte mit Laborstämmen und auch mit klinischen Isolaten beobachtet werden. Die antivirulente Aktivität wurde durch eine Transkriptom Analyse bestätigt. ABPP Experimente führten zu einer Auswahl an Protein Angriffszielen. Nach Validierungsexperimenten mit Transposonmutanten wurde die Mangantransporteruntereinheit C (MntC) als Angriffsziel-Protein mit einem Bezug zur Virulenz identifiziert. Das Hydroxyamid (*R**,*R**)-3 zeigte *in vitro* keine Resistenzentwicklung und war im systemischen Mausinfektionsmodell effektiv.

(2) Lalistat, ein Inhibitor der humanen lysosomalen saueren Lipase mindert *Mycobacterium tuberculosis* Wachstum durch seine Wirkung auf bakterielle Hydrolasen.

Lalistat, ein Inhibitor der humanen lysosomalen saueren Lipase zeigte in Zellkultur und in einem Makrophagen Infektionsmodell antibiotische Aktivität gegen *M. tuberculosis*. Zusätzlich konnten synergistische Effekte mit Vankomycin gemessen werden. ABPP Experimente inklusive einer Kompetitionskontrolle mit Lalistat zeigten ein eindeutiges Set an Hydrolasen. Unter den Hits waren sieben Proteine aus der Lipase Familie.

INTRODUCTION

STAPHYLOCOCCUS AUREUS

The human body includes 1-2 kg of bacterial cells. By cell number, bacteria outnumber human cells roughly by a factor of 10.[1] Nevertheless, bacteria are not evenly distributed. While most of the microbiome is located in the gut and on skin tissue, body fluids like blood are considered to be sterile. However, through open wounds, surgery, implants pathogenic bacteria like *Staphylococcus aureus* gain access to our body and cause bacteremia, an infection of the bloodstream. This infection can spread to heart tissue and cause infective endocarditis [2] or lead to sepsis and septic shock.[3] Not only skin barrier damage but also diabetes, AIDS and defects in neutrophil function are known risk factors.[4]

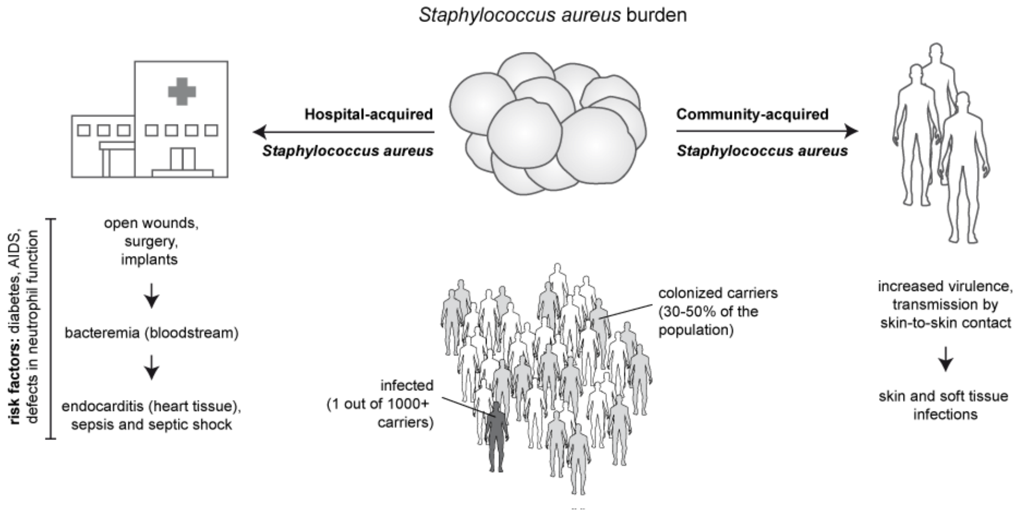
Staphylococcus aureus burden
Hospital-acquired
Staphylococcus aureus
Community-acquired
Staphylococcus aureus
risk factors: diabetes, AIDS, defects in neutrophil function
open wounds, surgery, implants
bacteremia (bloodstream)
endocarditis (heart tissue), sepsis and septic shock
colonized carriers (30-50% of the population)
infected (1 out of 1000+ carriers)
increased virulence, transmission by skin-to-skin contact
skin and soft tissue infections

Fig. 1 *Staphylococcus aureus* burden: Hospital-acquired and community-acquired (CA) strains.

In addition to these nosocomial infections, *S. aureus* can also be community acquired (CA-MRSA). Here, skin and soft tissue infections are most prevalent.[5] Despite its severe pathogenic characteristics the bacterium is also a commensal with a long history of co-evolution with the human species that colonizes 30-50% of the population.[2] These high numbers can be partially explained by the fact that transmission between carriers occurs mostly due to simple skin-to-skin contact.[4] While the risk of suffering from *S. aureus* infection increases by colonization, only one of at least 1000 carriers develops an invasive infection.[6] The pathogen maintains a large number of colonized hosts that carry and spread the bacterium among the population, with only a small fraction of colonized individuals actually developing an infection. This strategy allows *S. aureus* strains to spread and establish a stable basis of healthy carriers, which makes it impossible to eradicate and difficult to effectively control this dangerous microorganism.

Of major concern are methicillin-resistant *S. aureus* strains (MRSA): According to the WHO 20-80% of isolates are resistant to first-line drugs like methicillin and cloxacillin.[7] These strains express an additional penicillin-binding protein (PBP2A) encoded by the methicillin-resistance determinant mecA. PBP2A is a transpeptidase with reduced affinity for β-lactam antibiotics that takes over the function of the native β-lactam target penicillin-binding protein 2 (PBP2) that is involved in cell-wall biosynthesis.[8] MRSA infections are treated with second-line antibiotics that come with increased costs and side-effects: Examples include glycopeptides such as vancomycin and teicoplanin. Also linezolid and daptomycin represent more recent antibiotics. However, new strains like vancomycin-resistant *Staphylococcus aureus* (VRSA) demonstrate the following: New antibiotics are not a save backup solution but rather another milestone in the race of antibiotic drug development vs. bacterial resistance emergence and spread. On a molecular level resistances develop by rare chromosomal mutations in few bacterial cells. They enable adapted clones to escape the antibiotic pressure. This selective advantage then spreads mostly via horizontal gene transfer causing an epidemic wave of resistant staphylococci.[4]

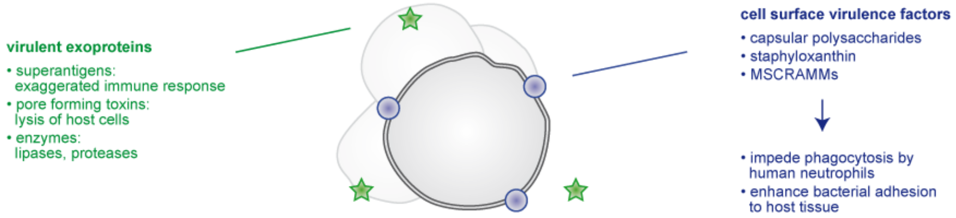
virulent exoproteins
• superantigens: exaggerated immune response
• pore forming toxins: lysis of host cells
• enzymes: lipases, proteases
cell surface virulence factors
• capsular polysaccharides
• staphyloxanthin
• MSCRAMMs
• impede phagocytosis by human neutrophils
• enhance bacterial adhesion to host tissue

Fig. 2 *Staphylococcus aureus* virulence.

The gram positive bacterium has a round shape and forms clusters (*staphylo* means *grape* in Greek). It has a characteristic carotenoid surface pigmentation (*aureus* means *golden* in Latin)[9]. The circular chromosome with 2.8 Mbp has a reduced G+C content [10] and includes prophages, plasmids and transposons. In addition to a cell wall that consists of 50 wt% peptidoglycan *S. aureus* cells are surrounded and protected by a thick polysaccharide cell capsule.[2] *S. aureus* expresses a diverse set of virulence factors: Cell surface virulence factors but also virulent exoproteins. Cell surface virulence factors include capsular polysaccharides, staphyloxanthin (carotenoid pigment) and microbial surface components recognizing adhesive matrix molecules (MSCRAMMs) like fibronectin-binding proteins (FnBP).[11] Their function is to impede phagocytosis by human neutrophils and enhance bacterial adhesion to host tissue and colonization. Exoproteins are superantigens like toxic shock syndrome toxin (TSST) or enterotoxins which trigger an exaggerated immune response, pore-forming toxins like hemolysin, leukocidin and phenol-soluble modulins that lyse host cells or enzymes like lipases and proteases (e.g. exfoliative toxins).[11] Especially CA-MRSA exhibits an increased virulence that leads to particularly severe tissue infections: necrotizing fasciitis (muscle tissue related infection); necrotizing pneumonia (lung tissue infection).[4] Overall, a complex regulatory network adjusts the expressed virulence factor arsenal to environmental challenges like nutrient availability, temperature, oxidative stress.[12, 13] However, not only environmental signals are detected in order to adapt to surrounding conditions but also cell-cell communication molecules like the autoinducing peptide AIP. These molecules allow coordination of multiple bacterial cells via quorum sensing, e.g. growth phase transition as a response to high cell density.[14]

MYCOBACTERIUM TUBERCULOSIS

Similar to *Staphylococcus aureus*, *Mycobacterium tuberculosis* is a lethal pathogen that maintains a large number of carriers with no active infection. A large basis of hosts with no symptoms is a major advantage for both bacterial strains. While *S. aureus* has colonized 30-50% of the population [2] one-third of the world's population is latently infected with *M. tuberculosis*.[15] In latent TB infections nonreplicating persistent cells are effectively controlled by the immune system without complete eradication of the pathogen.[16, 17]

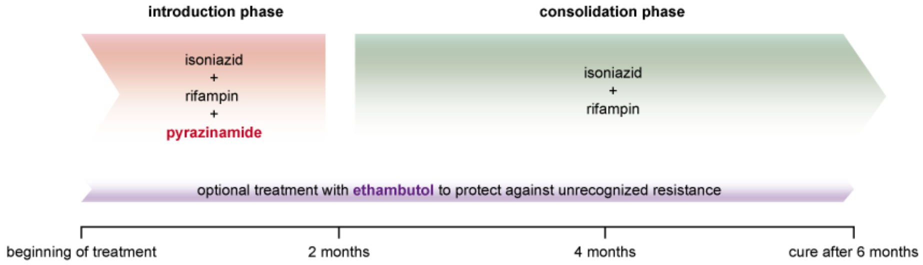
introduction phase
consolidation phase
isoniazid
+
rifampin
+
pyrazinamide
isoniazid
+
rifampin
optional treatment with ethambutol to protect against unrecognized resistance
beginning of treatment
2 months
4 months
cure after 6 months

Fig. 3 *Mycobacterium tuberculosis* treatment.[17]

To cure active tuberculosis a 6 month treatment with several antibiotics has to be applied as persistent bacterial cells are far less susceptible to drug treatment then fast replicating active *M. tuberculosis* bacteria. The introduction phase with isoniazid, rifampin and pyrazinamide is followed by a consolidation phase with isoniazid and rifampin treatment. Optionally ethambutol is used in addition as protection against unrecognized resistance to isoniazid, rifampin or pyrazinamide.[17] Due to the long treatment with up to four antibiotic drugs at the same time 11% of patients suffer from hepatotoxic effects (liver damage).[18] New treatment options are desperately needed due to side effects, bad patient adherence and due to the emergence of multi-drug resistant tuberculosis (MDR-TB) and extensively drug resistant tuberculosis (XDR TB).[19]

PHENOTYPE BASED ANTI-BACTERIAL DRUG DEVELOPMENT

Harmful infections with *S. aureus*, *M. tuberculosis* and with their drug resistant forms MRSA, MDR-TB are caused by bacterial cells that show an uncooperative, destructive behavior with regard to surrounding host cells. Just like cancer cells, bacterial cells attack and harm healthy tissue.[20] The ultimate goal of anti-infective and cancer drug treatment is to stop the hostile cells without impairing other cells, to selectively kill only bacteria or cancer tissue. This however leads to the development of resistances as single cells with random mutations can survive treatment and proliferate.[21] An alternative option is to focus drug development on the behavior of cells. Prevention of unwanted cellular phenotypes can be achieved by affecting intercellular communication, metabolic and virulence pathways. A deep understanding of how cells work, allows sophisticated phenotypic manipulation instead of simple killing.

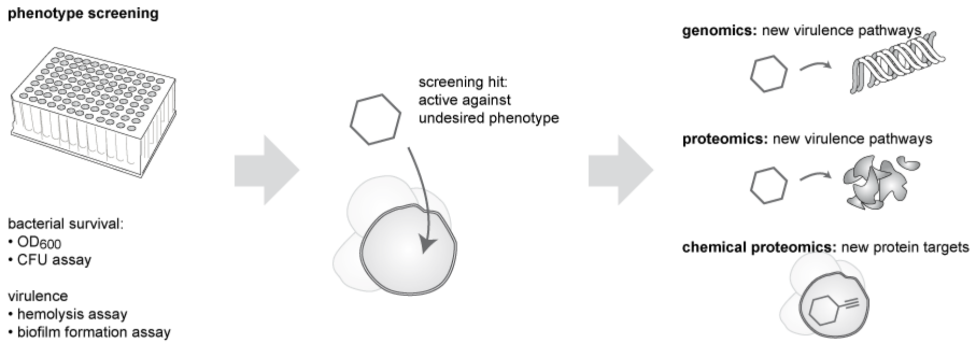
phenotype screening
bacterial survival:
• OD_{600}
• CFU assay
virulence
• hemolysis assay
• biofilm formation assay
screening hit:
active against
undesired phenotype
genomics: new virulence pathways
proteomics: new virulence pathways
chemical proteomics: new protein targets

Fig. 4 From phenotype screening to innovative drug development concepts.

When screening for new drugs, there is a huge potential of different phenotypes that can be monitored in addition to dead or alive status. For bacterial cells this means not only measuring bacterial growth with optical density / absorbance measurements at 600 nm wavelength (OD_{600}) or counting colony forming units (CFUs) on agar plates to test small sample volumes from liquid bacterial culture. Instead, also e.g. the amount of toxins (hemolysin, TSST, enterotoxin) that were produced by bacteria can be determined with and without compound treatment. Drug libraries can also be screened based on their potential to inhibit biofilm formation. Hits that are identified in these phenotypic screenings change cellular behavior in a desired way. Those active molecules can then be used to identify new cellular mechanisms and pathways linked to bacterial virulence using proteomic and genomic methods. With chemical proteomics methods (e.g. activity based protein profiling (ABPP [22]), cellular thermal shift assay (CETSA [23])) even direct protein targets or target spectra can be identified that explain why phenotype screening hit compounds have their effect on harmful cells.

ACTIVITY / AFFINITY BASED PROTEIN PROFILING

Activity based protein profiling (ABPP) [22] is a method to identify protein targets of bioactive substances in live cells with the help of chemical biology tool compounds: ABPP probes. These probes are close derivatives of the active chemical structures. They show the same or similar bioactivity compared to the original compound. Probes are equipped with an alkyne handle. Here, reporter structures like biotin for pulldown experiments or fluorescent moieties like rhodamine for SDS-PAGE analysis can be attached in a cellular context using bioorthogonal click chemistry. Quantitative mass spectrometric analysis of peptides from a tryptic digest is finally used to identify specific proteins based on known amino acid sequences. Figure 5 shows an overview of the process from medical need to new, validated protein target via ABPP that is described in the following sub-chapters.

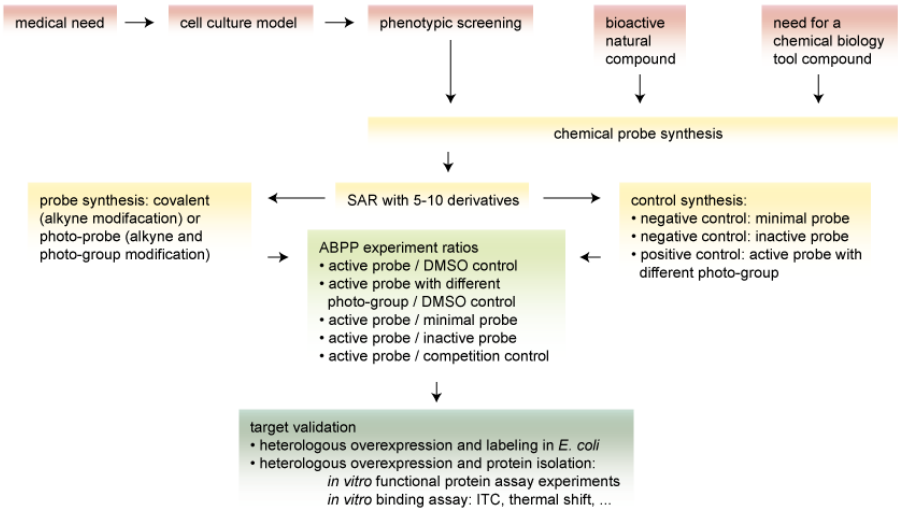
medical need
cell culture model
phenotypic screening
bioactive natural compound
need for a chemical biology tool compound
chemical probe synthesis
probe synthesis: covalent (alkyne modifacation) or photo-probe (alkyne and photo-group modification)
SAR with 5-10 derivatives
control synthesis:
• negative control: minimal probe
• negative control: inactive probe
• positive control: active probe with different photo-group
ABPP experiment ratios
• active probe / DMSO control
• active probe with different photo-group / DMSO control
• active probe / minimal probe
• active probe / inactive probe
• active probe / competition control
target validation
• heterologous overexpression and labeling in *E. coli*
• heterologous overexpression and protein isolation:
in vitro functional protein assay experiments
in vitro binding assay: ITC, thermal shift, ...

Fig. 5 Overview of process from medical need to new, validated protein target via ABPP.

Need for ABPP experiments

A reason for an ABPP analysis can be, as mentioned in the chapter 'phenotype based anti-bacterial drug development', a bioactive chemical compound from a phenotypic screening. In a phenotypic screening, a cell culture model is designed as a representation of a medical need. A simple model assay of an infection would be liquid bacterial culture in plastic tubes or 96-well plates. For example growth could be measured with optical density measurements at 600 nm after overnight growth. A hit compound added to the culture in different concentrations would then reduce growth and therefore optical density. A more advanced assay would be to centrifuge liquid cultures of bacteria after overnight growth and add erythrocytes to the supernatant to test for secreted hemolytic proteins by monitoring lysis of the red blood cells. With a successful hit compound added to the growth medium, less hemolytic proteins would be in the supernatant and subsequent blood lysis would be slower.[24] Typically, phenotypic screening hits are great drug development lead structures as they already have proven to be cell permeable and effective in a cellular context. However, compared to target based screening hits, where the screening assay is a simple *in vitro* protein assay and no cell culture based assay, the direct protein target is unknown.[25]

Not only phenotypic screening hits but also bioactive natural compounds can be used as a basis for the design of ABPP probes. Those structures are used to explore bioactivity in new and unexplored chemical spaces. Unfortunately, here the synthesis of chemical probes can be challenging when natural compound structures are complex and have multiple chiral centers.[26]

ABPP probes can also be designed as tool compounds without a primary focus on bioactivity. For example probes were used to target specific enzyme classes like serine or cysteine hydrolases, metallohydrolases or kinases.[27]

ABPP probe design

In general there are two kinds of ABPP probes: Covalent probes and photo-probes. Bioactive compounds with a structure that implies a covalent binding mode like esters are derived to covalent probes. Here, only an alkyne moiety has to be introduced. The alkyne tag serves as a handle where different functional groups can be attached via bioorthogonal click chemistry. This can be biotin for pulldown experiments or fluorescent moieties like rhodamine for SDS-PAGE visualization. To analyze covalent and non-covalent binding, in addition to an alkyne tag also a photoactivatable moiety like benzophenone or diazirine has to be introduced. These photo-probes can be activated with UV irradiation after binding non-covalently to proteins in the cell.

Upon UV activation these probes crosslink covalently with their non-covalent protein targets. In some cases ABPP with photo-probes is called AfBPP for affinity based protein profiling instead of ABPP (activity based protein profiling) as a faster covalent reaction is assumed to correlate with higher activity, a stronger non-covalent binding not.[28] However, in a complex cellular context affinity or speed of the covalent reaction is always hard to correlate with biological activity. A strong binding to a less relevant target can be misleading in the process of finding the mode and mechanism of action. As a consequence it is save to assume all ABPP target hits as binding-targets (affinity) that do not necessarily contribute to the biological effect (activity). A weak ABPP protein target can be crucial for bioactivity. A strong ABPP protein target can have a suitable pocket where the ABPP probe binds. However, it is possible that the binding event has no effect on the function of this protein or this proteins function is not relevant for the observed phenotypic effect. In addition, cellular protein abundance also has an influence on how high an APBB target ratio is. Therefore, all statistically significant targets can be relevant for the biological effect independent if they are obtained with covalent probes or photo-probes.

For the synthesis of an ABPP probe it is helpful to have structure activity relationship information about the molecule to know at which position the molecule can be altered without losing activity: A set of 5-10 derivatives of a phenotype screening hit. The goal is to retain bioactivity upon the introduction of an alkyne tag and/or a photoactivatable moiety. For the best ABPP results it is also beneficial to have a minimal probe, that contains just the introduced modifications (alkyne tag and photoactivatable group) and not the active structure of the original molecule as a negative control. A second negative control that improves ABPP experiments is an inactive probe. This probe should be structurally as close as possible to the active probe (ideally diastereomer or even enantiomer) but should have no or only very low biological activity. In addition, two active probes with different photoactivatable moieties (e.g. benzophenone, diazirine, aryl azide [29]) can be synthesized. Proteins found with both active probes are more likely to be active core structure hits. Hit proteins that were identified because they bind to the structure of the photoactivatable moiety can be excluded. Further possible control experiments that enhance the quality of ABPP experiment results are: Inactive concentration control (use probe concentration below the bioassay EC_{50}), competition control (preincubate cells with an excess of unmodified compound before labeling with probe to occupy target protein binding sites) and inactive cell line control (use different cell line / bacterial strain where no probe activity can be observed).

Gel-free ABPP protocol

A typical ABPP workflow with an active probe and two controls (DMSO control and inactive probe control) is depicted in Figure 6.

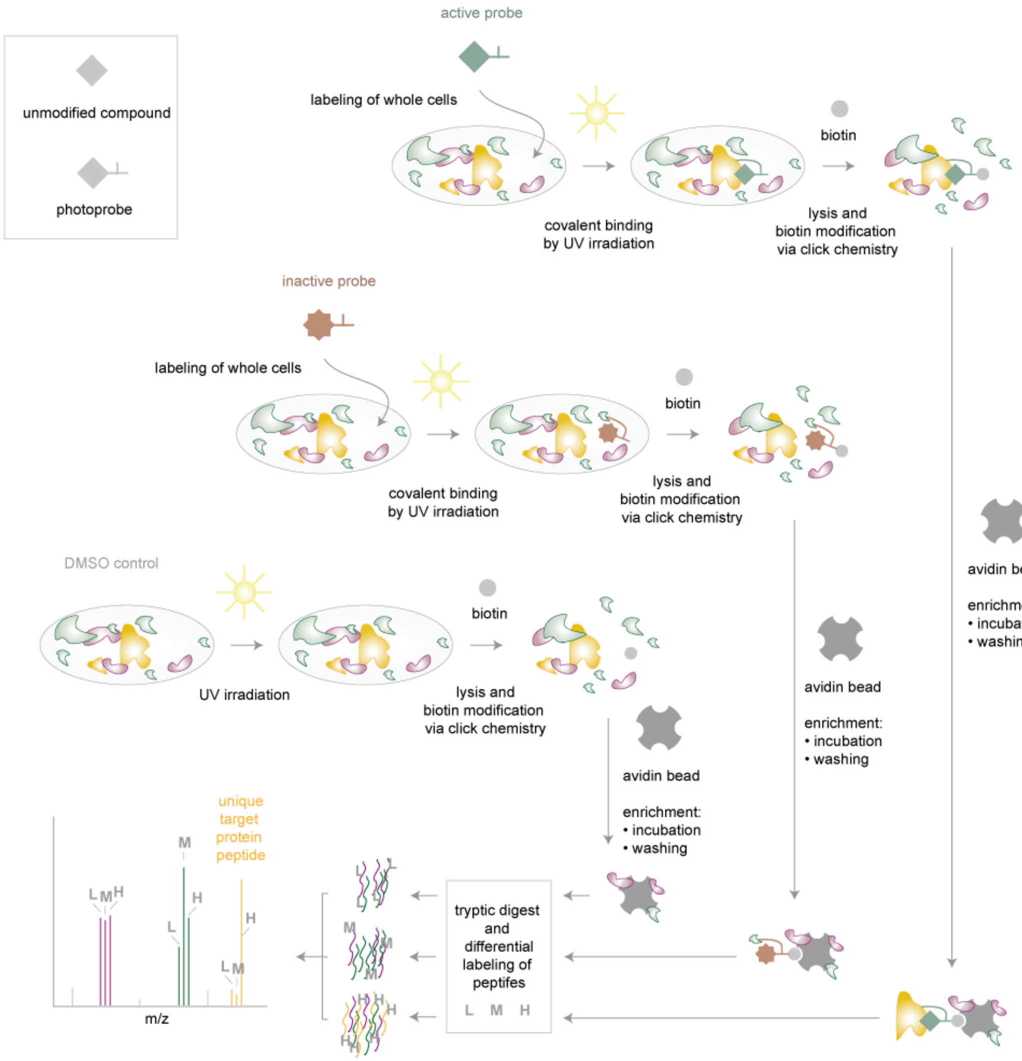
unmodified compound
photoprobe
active probe
labeling of whole cells
covalent binding by UV irradiation
biotin
lysis and biotin modification via click chemistry
inactive probe
labeling of whole cells
covalent binding by UV irradiation
biotin
lysis and biotin modification via click chemistry
DMSO control
UV irradiation
biotin
lysis and biotin modification via click chemistry
avidin bead
enrichment:
• incubation
• washing
avidin bead
enrichment:
• incubation
• washing
avidin bead
enrichment:
• incubation
• washing
tryptic digest and differential labeling of peptifes
L M H
unique target protein peptide
L M H
L M H
L M H
m/z

Fig. 6 ABPP workflow with active photoprobe, inactive photoprobe control and DMSO control.

Cells are cultured under the same conditions used for the bioassay. Temperature, growth time, culture volume and form and material of culture flasks / tubes have an effect on ABPP experiment results. Cells are harvested and incubated with ABPP probes (active and inactive) or DMSO as a control. Photo-probe labeled cells are irradiated with UV light to establish a covalent link between probe molecules and target proteins. The labeling and irradiation process is done in whole cells to analyze proteins under physiological conditions unaffected by chemical or mechanical lysis. Only after covalent linkage of protein and probe the cells are lysed. Then a biotin tag is attached to the chemical probe using bioorthogonal click chemistry [30-32]. After a pulldown experiment with avidin or streptavidin beads, samples are treated with trypsin to obtain peptide fragments. Primary amines of those peptide fragments are labeled with different formaldehyde isotopes (light, medium, heavy) for different probes and DMSO control. In figure 6 DMSO control is labeled with light formaldehyde (CH_2O), inactive probe with medium (CD_2O) and active probe with heavy formaldehyde ($^{13}CD_2O$). Then the three samples can be merged and measured as one sample in a LC-MS/MS mass spectrometer setup. MS-signal intensity ratios (e.g. heavy / light) are the evaluated. In figure 6 a peptide with a high heavy / light ratio indicates, that its protein is a target as it could be enriched by the preceding pulldown experiment. If this peptide is also enriched compared to the biologically inactive probe (high heavy / medium ratio) the corresponding protein is a biologically relevant ABPP protein target hit. In this case other peptides of the target protein should confirm the result by similar heavy / light and heavy / medium ratios.

ABPP target validation

ABPP target protein hits can be validated by a diverse set of assays. Validation is important to show that a protein is not only a binding partner of the compound or the probe but also is relevant for the observed biological effect. Heterologous overexpression of a putative hit-protein in *Escherichia coli* and subsequent ABPP experiments with this different strain should confirm the overexpressed protein as a hit. The interaction of purified protein with compound can be tested in binding assays like thermal shift assay (differential scanning calorimetry; DSC), isothermal titration calorimetry (ITC) or microscale thermophoresis (MST). An effect of compound on protein function can be shown with *in vitro* protein assays.

REFERENCES

1. Wexler, H.M., *Bacteroides: the good, the bad, and the nitty-gritty.* Clin Microbiol Rev, 2007. **20**(4): p. 593-621.
2. Lowy, F.D., *Staphylococcus aureus infections.* N Engl J Med, 1998. **339**(8): p. 520-32.
3. Lam, S.W., S.R. Bauer, and E.A. Neuner, *Predictors of septic shock in patients with methicillin-resistant Staphylococcus aureus bacteremia.* Int J Infect Dis, 2012. **16**(6): p. e453-6.
4. Chambers, H.F. and F.R. Deleo, *Waves of resistance: Staphylococcus aureus in the antibiotic era.* Nat Rev Microbiol, 2009. **7**(9): p. 629-41.
5. Tong, S.Y., et al., *Staphylococcus aureus infections: epidemiology, pathophysiology, clinical manifestations, and management.* Clin Microbiol Rev, 2015. **28**(3): p. 603-61.
6. Brown, A.F., et al., *Staphylococcus aureus Colonization: Modulation of Host Immune Response and Impact on Human Vaccine Design.* Front Immunol, 2014. **4**: p. 507.
7. WHO, *Antimicrobial resistance: global report on surveillance.* 2014.
8. Grundmann, H., et al., *Emergence and resurgence of meticillin-resistant Staphylococcus aureus as a public-health threat.* Lancet, 2006. **368**(9538): p. 874-85.
9. Liu, G.Y., et al., *Staphylococcus aureus golden pigment impairs neutrophil killing and promotes virulence through its antioxidant activity.* J Exp Med, 2005. **202**(2): p. 209-15.
10. Baba, T., et al., *Genome sequence of Staphylococcus aureus strain Newman and comparative analysis of staphylococcal genomes: polymorphism and evolution of two major pathogenicity islands.* J Bacteriol, 2008. **190**(1): p. 300-10.
11. Lin, Y.C. and M.L. Peterson, *New insights into the prevention of staphylococcal infections and toxic shock syndrome.* Expert Rev Clin Pharmacol, 2010. **3**(6): p. 753-767.
12. Mekalanos, J.J., *Environmental signals controlling expression of virulence determinants in bacteria.* J Bacteriol, 1992. **174**(1): p. 1-7.
13. Thomas, M.S. and S. Wigneshweraraj, *Regulation of virulence gene expression.* Virulence, 2014. **5**(8): p. 832-4.
14. Yarwood, J.M. and P.M. Schlievert, *Quorum sensing in Staphylococcus infections.* J Clin Invest, 2003. **112**(11): p. 1620-5.
15. Gengenbacher, M. and S.H. Kaufmann, *Mycobacterium tuberculosis: success through dormancy.* FEMS Microbiol Rev, 2012. **36**(3): p. 514-32.
16. Lin, P.L. and J.L. Flynn, *Understanding latent tuberculosis: a moving target.* J Immunol, 2010. **185**(1): p. 15-22.
17. Horsburgh, C.R., Jr., C.E. Barry, 3rd, and C. Lange, *Treatment of Tuberculosis.* N Engl J Med, 2015. **373**(22): p. 2149-60.
18. Ramappa, V. and G.P. Aithal, *Hepatotoxicity Related to Anti-tuberculosis Drugs: Mechanisms and Management.* J Clin Exp Hepatol, 2013. **3**(1): p. 37-49.
19. CDC, N.C.f.H.A., Viral Hepatitis, STD, and TB Prevention, Division of Tuberculosis Elimination, *Multidrug-Resistant Tuberculosis (MDR TB) fact sheet*. 2012.
20. Ben-Jacob, E., D.S. Coffey, and H. Levine, *Bacterial survival strategies suggest rethinking cancer cooperativity.* Trends Microbiol, 2012. **20**(9): p. 403-10.
21. Lambert, G., et al., *An analogy between the evolution of drug resistance in bacterial communities and malignant tissues.* Nat Rev Cancer, 2011. **11**(5): p. 375-82.
22. Evans, M.J. and B.F. Cravatt, *Mechanism-based profiling of enzyme families.* Chem Rev, 2006. **106**(8): p. 3279-301.

23. Martinez Molina, D., et al., *Monitoring drug target engagement in cells and tissues using the cellular thermal shift assay.* Science, 2013. **341**(6141): p. 84-7.
24. Vomacka, J., Korotkov, V.S., Bauer, B., Weinandy, F., Kunzmann, M.H., Krysiak, J., Baron, O., Böttcher, T., Lorenz-Baath, K., Sieber, S.A., *An aromatic hydroxyamide attenuates multiresistant Staphylococcus aureus toxin expression.* Chemistry - A European Journal, 2016.
25. Swinney, D.C., *Phenotypic vs. target-based drug discovery for first-in-class medicines.* Clin Pharmacol Ther, 2013. **93**(4): p. 299-301.
26. Lehmann, J., M.H. Wright, and S.A. Sieber, *Making a Long Journey Short: Alkyne Functionalization of Natural Product Scaffolds.* Chemistry, 2016. **22**(14): p. 4666-78.
27. Cravatt, B.F., A.T. Wright, and J.W. Kozarich, *Activity-based protein profiling: from enzyme chemistry to proteomic chemistry.* Annu Rev Biochem, 2008. **77**: p. 383-414.
28. Ge, J. and S.Q. Yao, *Chemical proteomics of host-pathogen interaction.* Chem Biol, 2015. **22**(4): p. 434-5.
29. Tate, J.J., J. Persinger, and B. Bartholomew, *Survey of four different photoreactive moieties for DNA photoaffinity labeling of yeast RNA polymerase III transcription complexes.* Nucleic Acids Res, 1998. **26**(6): p. 1421-6.
30. Huisgen, R., *1,3-Dipolar Cycloadditions.* Proc. Chem. Soc., 1961: p. 357-96.
31. Rostovtsev, V.V., et al., *A stepwise huisgen cycloaddition process: copper(I)-catalyzed regioselective "ligation" of azides and terminal alkynes.* Angew Chem Int Ed Engl, 2002. **41**(14): p. 2596-9.
32. Tornoe, C.W., C. Christensen, and M. Meldal, *Peptidotriazoles on solid phase: [1,2,3]-triazoles by regiospecific copper(i)-catalyzed 1,3-dipolar cycloadditions of terminal alkynes to azides.* J Org Chem, 2002. **67**(9): p. 3057-64.

AN AROMATIC HYDROXYAMIDE ATTENUATES MULTIRESISTANT STAPHYLOCOCCUS TOXIN EXPRESSION

Published in Chemistry - A European Journal **2016**, *22* (5), 1622 - 1630, by Jan Vomacka, Vadim S. Korotkov, Bianca Bauer, Franziska Weinandy, Martin H. Kunzmann, Joanna Krysiak, Oliver Baron, Thomas Böttcher, Katrin Lorenz-Baath and Stephan A. Sieber.

Reproduced from J. Vomacka, V.S. Korotkov, B. Bauer, F. Weinandy, M.H. Kunzmann, J. Krysiak, O. Baron, T. Böttcher, K. Lorenz-Baath, S.A. Sieber, *Chem. Eur. J.* **2016**, 22, 1622, DOI: 10.1002/chem.201503981 with permission from John Wiley and Sons.

SUMMARY

Methicillin-resistant *Staphylococcus aureus* (MRSA) causes severe infections with only few effective antibiotic therapies currently available. To approach this challenge, chemical entities with a novel and resistance-free mode of action are desperately needed. Here, a new hydroxyamide compound is introduced, that effectively reduces the expression of devastating toxins in various *S. aureus* and MRSA strains. The molecular mechanism was investigated by transcriptome analysis as well as by affinity-based protein profiling. Down-regulation of several pathogenesis associated genes suggested the inhibition of a central virulence-related pathway. Mass spectrometry-based chemical proteomics revealed putative molecular targets. Systemic treatment with the hydroxyamide showed significant reduction of abscess sizes in a MRSA mouse skin infection model. The absence of resistance development *in vitro* further underlines the finding that targeting virulence could lead to prolonged therapeutic options in comparison to antibiotics that directly address bacterial survival.

This summary is an altered version of the abstract accompanying the publication.

AUTHOR CONTRIBUTIONS

S.A. Sieber and K. Lorenz-Baath conceived and supervised the project. J. Vomacka performed all experiments unless noted otherwise. V.S. Korotkov synthesized all chemical compounds. F.

Weinandy and K. Lorenz-Baath performed the *in vivo* experiments. J. Vomacka, B. Bauer and M.H. Kunzmann performed the resistance development experiments. B. Bauer and J. Vomacka performed the transcriptome analysis. J. Vomacka, B. Bauer, K. Lorenz-Baath and F. Weinandy performed the virulence factor detection assays. J. Vomacka, S.A. Sieber and K. Lorenz-Baath wrote the manuscript with input from J. Krysiak, O. Baron and T. Böttcher.

ChemPubSoc Europe

DOI: 10.1002/chem.201503981

CHEMISTRY
A European Journal
Full Paper

Drug Discovery |*Hot Paper*|

An Aromatic Hydroxyamide Attenuates Multiresistant *Staphylococcus aureus* Toxin Expression

Jan Vomacka,[b] Vadim S. Korotkov,[b] Bianca Bauer,[b] Franziska Weinandy,[b] Martin H. Kunzmann,[a] Joanna Krysiak,[a] Oliver Baron,[c] Thomas Böttcher,[d] Katrin Lorenz-Baath,[b] and Stephan A. Sieber*[a]

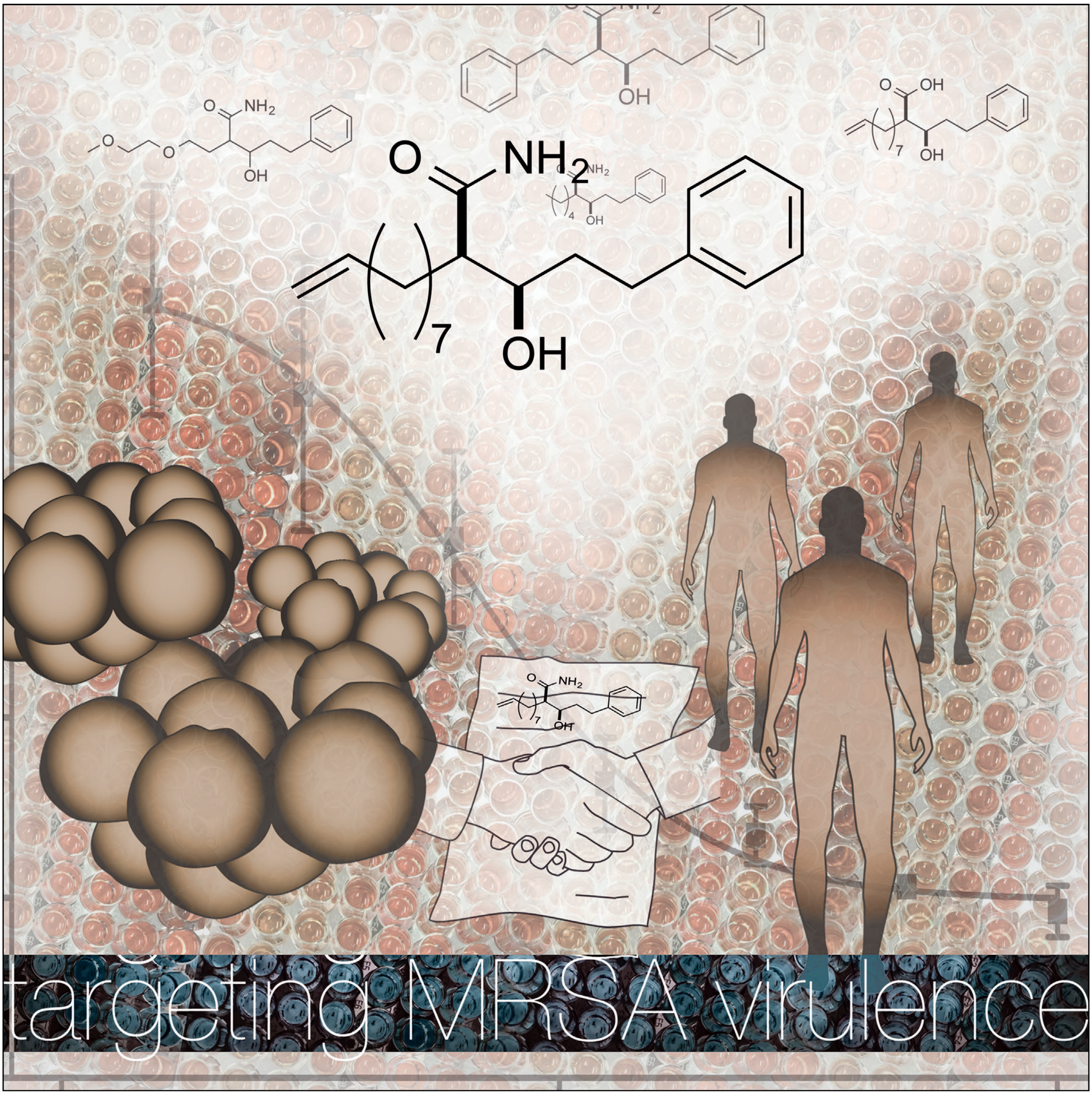

© 2016 Wiley-VCH Verlag GmbH & Co. KGaA, Weinheim

Abstract: Methicillin-resistant *Staphylococcus aureus* (MRSA) causes severe infections with only few effective antibiotic therapies currently available. To approach this challenge, chemical entities with a novel and resistance-free mode of action are desperately needed. Here, we introduce a new hydroxyamide compound that effectively reduces the expression of devastating toxins in various *S. aureus* and MRSA strains. The molecular mechanism was investigated by transcriptome analysis as well as by affinity-based protein profiling. Down-regulation of several pathogenesis associated genes suggested the inhibition of a central virulence-related pathway. Mass spectrometry-based chemical proteomics revealed putative molecular targets. Systemic treatment with the hydroxyamide showed significant reduction of abscess sizes in a MRSA mouse skin infection model. The absence of resistance development in vitro further underlines the finding that targeting virulence could lead to prolonged therapeutic options in comparison to antibiotics that directly address bacterial survival.

Introduction

The spread of methicillin-resistant *Staphylococcus aureus* (MRSA) poses a major threat to public health and represents one of the greatest challenges for clinicians today.[1] In addition to the ability of MRSA to cause life-threatening diseases such as endocarditis, pneumonia, or sepsis as well as severe skin and soft tissue infections, its high mutation frequency by which it rapidly accumulates multiple antibiotic resistances, is of major concern.[2]

Alternative treatment strategies targeting bacterial pathogenicity are emerging, that is, inhibiting virulence instead of bacterial viability.[3,4] Bacterial virulence is determined by a diverse set of molecules, including toxins and adhesins, which are needed to establish and propagate infection.[5] Inhibition of central virulence pathways disarms bacteria without directly affecting their viability, thus leading to less selective pressure and decreased resistance development.[6–10] Several mouse studies have already confirmed the success of this concept by showing that anti-virulence compounds improve the outcome of *S. aureus* induced sepsis, pneumonia or skin infections.[11–15] These approaches addressed very different targets—from interference with cholesterol biosynthesis[11–13] to the inhibition of toxins[14,15] or cell adhesion.[16] Moreover, the efficacy of therapeutic antibodies that block diverse virulence determinants of *S. aureus* has been reported from animal studies.[17,18] However, immunotherapeutics against a single virulence factor were only moderately effective in phase 1 or 2 clinical trials; therefore, current approaches are starting to combine multiple antibody formulations directed against a series of key staphylococcal toxins.[18] Consequently, we focused our study on the discovery of anti-virulence small molecules that inhibit not only one but multiple staphylococcal virulence factors.

S. aureus virulence is controlled by complex pathways such as the accessory gene regulator (agr) two-component system.[19] Small autoinducing peptides (AIPs), encoded by agrD, are secreted and sensed by a growing population.[19] Once a critical density is reached, AIPs bind to histidine kinase AgrC on the cell surface and induces phosphorylation of an intracellular response regulator (AgrA) to activate transcription of RNAIII, which is an effector of a broad range of diverse virulence factors.[20] Synthetic derivatives of AIPs have been shown to effectively repress this sensing mechanism.[21–23] In addition, staphylococcal accessory regulator (SarA) and homologous proteins such as SarX independently control the transcription of toxins through direct binding to promoter regions.[24,25]

Herein we report the identification of a new chemical virulence inhibitor (*R**,*R**)-**3** (Figure 1 a), bearing an aromatic hydroxyamide functional group that blocks a variety of different staphylococcal virulence factors. Systemic treatment with the inhibitor in mice led to a significant reduction of MRSA induced skin abscesses. Together with the lack of in vitro resistance development of (*R**,*R**)-**3** treated bacteria, the new compound represents a promising starting point for further medicinal development.

Results and Discussion

Hydroxyamide (*R**,*R**)-3 broadly inhibits virulence factors of *S. aureus* in multiresistant clinical isolates

In previous studies we identified β-lactones as specific inhibitors of bacterial caseinolytic protease P (ClpP), which is a virulence associated protein, that attenuates pathogenicity in bacterial cultures as well as in a murine infection model.[15,26]

---

[a] Dr. M. H. Kunzmann, Dr. J. Krysiak, Prof. S. A. Sieber
Department of Chemistry, Chair of Organic Chemistry II
Center for Integrated Protein Science (CIPSM)
Institute of Advanced Studies (IAS), Technische Universität München (TUM)
Lichtenbergstrasse 4, 85747 Garching (Germany)
E-mail: stephan.sieber@tum.de

[b] J. Vomacka, Dr. V. S. Korotkov, Dr. B. Bauer, Dr. F. Weinandy, Dr. K. Lorenz-Baath
Department of Chemistry, AVIRU, GO-Bio-project of the Federal Ministry of Education and Research, FKZ: 031A131
Technische Universität München (TUM)
Lichtenbergstrasse 4, 85747 Garching (Germany)

[c] Dr. O. Baron
Department of Chemistry, Center for Integrated Protein Science (CIPSM)
Ludwig-Maximilians-Universität München (LMU)
Butenandtstrasse 5–13, 81377 Munich (Germany)

[d] Dr. T. Böttcher
Department of Chemistry, Universität Konstanz
Universitätsstrasse 10, 78457 Konstanz (Germany)

Supporting information, including detailed experimental descriptions for all experiments, and ORCID(s) from the author(s) for this article are available on the WWW under http://dx.doi.org/10.1002/chem.201503981.

© 2016 Wiley-VCH Verlag GmbH & Co. KGaA, Weinheim

These are not the final page numbers!

Further progress was mainly limited by the low plasma stability of the β-lactones.[15] In the search for antivirulence compounds with improved pharmacological properties, we opened the lactone ring of **1** through hydrolysis or aminolysis to obtain open-chain β-hydroxyacid **2** and β-hydroxyamide **3**, respectively, both as (*R**,*R**)-diastereomers (Figure 1 a). Initially, the biological activity of the newly synthesized substances was investigated. To rule out an antibiotic mode of action and focus on substances with antivirulence activity, we performed a minimum inhibitory concentration (MIC) test with *S. aureus* (NCTC 8325). Only compound **2** exhibited a MIC of 400 μM (127 $\mu g\,mL^{-1}$), and was thus excluded from further investigations (Figure 1 a). Given that no inhibition of bacterial growth was obtained after treatment with (*R**,*R**)-**3** up to concentrations of 1 mM (317 $\mu g\,mL^{-1}$), we focused on this compound for further studies.

Hemolysin alpha (hla), a pore-forming cytotoxin that causes lysis of immune cells and erythrocytes, is one of the major staphylococcal virulence factors. Remarkably, (*R**,*R**)-**3** inhibited hemolytic activity of two major *S. aureus* strains (NCTC 8325 and MRSA USA 300) with EC_{50} values of 13 μM (4.1 $\mu g\,mL^{-1}$; Figure 1 b) and 18 μM (5.7 $\mu g\,mL^{-1}$; see the Supporting Information, Figure S1 a), respectively. Western blot analysis revealed that reduced hemolysis was based on decreased production of hla (Figure 1 b and Figure S1 a). Importantly, a broad spectrum of 16 independent clinical isolates from different disease origins containing different resistance types (methicillin-sensitive *S. aureus* (MSSA) and methicillin-resistant *S. aureus* (MRSA)) were largely sensitive to treatment with (*R**,*R**)-**3**, showing reduced hemolysis of erythrocytes (Figure 1 c). Whereas some isolates did not show effective hemolysis at all (BK97296, VA402525, VA417350, VA12350), only two haemolytic strains did not respond to the treatment with (*R**,*R**)-**3**. Importantly, the production of sepsis causing toxic shock syndrome toxin (TSST-1) was also decreased with an EC_{50} of 7 μM (2.22 $\mu g\,mL^{-1}$) in TSST-1 producing strain Mu 50 (Figure 1 d). In addition, (*R**,*R**)-**3** attenuated the production of other staphylococcal virulence factors, including diarrhea causing enterotoxins (SAE A-E; see the Supporting Information, Figure S1 b) in a concentration-dependent manner. Furthermore, the (*R**,*R**)-**3** mediated inhibition of toxin secretion led to a protection of eukaryotic, alveolar cells from cell death in an in vitro model of *S. aureus* toxin-induced cell injury during lung infection (see the Supporting Information, Figure S1 c).

To investigate structure-activity relationships we tested various hydroxyamide derivatives. Several analogues featuring aromatic and aliphatic substituents as putative protein-binding ligands were synthesized according to two different routes (Scheme 1). In brief, β-lactone ring-opening reactions with ammonia in isopropanol stereoselectively led to the desired compounds (Route I). *trans*-β-Lactones were obtained by $ZnCl_2$-catalyzed tandem Mukaiyama aldol-lactonization (TMAL)[27,28] from aldehydes and ketene acetals. Alternatively, hydroxyamides were synthesized by utilizing aldol condensation (Route II). Given that the reaction is not stereoselective, a mixture of both diastereomers was formed; these were successfully separated by column chromatography and further converted into the desired compounds. The effect of the derivatives on hla inhibition was examined by hemolysis assay (Figure 1 e). Interestingly, diastereomer (*R**,*S**)-**3** was almost inactive. In addition, the orientation of both side chains was crucial for anti-hemolytic activity, because substance **4**, with exchanged substituents, showed a reduced effect in the hemolysis assay. All attempts to replace the nonenyl chain, for example, by the introduction of pentyl (**5**), phenylethyl (**6**), or 1-ethoxy-2-methoxyethane (**7**), resulted in molecules with impaired activity compared with (*R**,*R**)-**3** (Figure 1 e).

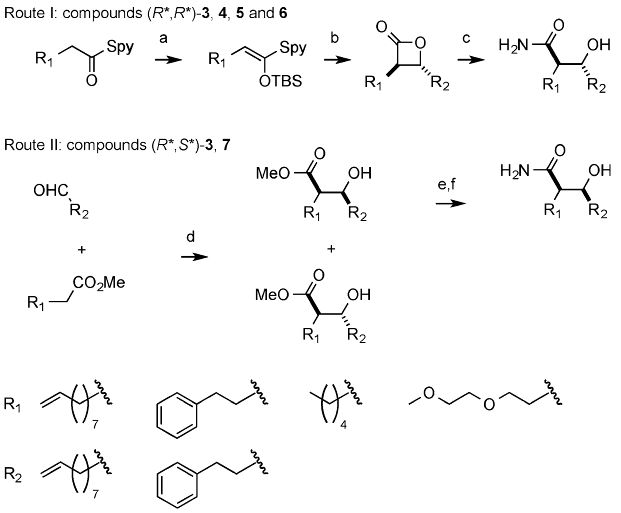
Route I: compounds (R*,R*)-3, 4, 5 and 6
a
b
c
Spy
OTBS
H_2N
OH
R_1
R_2
Route II: compounds (R*,S*)-3, 7
OHC
CO_2Me
MeO
d
e,f
+
7
4

Scheme 1. Two routes for the synthesis of hydroxyamide derivatives. Reagents and conditions: a) TBSCl, LHMDS, Et_3N, THF, DMF, −78 to 0 °C, 2 h; b) $ZnCl_2$, R_2CHO, CH_2Cl_2, RT, 4 d; c) NH_3 in *i*PrOH, RT, 18 h; d) LHMDS, THF, −78 °C, (no separation of diastereomers for compound **7**; e) NaOH, H_2O, MeOH, RT, 18 h; f) NH_4HCO_3, Boc_2O, py, CH_3CN, RT, 18 h. TBS = tri-*n*-butylsilyl; LHMDS = lithium hexamethyldisilazide.

Unlike the parent β-lactones,[15,26] (*R**,*R**)-**3** did not inhibit ClpP activity in vitro (see the Supporting Information, Figure S2), suggesting a different antivirulence mode of action.

Transcriptome analysis revealed a strong impact of (*R**,*R**)-3 treatment on virulence factor regulation

To elucidate the inhibitory molecular mechanisms of (*R**,*R**)-**3**, next generation sequencing was applied to analyze transcriptional changes of NCTC 8325 cells after treatment with (*R**,*R**)-**3**. Cells treated with dimethyl sulfoxide (DMSO) were used as control. Significant (>1 or <-1 $\log_2$ fold change, $p<0.05$) regulation of 197 genes (6.9 % of all genes) was observed, with 149 genes being down-regulated and 48 being up-regulated (Figure 2 a). A DAVID database[29,30] gene cluster analysis based on gene annotation terms revealed that a substantial number of down-regulated genes clustered within the pyruvate metabolism, metal ion binding processes, and virulence associated mechanisms (see the Supporting Information, Figure S3). Remarkably, several enzymes connecting glycolysis with the citrate acid cycle via pyruvate were significantly down-regulated, suggesting a strong effect on central carbon metabolism. Consistent with the antihemolytic effect, hla transcript levels were

© 2016 Wiley-VCH Verlag GmbH & Co. KGaA, Weinheim

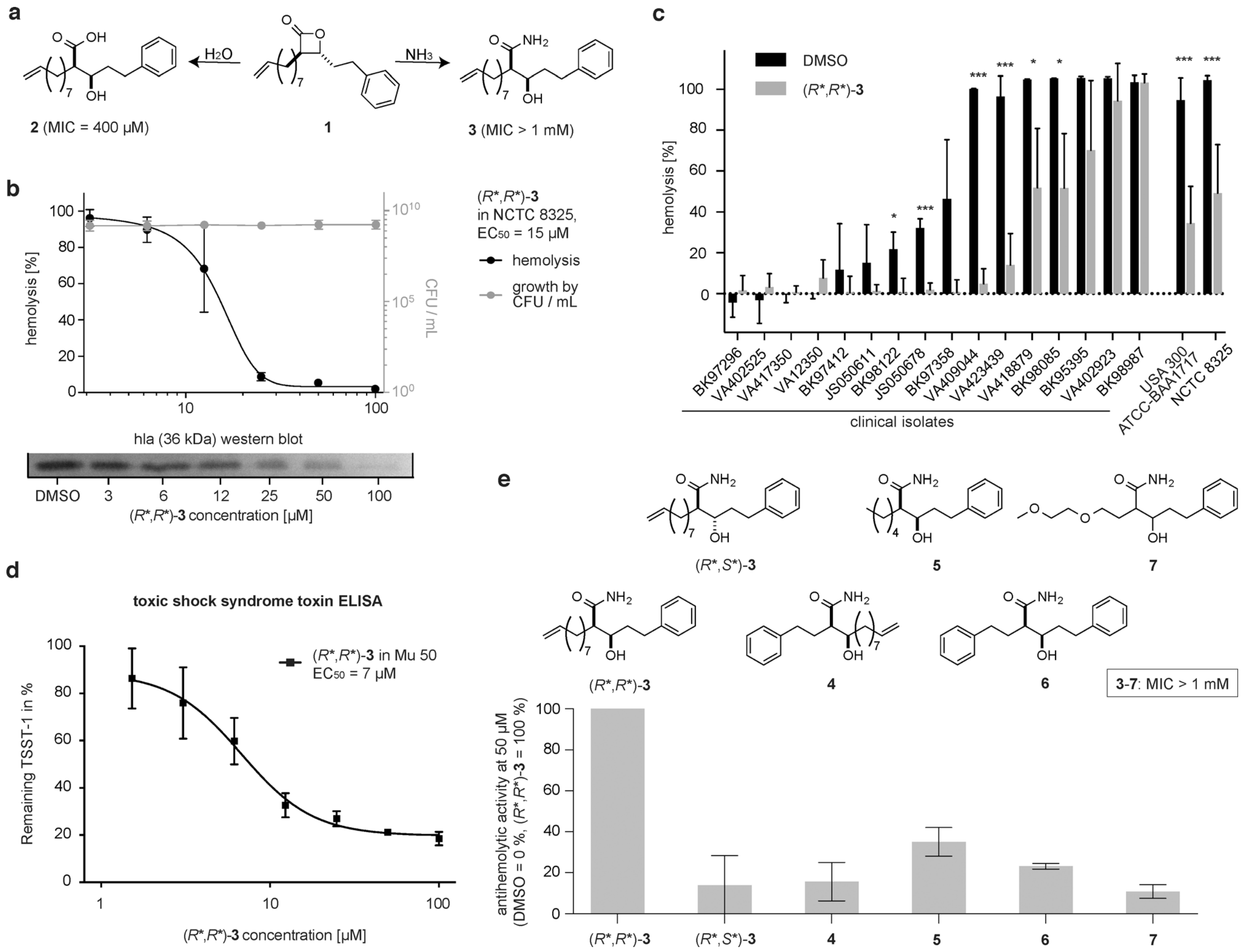

Figure 1. (*R**,*R**)-**3** strongly inhibits hemolysis in *S. aureus*. a) Ring opening of anti-virulence compound **1** through hydrolysis or aminolysis yields an open chain β-hydroxyacid **2** and β-hydroxyamide **3**, respectively, both as (*R**,*R**)-diastereomers. Antibiotic effects were determined by measuring minimum inhibitory concentrations (MIC) up to 1 mM for three biological replicates. b) Hemolysis inhibition with (*R**,*R**)-**3** in *S. aureus* NCTC 8325. The mean value of three technical replicates is shown. These findings were further confirmed by western blot analysis of hla (lower panel). Growth is indicated by colony-forming units (CFU)/mL culture. c) Inhibition of hemolysis by 100 μM (*R**,*R**)-**3** in clinical isolates originating from blood cultures (BK95395#, BK98122, BK98085, BK97358, BK97472, BK97296#, BK98987), abscesses (VA423439, VA409044#, VA402525#, VA402923#, VA412350#) and pneumonia (VA418879#, IS050611#, IS050678#, VA417350#). MRSA strains are marked by (#). The mean value of three biological replicates ± SD is shown. Significant difference of compound treated compared with DMSO control treated samples (one-sample Student's t-test, * $p < 0.05$, *** $p < 0.001$). d) Toxic shock syndrome toxin 1 (TSST-1) reduction by (*R**,*R**)-**3** in *S. aureus* Mu 50 was detected by ELISA in three biological replicates. e) Structures of anti-virulence compounds and their derivatives used for structure activity relationship studies (**1**–**7**) and target identification (**8**). Antibiotic effects were determined by measuring minimum inhibitory concentrations (MIC) up to 1 mM for three biological replicates. Antihemolytic activity of hydroxyamide derivatives (50 μM) **3**–**7**: Measurements were normalized according to DMSO control (0 % activity) and (*R**,*R**)-**3** (100 % activity). The mean value of at least three biological replicates ± SD is shown.

3.29 fold reduced (1.72 $\log_2$ fold). Several major virulence-associated transcriptional activators such as SarA and SarR[31] were among the strongest down-regulated genes (Figure 2 b and Figure S3in the Supporting Information). In contrast, SarX,[25] a negative regulator of agr promoted virulence, was found to be the only virulence-associated up-regulated gene. Thus, transcriptional analysis supports the global antivirulence properties of (*R**,*R**)-**3**.

Chemical proteomics reveal target proteins

To identify protein target(s) of (*R**,*R**)-**3**, we synthetically equipped the active and inactive core structures (*R**,*R**)-**3** and (*R**,*S**)-**3** with an alkyne handle at the terminal end of the alkyl chain, and replaced the phenyl ring with a benzophenone photocrosslinker (Scheme 2). Synthesis started with the Heck reaction of the protected 4-bromobenzophenone with acrylic acid. The product obtained was hydrogenated and converted into the corresponding aldehyde. Its aldol reaction with TMS-protected methyl undec-10-ynoate yielded a mixture of two diastereomeric 3-hydroxyesters. Diastereomers of the 3-hydroxyacid obtained after deprotection steps were separated by column chromatography and converted into the desired photo-probes (*R**,*R**)-**8** and (*R**,*S**)-**8**.

The functionalized affinity-based protein profiling (AfBPP) probe[32] (*R**,*R**)-**8** retained anti-hemolytic properties, albeit

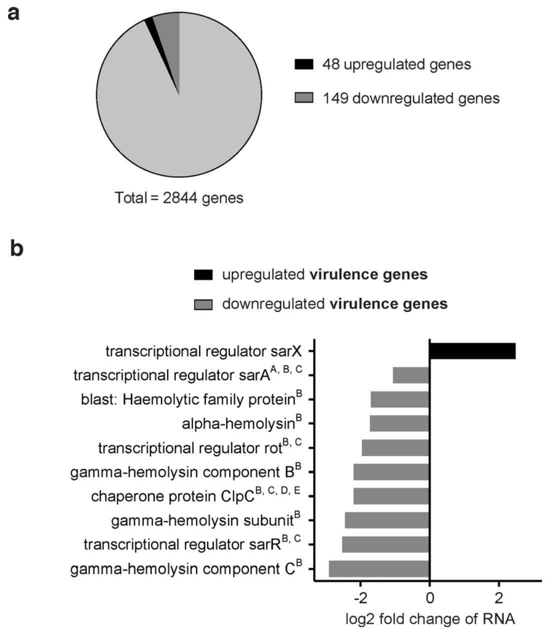

Figure 2. Next generation sequencing of NCTC 8325 cells treated with 100 μM (31.7 μg mL^{-1}) (R^*,R^*)-**3** compared with DMSO control. a) Fraction of up- and down-regulated genes (>1 or <-1 log$_2$ fold change, *p*-value <0.05). b) Up- and down-regulated virulence associated genes. Virulence genes were identified by searching the DAVID[29,30] functional annotation table for the terms: virulence, pathogenesis, cell killing and cytolysis. For regulated DAVID database gene clusters, see the Supporting Information (Figure S3). A–E: gene is part of the following DAVID gene clusters (enrichment score): A: metal ion binding (2.27); B: virulence (2.26); C: virulence regulation (0.80). D: DNA repair, stress response (0.43); E: nucleotide binding (0.41). See also the supporting transcriptome analysis.xlsx file.

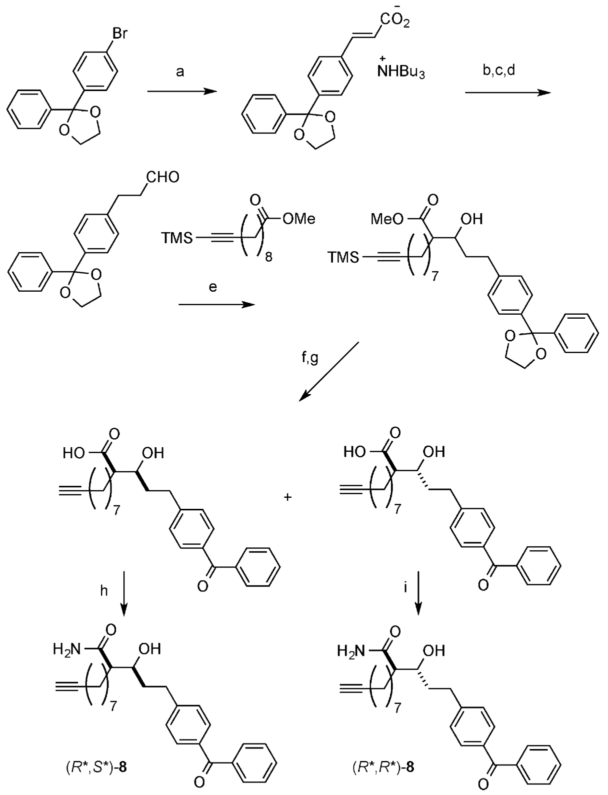

Scheme 2. Synthesis of the affinity-based protein profiling (AfBPP) probes. Reagents and conditions: a) acrylic acid, Pd(OAc)$_2$, Bu$_3$N, P(2-MeC$_6$H$_4$)$_3$, *o*-xylene, H$_2$O, 150 °C, 5 h, 74 %; b) H$_2$/Pd/C, MeOH, RT, 16 h, 97 %; c) LiAlH$_4$, THF, 80 °C, 2 h, 50 %; d) PCC, CH$_2$Cl$_2$, RT, 4 h, 80 %; e) LHMDS, THF, −78 °C to RT, 4 h, 28 %; f) trifluoroacetic acid, RT, 20 h; g) NaOH, THF, H$_2$O, MeOH, separation of diastereomers; h) NH$_4$HCO$_3$, Boc$_2$O, py, CH$_3$CN, RT, 22 %; i) NH$_4$HCO$_3$, Boc$_2$O, py, CH$_3$CN, RT, 22 %.

with reduced potency compared with the parent structure (Figure 3 a). As expected, the (R^*,S^*)-**8** diastereomer was almost inactive. Both probes were incubated with live *S. aureus* (NCTC 8325 and USA 300 Lac) cells and irradiated with UV light to establish a covalent link between the target protein and the photolinker. Cells were lysed and the probe-labeled proteome was modified with fluorescent biotin tags through the use of click chemistry.[33–35] Avidin bead enrichment, SDS-PAGE analysis and fluorescent scanning revealed two intense bands at approximately 90 and 35 kDa (Figure 3 b) that were analyzed by LC-MS/MS following tryptic digest. The upper band was identified as 3-hydroxyacyl-CoA dehydrogenase (see the Supporting Information, Figure S4) and the lower band as MntC, which is a binding domain for a manganese membrane transporter (MntABC; see the Supporting Information, Figure S5).

Importantly, labeling with the inactive probe (R^*,S^*)-**8** revealed comparable intensity of the upper band but reduced intensity of the lower band (see the Supporting Information, Figure S6). Labeling in *S. aureus* NCTC 8325 was dose-dependent and the lower band could be detected down to a concentration of 3.5 μM (1.5 μg mL^{-1}) of (R^*,R^*)-**8** (see the Supporting Information, Figure S7).

To comprehensively identify and confirm putative target proteins through quantitative proteomics, we utilized a gel-free approach with dimethyl labeling to introduce light-, medium-, and heavy-isotope tags to peptides after enrichment and digest.[36] Differentially labeled peptides derived from cells treated with the active probe (R^*,R^*)-**8**, the inactive probe (R^*,S^*)-**8** or DMSO, respectively, were mixed and analyzed by MS (see the Supporting Information, Figure S8). Results were ranked according to highest enrichment ratios derived from the active probe in comparison to the DMSO control (Figure 3 c) and to the inactive probe (Figure 3 d). Only proteins with enrichment higher than one-fold standard deviation (SD) and a *p* value <0.01 were considered. The four hits throughout all experiments were MntC, an uncharacterized esterase, a proline dehydrogenase, and the FtsH metalloprotease (Figure 3 e, Supporting Information ABPP_analysis.xlsx file). The 90 kDa 3-hydroxyacyl-CoA dehydrogenase was not enriched by using this method, suggesting that it is an unspecific target of gel-based labeling.

Hit validation was performed by using selective transposon mutants (TN mut.) of *S. aureus* NCTC 8325 that were obtained by phage transduction from USA 300 Lac TN mutant strains from the Nebraska transposon mutant library (NTML, University of Nebraska Medical Center). Fluorescent gel analysis following labeling with (R^*,R^*)-**8** in the MntC-deficient strain revealed

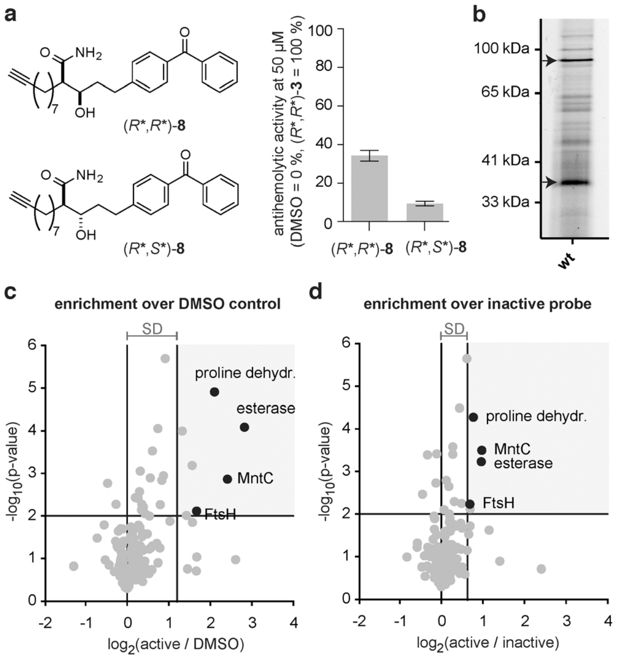

e

uniprot		N	active / DMSO (av. enrichment (p-value))	active / inactive (av. enrichment (p-value))
Q2FV90	uncharacterized protein (blast: esterase)	8	7.09 (8.2E-5)	1.95 (5.9E-4)
Q2G2D8	ABC transporter (MntC), substrate-binding protein	8	5.33 (1.3E-3)	1.96 (3.2E-4)
Q2FXG3	proline dehydrogenase	9	4.30 (1.2E-5)	1.71 (5.3E-5)
Q2G0R0	ATP-dependent zinc metalloprotease FtsH	4	2.69 (9.8E-3)	1.61 (5.9E-3)

Figure 3. MS based target identification. a) Structure and antihemolytic activity of 50 µM photo-probes (*R**,*R**)-**8** and (*R**,*S**)-**8**. Measurements were normalized according to DMSO control (0 % activity) and (*R**,*R**)-**3** (100 % activity). The mean value of at least three biological replicates ± SD is shown. b) Labeling of NCTC 8325 wt with 50 µM (21.0 µg mL^{-1}) photo-probe (*R**,*R**)-**8**. c), d) Volcano plots showing *p* value ($-\log_{10}$ transformed) and enrichment factor ($\log_2$ transformed) for 35 µM (*R**,*R**)-**8** vs. DMSO control (c) and for (*R**,*R**)-**8** (35 µM) vs. the inactive diastereomer photo-probe (*R**,*S**)-**8** control (35 µM) (d). SD represents the enrichment factor standard deviation over all proteins. Black dots represent proteins that were enriched over both controls. 10 independent biological experiments (five replicates NCTC 8325 and five replicates USA 300 Lac) were performed. Both strains were analyzed together. Separate analysis of each strain can be found in a separate excel file (ABPP_analysis.xlsx). To be considered a hit, the mean of both enrichment factors (active diastereomer (*R**,*R**)-**8** over DMSO and active diastereomer (*R**,*R**)-**8** over inactive diastereomer (*R**,*S**)-**8**) had to be greater than the respective average enrichment factor of all proteins by at least one standard deviation (SD). In addition, the enrichment had to be significant according to a one-sample Student's t-test for enrichment greater than 1 (one-tailed, $p < 0.01$). e) Hits enriched over DMSO and inactive diastereomer photo-probe (*R**,*S**)-**8** control: Uniprot[37] accession numbers and protein names from fasta entries are shown. Uncharacterized proteins were identified by using blast (uniprot). Number of experiments (out of 10 replicates) in which the protein was identified (*N*), average (av.) enrichment factors and corresponding *p* values are shown for both controls.

a similar labeling pattern to that of wild type (wt), except for the loss of the strong fluorescent band at 35 kDa, confirming the previous gel-based assignment of this band as MntC (Figure 4a). To examine the impact of all putative hits revealed by gel-free MS analysis (Figure 3c–e), TN mutations of MntC, the uncharacterized esterase, the proline dehydrogenase, and FtsH were tested for their ability to reduce hemolysis in *S. aureus* USA 300 Lac and NCTC 8325 (Figure 4b). Whereas FtsH and the esterase showed no or only a slight reduction in hemolysis production, respectively, a significant effect was observed for proline dehydrogenase and MntC in the NCTC 8325 strain. It is thus possible that multiple targets are involved in the observed phenotype.

Hydroxyamide (*R**,*R**)-3 does not induce resistance in vitro

Targeting nonessential virulence pathways is believed to decrease selective pressure and limit the development of resistances.[10] To test this concept, the antivirulence compound (*R**,*R**)-**3** and a control antibiotic ofloxacin were compared in a resistance development assay (Figure 5). Bacterial *S. aureus* cultures (NCTC 8325) were treated with either 16 µM (5.2 µg mL^{-1}) (*R**,*R**)-**3** (EC_{50} concentration in the hemolysis assay) or 3.5 µM (1.5 µg mL^{-1}) ofloxacin (no growth inhibition at this concentration based on OD_{600}) over 12 passages. Importantly, whereas treatment with ofloxacin resulted in an increased EC_{50} already after four passages, no change in hemolysis EC_{50} could be observed with the antivirulence compound (*R**,*R**)-**3** (Figure 5). In an independent long-term experiment with (*R**,*R**)-**3**, no resistance development could be observed even after 45 passages (see the Supporting Information, Figure S9).

In vivo efficacy in methicillin-resistant *S. aureus* (MRSA) skin infections

In contrast to β-lactones, which undergo rapid hydrolysis,[15] the related β-hydroxyamide (*R**,*R**)-**3** displayed significantly improved stability in both mouse and human plasma, indicating that it may be suitable for pharmacological application (Figure 6a). We thus evaluated the phase-1 metabolism of (*R**,*R**)-**3** in mouse and human microsomes and observed by LC-MS analysis a dihydroxylation product as the major metabolite. This assignment was confirmed by chemical synthesis of the expected metabolite **9**, which exhibited an identical fragmentation pattern (see the Supporting Information, Figure S10). In vivo pharmacokinetics were performed by using a single dose of 0.42 mg (*R**,*R**)-**3** by intravenous (i.v.) administration in Balb/cOlaHsd mice. Rapid elimination with a half-life of $t_{1/2} = 7.7$ min was observed. Further studies, however, showed that intraperitoneal (i.p.) administration of 3.17 mg of (*R**,*R**)-**3** prolonged the elimination half-life to 4.3 h (Figure 6b). By using a repetitive dosing regimen (three times during 18 h), animals were tightly monitored for clinical symptoms during an explorative toxicity assessment and finally this delivery route was utilized to determine the efficacy of (*R**,*R**)-**3** in an in vivo *S. aureus* mouse abscess model by systemic (i.p.) compound administration. We induced dorsal skin abscesses by subcutaneous infection with MRSA strain USA 300 BAA 1717 in Crl:SKH1-Hr^{hr} hairless mice. To ensure optimal compound availability, we admin-

© 2016 Wiley-VCH Verlag GmbH & Co. KGaA, Weinheim

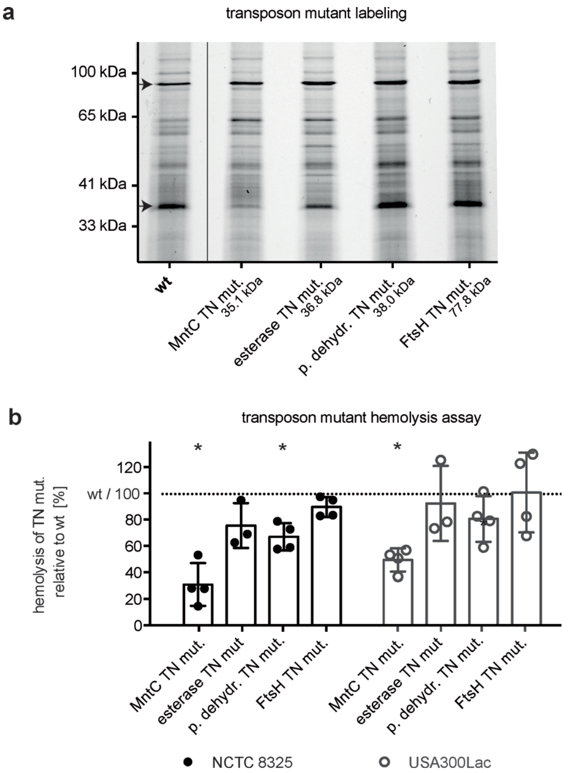

Figure 4. Validation of (R^*,R^*)-**3** targets. a) Labeling of NCTC 8325 wt and transposon mutants (TN mut.) with 50 μM (21.0 μg mL^{-1}) photo-probe (R^*,R^*)-**8**. b) Hemolysis assay of wild type (wt) and transposon mutants (TN mut.) in NCTC 8325 and USA 300 Lac background. * $p < 0.05$ (one sample t test); four biological replicates (three biological replicates for esterase TN mut.).

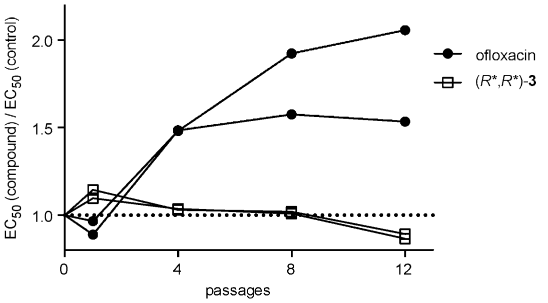

Figure 5. Resistance development assay with antihemolytic compound (R^*,R^*)-**3** (16 μM (5.2 μg mL^{-1})) and ofloxacin (3.5 μM (1.5 μg mL^{-1})). Relative EC_{50} values in hemolysis inhibition of (R^*,R^*)-**3** and growth inhibition of ofloxacin are plotted against the number of passages. Relative EC_{50}: EC_{50} of long-term compound treated bacteria/EC_{50} of long-term vehicle-treated bacteria (DMSO control for (R^*,R^*)-**3** or 0.1 N NaOH control for ofloxacin). The curves for two biological replicates are shown. An independent long-term experiment with compound (R^*,R^*)-**3** with no resistance development over 45 passages is shown in the Supporting Information (Figure S9).

istered the first dose of 3.17 mg (159 mg per kg body weight) (R^*,R^*)-**3** one hour prior to infection and repeated the same dosing six and 18 h after infection (Figure 6c). Abscess lesions were fully developed after one to two days in untreated mice. The necrotic areas were measured over the entire experimental duration for 13 days. The abscess size was significantly decreased to about 60% compared with abscesses obtained in vehicle treated control animals (Figure 6c).

Conclusions

The dramatic increase in bacterial resistance to commonly used antibiotics has been paralleled by a decrease in antibiotic drug development, leading to a poor prognosis for future treatment of infectious diseases. As current antibiotics address only a limited spectrum of essential targets such as cell wall biosynthesis, DNA replication and translation, viability-independent pathways that significantly limit bacterial pathogenesis represent attractive alternatives. Here, we present hydroxyamide (R^*,R^*)-**3** as a potent inhibitor of *S. aureus* virulence. The global reduction of toxin levels such as hla, enterotoxin SAE A-D, and TSST-1, suggests that (R^*,R^*)-**3** hits major target(s) that are responsible for virulence regulation. This observation was further validated by transcriptome analysis of hydroxyamide-treated *S. aureus* cells. Parallel down-regulation of common virulence associated transcriptional activators and up-regulation of the virulence repressor protein SarX was observed. Target identification revealed four protein hits. Among these, proline dehydrogenase and MntC revealed the most significant down-regulation of hemolysis in the NCTC 8325 strain. In fact, MntC is an essential component of the MntABC Mn^{2+} transport system, which consists of an ATP-binding protein (MntA), an integral membrane transporter (MntB), and the metal-binding lipoprotein (MntC).[38,39] A recent study demonstrated severe inhibition of murine systemic infection with a deletion of solely MntC in *S. aureus* USA 300.[40] However, *S. aureus* also encodes MntH, a second manganese uptake system related to the Nramp metal transport family. The individual contribution of both transporters to pathogenesis remains elusive.[41,42]

Future studies will thus investigate a putative synergistic role of other identified targets for the broad antivirulence mechanism. Given the inhibition of devastating toxin expression in various *S. aureus* isolates, the corresponding beneficial effect in a systemic mouse abscess model with an MRSA (USA 300) strain and the lack of resistance development in vitro, aromatic hydroxyamides represent promising starting points for antivirulence drug development.

Experimental Section

Phenotype assays: Bioactivity assays (inhibition of hemolysis, enterotoxins, and TSST) were performed with supernatants from *S. aureus* cultures grown for 20 h at 37 °C. Shortly thereafter, to monitor hemolysis, heparinized sheep blood was added and lysis of erythrocytes was monitored. Enterotoxin and toxic shock syndrome toxin levels in supernatants were determined by ELISA (Ridascreen from R-Biopharm and antibodies from Toxin Technology). Detection of α-hemolysin was performed by Western Blot analysis using ab50536 (Abcam) as the primary antibody. For the long-term resistance assay, cultures were passaged daily with an inoculum of each 3.4×10^4 colony-forming units. Animal experiments were performed with Balb/cOlaHsd (Harlan) and Crl:SKH1-Hr^{hr} (Charles River) mice.

© 2016 Wiley-VCH Verlag GmbH & Co. KGaA, Weinheim
These are not the final page numbers! ↗↗

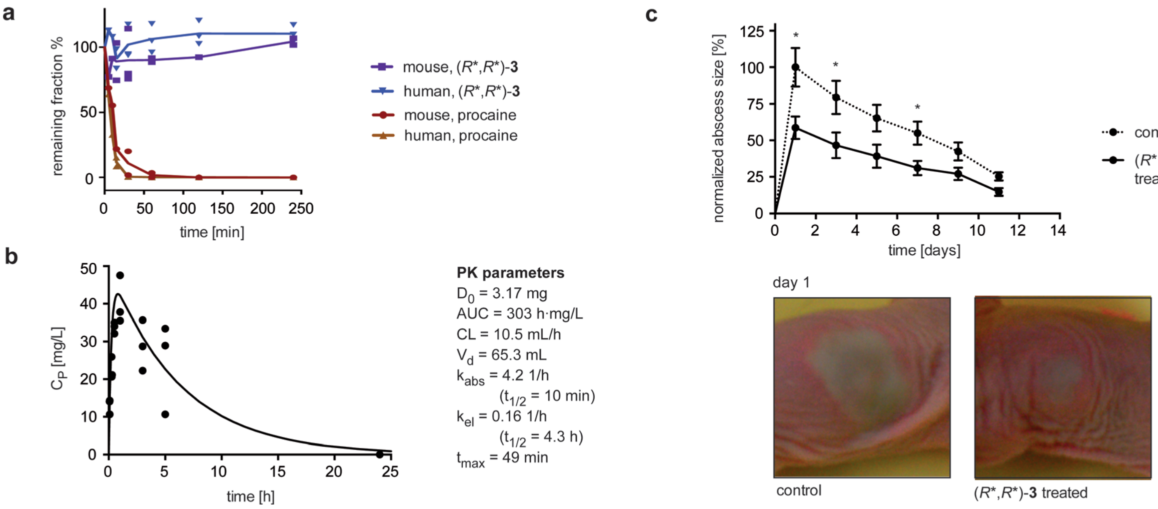

Figure 6. a) In vitro plasma levels of (*R**,*R**)-**3** remain stable for >4 h, whereas the positive control compound procaine is rapidly disintegrated. Three technical replicates are shown. b) In vivo pharmacokinetic parameters were determined following a single-dose i.p. injection of 3.17 mg (*R**,*R**)-**3** in corn oil. The group size comprised four mice ($n=4$) using three groups and an alternating blood withdrawal scheme. c) Systemic treatment of skin infections with compound (*R**,*R**)-**3** significantly ($^*p<0.05$) decreased the size of lesions induced by *S. aureus* USA 300 BAA-1717 (antihemolytic activity of (*R**,*R**)-**3** in this strain is shown in the Supporting Information, Figure S1 a). Graphs represent abscess sizes normalized to control animals at day one for control- and (*R**,*R**)-**3**-treated animals monitored over 13 days post-infection. All results are shown as mean values ±SEM for $n=32$ animals from four independent experiments. During the course of the experiments with *S. aureus* BAA-1717, six animals died prematurely (two control animals and four (*R**,*R**)-**3** treated animals).

Mode of action analysis: Transcriptome analysis was performed by RNA-seq analysis described by Dugar et al.[43] Target identification was performed with AfBPP[32] using photo-probes and quantitative dimethyl-labeling for mass-spectrometry, as previously described.[36] Validation experiments include functional studies of transposon mutants (Nebraska Transposon Mutant Library).

Conflict of interest: S. Sieber, T. Böttcher, K. Lorenz-Baath, O. Baron, V. Korotkov, F. Weinandy are named inventors on a patent ("Beta-O/S/N fatty acids and derivatives as anti-virulence drugs") related to this study. S. Sieber, O. Baron, T. Böttcher founded a company (AVIRU).

Acknowledgements

We thank the Network on Antimicrobial Resistance in *Staphylococcus aureus* (NARSA) for the supply of the Nebraska Transposon Mutant Library (NTML). Furthermore, we thank Professor Markus Gerhard for excellent scientific advice and the permission to perform animal experiments in his group at the Institute of Medical Microbiology, Immunology and Hygiene (Technische Universität München) as well as for the supply of clinical isolates. Animal studies were approved by the Government of Upper Bavaria under the accreditation number 55.2-1/54-2531-114/10. The work was funded by an ERC starting grant (250924-antibacterials) and by the Federal Ministry of Education and Research, Germany, FKZ: 031A131. The authors account for the content of the work. We would also like to thank Josef Schachtner for contribution to the synthesis of photoreactive chemical probes and Dr. Malte Gersch for an introduction to ABPP. Finally, we thank Ernst Bernges, Heike Hofmann, Mona Wolff, Burghard Cordes, and Katja Bäuml for excellent technical support.

Keywords: click chemistry · drug discovery · proteomics · medicinal chemistry · toxicology

[1] CDC Antibiotic resistance threats in the United States, U.S. Department of Health and Human Services, Centers for Disease Control and Prevention, **2013**.

[2] M. M. Mwangi, S. W. Wu, Y. Zhou, K. Sieradzki, H. de Lencastre, P. Richardson, D. Bruce, E. Rubin, E. Myers, E. D. Siggia, A. Tomasz, *Proc. Natl. Acad. Sci. USA* **2007**, *104*, 9451–9456.

[3] A. E. Clatworthy, E. Pierson, D. T. Hung, *Nat. Chem. Biol.* **2007**, *3*, 541–548.

[4] D. A. Rasko, V. Sperandio, *Nat. Rev. Drug Discovery* **2010**, *9*, 117–128.

[5] S. Ruer, N. Pinotsis, D. Steadman, G. Waksman, H. Remaut, *Chem. Biol. Drug Des.* **2015**, *86*, 379–399.

[6] D. T. Hung, E. A. Shakhnovich, E. Pierson, J. J. Mekalanos, *Science* **2005**, *310*, 670–674.

[7] D. A. Rasko, C. G. Moreira, D. R. Li, N. C. Reading, J. M. Ritchie, M. K. Waldor, N. Williams, R. Taussig, S. Wei, M. Roth, D. T. Hughes, J. F. Huntley, M. W. Fina, J. R. Falck, V. Sperandio, *Science* **2008**, *321*, 1078–1080.

[8] V. Khodaverdian, M. Pesho, B. Truitt, L. Bollinger, P. Patel, S. Nithianantham, G. Yu, E. Delaney, E. Jankowsky, M. Shoham, *Antimicrob. Agents Chemother.* **2013**, *57*, 3645–3652.

[9] F. Tang, W.-H. Li, X. Zhou, Y.-H. Liu, Z. Li, Y.-S. Tang, X. Kou, S.-D. Wang, M. Bao, L.-D. Qu, M. Li, B. Li, *Microb. Drug Resist.* **2014**, *20*, 357–363.

[10] R. C. Allen, R. Popat, S. P. Diggle, S. P. Brown, *Nat. Rev. Microbiol.* **2014**, *12*, 300–308.

[11] G. Y. Liu, A. Essex, J. T. Buchanan, V. Datta, H. M. Hoffman, J. F. Bastian, J. Fierer, V. Nizet, *J. Exp. Med.* **2005**, *202*, 209–215.

[12] C. I. Liu, G. Y. Liu, Y. Song, F. Yin, M. E. Hensler, W. Y. Jeng, V. Nizet, A. H. Wang, E. Oldfield, *Science* **2008**, *319*, 1391–1394.

[13] Y. Song, C. I. Liu, F. Y. Lin, J. H. No, M. Hensler, Y. L. Liu, W. Y. Jeng, J. Low, G. Y. Liu, V. Nizet, A. H. Wang, E. Oldfield, *J. Med. Chem.* **2009**, *52*, 3869–3880.

[14] J. Qiu, X. Niu, J. Dong, D. Wang, J. Wang, H. Li, M. Luo, S. Li, H. Feng, X. Deng, *J. Infect. Dis.* **2012**, *206*, 292–301.

[15] F. Weinandy, K. Lorenz-Baath, V. S. Korotkov, T. Bottcher, S. Sethi, T. Chakraborty, S. A. Sieber, *ChemMedChem* **2014**, *9*, 710–713.

© 2016 Wiley-VCH Verlag GmbH & Co. KGaA, Weinheim

[16] J. Zhang, H. Liu, K. Zhu, S. Gong, S. Dramsi, Y. T. Wang, J. Li, F. Chen, R. Zhang, L. Zhou, L. Lan, H. Jiang, O. Schneewind, C. Luo, C. G. Yang, *Proc. Natl. Acad. Sci. USA* **2014**, *111*, 13517 – 13522.
[17] M. Otto, *Expert Opin. Biol. Ther.* **2010**, *10*, 1049 – 1059.
[18] G. Y. C. Cheung, M. Otto, *Expert Opin. Ther. Targets* **2012**, *16*, 601 – 612.
[19] E. A. George, T. W. Muir, *ChemBioChem* **2007**, *8*, 847 – 855.
[20] R. P. Novick, *Mol. Microbiol.* **2003**, *48*, 1429 – 1449.
[21] E. A. George, R. P. Novick, T. W. Muir, *J. Am. Chem. Soc.* **2008**, *130*, 4914 – 4924.
[22] Y. Tal-Gan, D. M. Stacy, M. K. Foegen, D. W. Koenig, H. E. Blackwell, *J. Am. Chem. Soc.* **2013**, *135*, 7869 – 7882.
[23] E. J. Murray, R. C. Crowley, A. Truman, S. R. Clarke, J. A. Cottam, G. P. Jadhav, V. R. Steele, P. O'Shea, C. Lindholm, A. Cockayne, S. R. Chhabra, W. C. Chan, P. Williams, *J. Med. Chem.* **2014**, *57*, 2813 – 2819.
[24] Y. Chien, A. C. Manna, S. J. Projan, A. L. Cheung, *J. Biol. Chem.* **1999**, *274*, 37169 – 37176.
[25] A. C. Manna, A. L. Cheung, *J. Bacteriol.* **2006**, *188*, 4288 – 4299.
[26] T. Böttcher, S. A. Sieber, *J. Am. Chem. Soc.* **2008**, *130*, 14400 – 14401.
[27] E. Zeiler, V. S. Korotkov, K. Lorenz-Baath, T. Bottcher, S. A. Sieber, *Bioorg. Med. Chem.* **2012**, *20*, 583 – 591.
[28] S. W. Cho, D. Romo, *Org. Lett.* **2007**, *9*, 1537 – 1540.
[29] D. W. Huang, B. T. Sherman, R. A. Lempicki, *Nat. Protoc.* **2008**, *4*, 44 – 57.
[30] D. W. Huang, B. T. Sherman, R. A. Lempicki, *Nucleic Acids Res.* **2009**, *37*, 1 – 13.
[31] A. L. Cheung, A. S. Bayer, G. Zhang, H. Gresham, Y. Q. Xiong, *FEMS Immunol. Med. Microbiol.* **2004**, *40*, 1 – 9.
[32] M. J. Evans, B. F. Cravatt, *Chem. Rev.* **2006**, *106*, 3279 – 3301.
[33] R. Huisgen, *Proc. Chem. Soc.* **1961**, 357 – 396.
[34] V. V. Rostovtsev, L. G. Green, V. V. Fokin, K. B. Sharpless, *Angew. Chem. Int. Ed.* **2002**, *41*, 2596 – 2599; *Angew. Chem.* **2002**, *114*, 2708 – 2711.
[35] C. W. Tornøe, C. Christensen, M. Meldal, *J. Org. Chem.* **2002**, *67*, 3057 – 3064.
[36] J. L. Hsu, S. Y. Huang, N. H. Chow, S. H. Chen, *Anal. Chem.* **2003**, *75*, 6843 – 6852.
[37] *Uni*Prot, *Nucleic Acids Res.* **2015**, 43, D204 – D212.
[38] H. J. Tseng, Y. Srikhanta, A. G. McEwan, M. P. Jennings, *Mol. Microbiol.* **2001**, *40*, 1175 – 1186.
[39] K. M. Papp-Wallace, M. E. Maguire, *Annu. Rev. Microbiol.* **2006**, *60*, 187 – 209.
[40] B. A. Diep, Q. Phung, S. Date, D. Arnott, C. Bakalarski, M. Xu, G. Nakamura, D. L. Swem, M. K. Alexander, H. N. Le, T. T. Mai, M.-W. Tan, E. J. Brown, M. Nishiyama, *J. Infect. Dis.* **2014**, *209*, 1533 – 1541.
[41] M. J. Horsburgh, S. J. Wharton, A. G. Cox, E. Ingham, S. Peacock, S. J. Foster, *Mol. Microbiol.* **2002**, *44*, 1269 – 1286.
[42] T. E. Kehl-Fie, Y. Zhang, J. L. Moore, A. J. Farrand, M. I. Hood, S. Rathi, W. J. Chazin, R. M. Caprioli, E. P. Skaar, *Infect. Immun.* **2013**, *81*, 3395 – 3405.
[43] G. Dugar, A. Herbig, K. U. Forstner, N. Heidrich, R. Reinhardt, K. Nieselt, C. M. Sharma, *PLoS Genet.* **2013**, *9*, e1003495.

Received: October 5, 2015
Published online on ■■ ■■, 0000

© 2016 Wiley-VCH Verlag GmbH & Co. KGaA, Weinheim
These are not the final page numbers! ↗↗

FULL PAPER

Drug Discovery

*J. Vomacka, V. S. Korotkov, B. Bauer, F. Weinandy, M. H. Kunzmann, J. Krysiak, O. Baron, T. Böttcher, K. Lorenz-Baath, S. A. Sieber**

■■ – ■■

An Aromatic Hydroxyamide Attenuates Multiresistant *Staphylococcus aureus* Toxin Expression

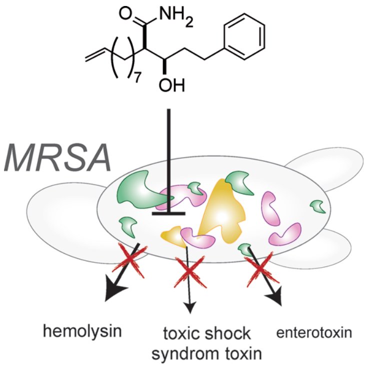

Disarming MRSA: A new hydroxyamide compound effectively reduces the expression of devastating toxins in various *S. aureus* and MRSA strains. The molecular mechanism was investigated by transcriptome analysis, as well as by affinity-based protein profiling. Systemic treatment with the hydroxyamide showed significant reduction of abscess sizes in an MRSA mouse skin infection model.

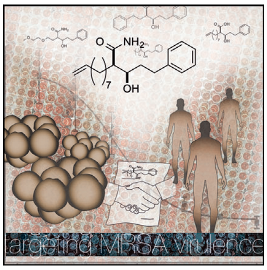

Anti-Virulence Strategy

The agreement depicted in the figure is between humans, who, instead of killing bacterial cells, just reduce their arsenal of virulence factors, and *S. aureus* which, as a reward, don't respond with resistance development. In their Full Paper on page ■■ ff., S. A. Sieber et al. report that the molecule represented in the middle and on the contract is one of the most powerful among a set of hydroxyamide derivatives to exhibit this remarkable bioactivity.

© 2016 Wiley-VCH Verlag GmbH & Co. KGaA, Weinheim

Supporting Information

An aromatic hydroxyamide attenuates multireststant *Staphylococcus aureus* toxin expression.

Jan Vomacka,[b] Vadim S. Korotkov,[b] Bianca Bauer,[b] Franziska Weinandy,[b] Martin H. Kunzmann,[a] Joanna Krysiak,[a] Oliver Baron,[c] Thomas Böttcher,[d] Katrin Lorenz-Baath[b] and Stephan A. Sieber*[a]

[a] Dr. Martin H. Kunzmann, Dr. Joanna Krysiak, Prof. Stephan A. Sieber
Department of Chemistry, Chair of Organic Chemistry II
Center for Integrated Protein Science (CIPSM), Institute of Advanced Studies (IAS), Technische Universität München (TUM)
Lichtenbergstrasse 4, D-85747 Garching, Germany
E-mail: stephan.sieber@tum.de
[b] Jan Vomacka, Dr. Vadim S. Korotkov, Dr. Bianca Bauer, Dr. Franziska Weinandy, Dr. Katrin Lorenz-Baath
Department of Chemistry
AVIRU, GO-Bio-project of the Federal Ministry of Education and Research, FKZ: 031A131, Technische Universität München (TUM)
Lichtenbergstrasse 4, D-85747 Garching, Germany
[c] Dr. Oliver Baron
Department of Chemistry
Center for Integrated Protein Science (CIPSM), Ludwig-Maximilians-Universität München (LMU)
Butenandtstrasse 5-13, D-81377 Munich, Germany
[d] Dr. Thomas Böttcher
Department of Chemistry
Universität Konstanz
Universitätsstrasse 10, D-78457 Konstanz, Germany

FIGURES

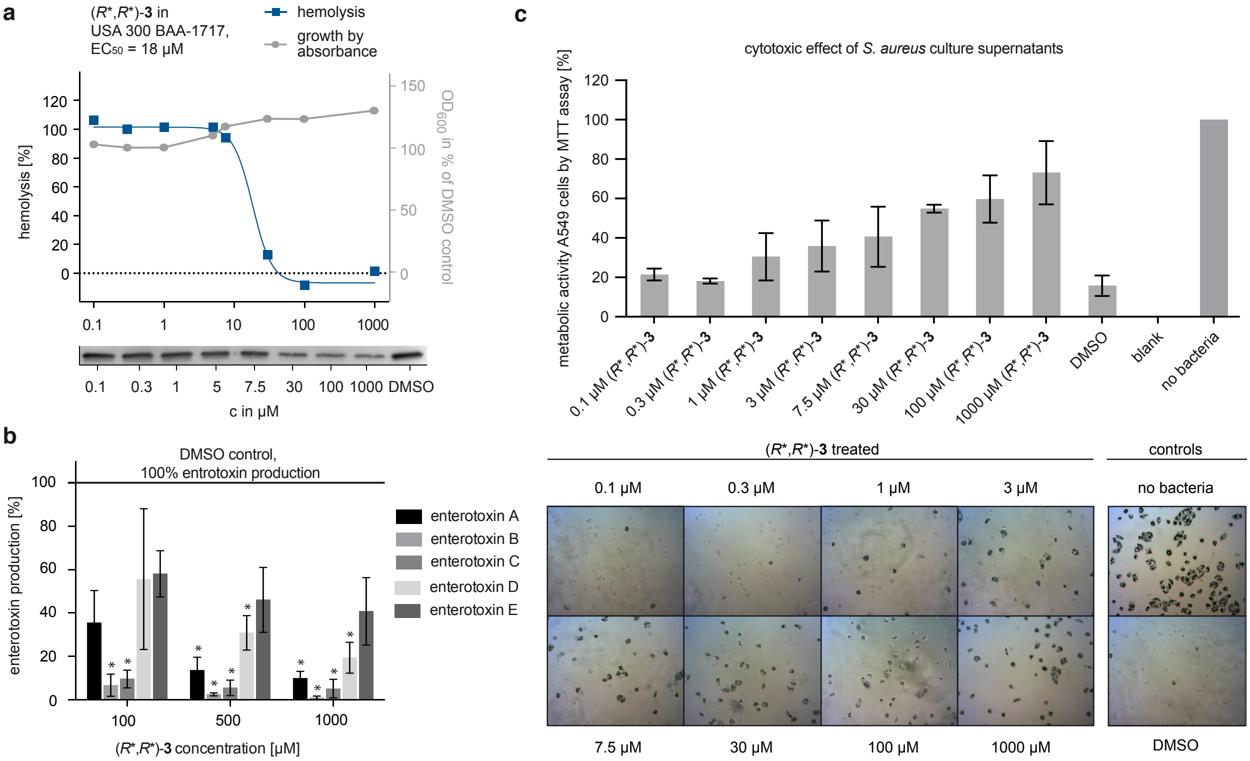

Figure S1. Anti-virulence activity of (*R**,*R**)-**3**. a) Hemolysis inhibition with (*R**,*R**)-**3** in *S. aureus* USA 300 BAA-1717. The mean value of three technical replicates is shown. These findings were further confirmed by western blot of hla in each 10 µl of bacterial supernatant (shown below). Growth is indicated by OD_{600} values in % of DMSO control. b) The reduced production of enterotoxins by *S. aureus* NCTC 8325 upon treatment with (*R**,*R**)-**3** was determined by sandwich ELISA (RIDASCREEN Set A,B,C,D,E). The mean value of three biological replicates ± SD is shown. (* significantly different to DMSO control; $p < 0.01$ (one sample t test)). c) The cytotoxic effect of *S. aureus* NCTC 8325 culture supernatants detected by MTT assay on the human lung carcinoma cell line A549 could be significantly reduced by treatment of NCTC 8325 (*R**,*R**)-**3**. Formazan formation from MTT by viable A549 cells is concentration dependently restored upon bacterial treatment with (*R**,*R**)-**3.** The mean value of three biological replicates ± SD and phase contrast microscopy is shown.

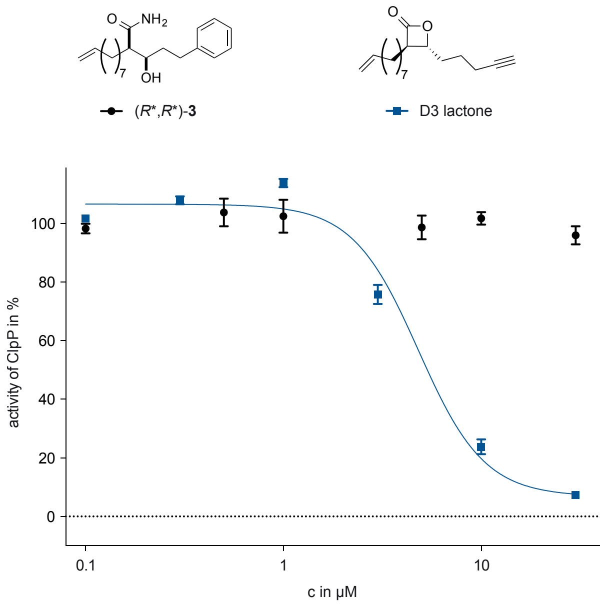

Figure S2. ClpP assay with (*R**,*R**)-**3**. Unlike the beta-lactones (shown by the example of D3 lactone [1]), compound (*R**,*R**)-**3** is unable to inhibit the peptidase activity of recombinant *S. aureus* ClpP. The results represent the mean value of three technical replicates ± SD.

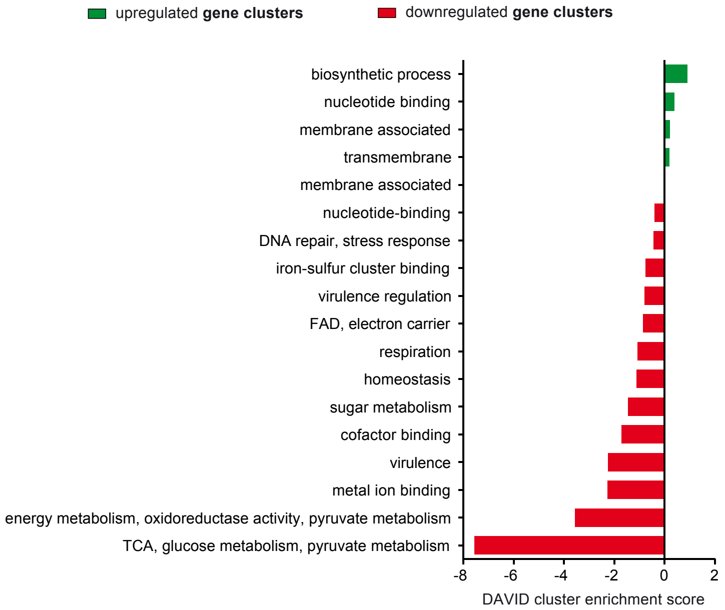

Figure S3. Next generation sequencing of NCTC 8325 cells treated with 100 µM (31.7 µg/mL) compound (*R**,*R**)-**3** compared to DMSO control. DAVID database enrichment score for gene clusters (positive enrichment score for clusters of upregulated genes and negative enrichment score for clusters of downregulated genes). See also the supporting transcriptome_analysis.xlsx file.

a

uniprot	protein	MW [kDa] (mass range: 81.6-91.6)	enrichment (by area: 8 / DMSO)	Score
Q2G1C9	Uncharacterized protein (blast: 3-hydroxyacyl-CoA dehydrogenase)	84.6	0.85	1051.42
Q2G0P5	ATP-dependent Clp protease ATP-binding subunit ClpC	91.0	0.89	144.58
Q2G1D8	Formate acetyltranferase	84.8	0.17	40.72
Q2G122	5-methyltetrahydropteroyltriglutamate--homocysteine methyltransferase	85.0	1.14	39.55
Q2FZ94	Penicillin-binding protein 1	82.7	infinite	8.89
Q2FZD8	Phenylalanin-tRNA synthetas, beta subunit	88.9	0.21	6.88
Q2FZD3	MutS2 protein	88.6	0.95	6.61

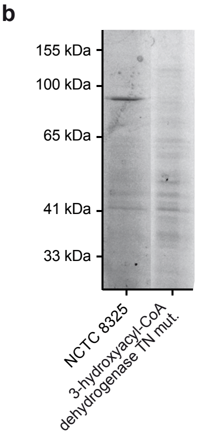

Figure S4. 3-Hydroxyacyl-CoA dehydrogenase is not a (*R**,*R**)-**3** virulence-related target. a) 3-Hydroxyacyl-CoA dehydrogenase was identified by score (Proteome Discoverer software) of in gel-based AfBPP experiments (one experiment, prominent band at 90 kDa). All protein hits in the mass range from 81.6 kDa to 91.6 kDa are shown. b) Labeling without avidin bead enrichment of NCTC 8325 wt and transposon mutants (TN mut.) with 50 µM (21.0 µg/mL) photoprobe (*R**,*R**)-**8** lacking a band at 90 kDa for the 3-hydroxyacyl-CoA dehydrogenase reductase transposon mutant. The 35 kDa band (MntC, Figure 3b) could not be observed without avidin bead enrichment suggesting that MntC is of lower abundance than 3-hydroxyacyl-CoA dehydrogenase reductase.

uniprot	protein	MW [kDa] (mass range: 29.4-39.4)	enrichment repl. 1 (by area: 8 / DMSO)	enrichment repl. 2 (by area: 8 / DMSO)	Score
Q2G2D8	ABC transporter, substrate-binding protein (MntC)	35.1	infinite	infinite	37.88
G2G0M5	Uncharacterized epimerase/dehydratase	36.0	3.21	1.97	118.45
Q2FVA3	D-lactate dehydrogenase, putative	34.8	13.43	not found	34.57
Q2FXZ9	UPF0365	35.2	9.57	not found	45.88
Q2G258	BirA bifunctional protein	37.0	1.61	not found	21.39
Q2FYG1	Glycerol-3-phosphate dehydrogenase [NAD(P)+]	36.0	not found	infinite	9.51

Figure S5. MntC was identified at „infinite“ enrichment (not detected in DMSO control) in two replicates with gel based AfBPP experiments (band at 35 kDa). All protein hits in the mass range from 29.4 kDa to 39.4 kDa are shown. Score refers to the Proteome Discoverer software score.

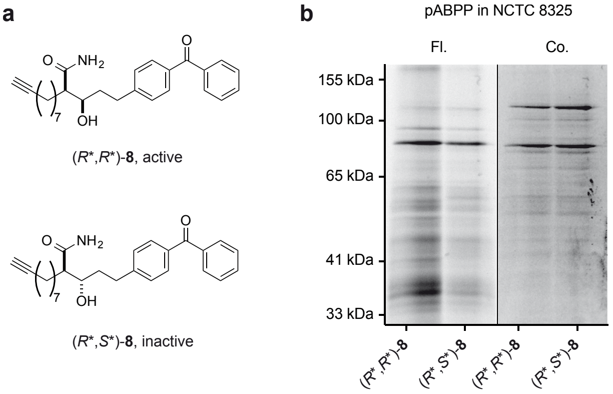

(*R**,*R**)-**8**, active

(*R**,*S**)-**8**, inactive

Figure S6. Photoreactive probes (*R**,*R**)-**8** and (*R**,*S**)-**8**. a) Active ((*R**,*R**)-**8**) and inactive ((*R**,*S**)-**8**) photoprobe used for gel-based and gel-free target identification. b) Affinity-based protein profiling with photoprobes (AfBPP) fluorescent labeling in NCTC 8325 with 50 µM (21.0 µg/mL) photoprobes (*R**,*R**)-**8** and (*R**,*S**)-**8** (Fl.) and the corresponding coomassie stained gel (Co.).

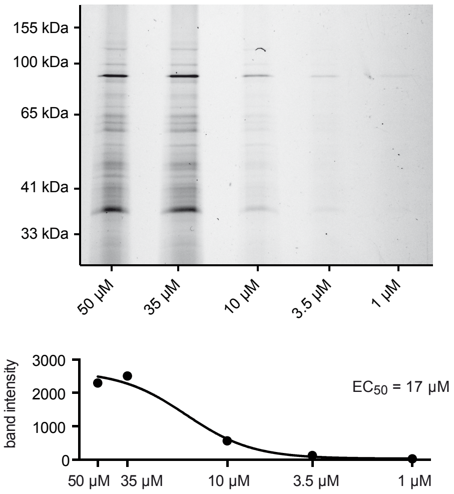

Figure S7. Concentration dependent AfBPP experiment in NCTC 8325 with photoprobe (*R**,*R**)-**8**. Quantification of the MntC band (35 kDa) was done with Gel Analyzer 2010 (Dr. Istvan Lazar). Concentrations in the quantification graph are plotted in logarithmic scale.

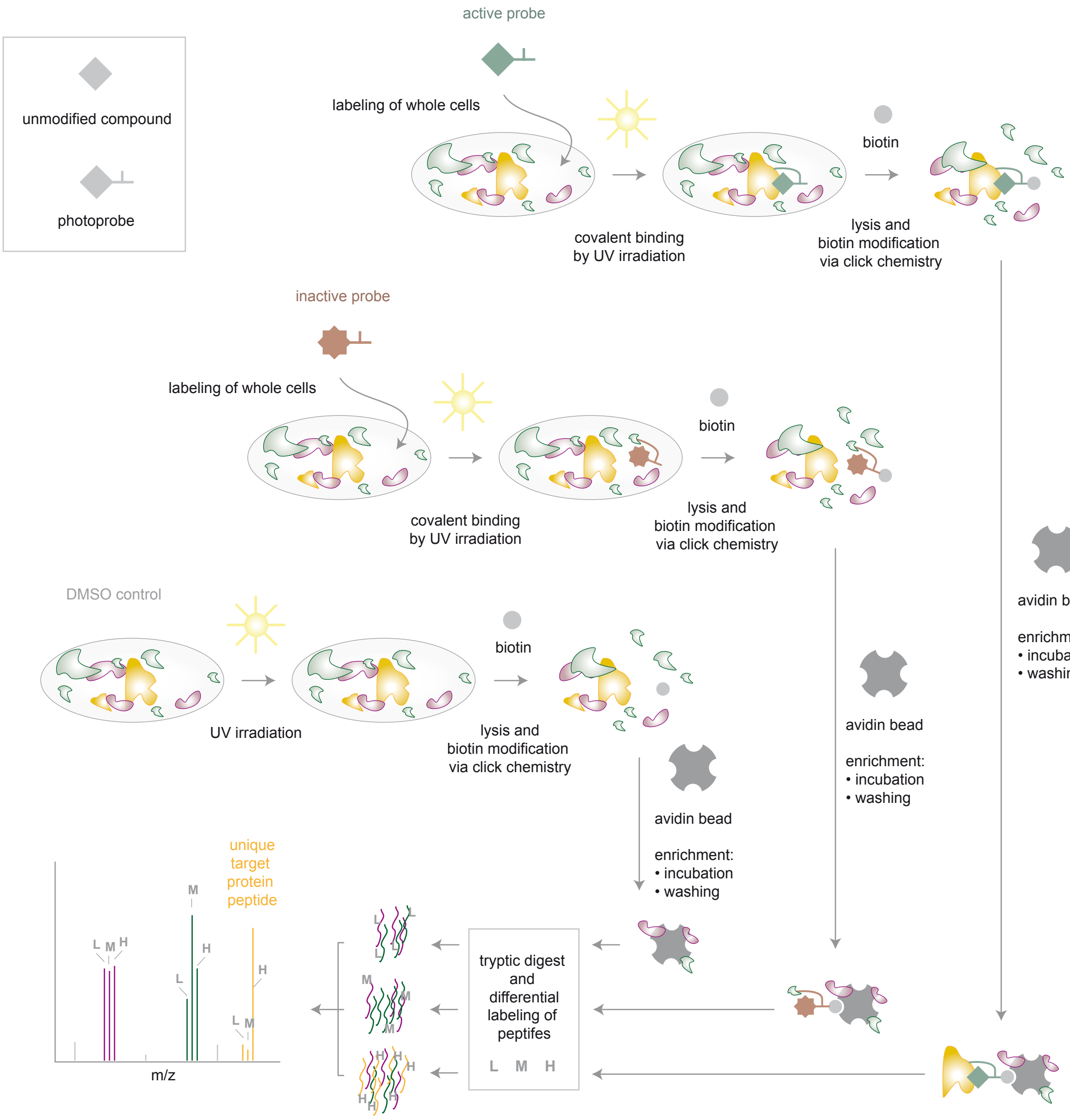
active probe
unmodified compound
photoprobe
labeling of whole cells
covalent binding by UV irradiation
biotin
lysis and biotin modification via click chemistry
inactive probe
labeling of whole cells
covalent binding by UV irradiation
biotin
lysis and biotin modification via click chemistry
DMSO control
UV irradiation
biotin
lysis and biotin modification via click chemistry
avidin bead
enrichment:
• incubation
• washing
avidin bead
enrichment:
• incubation
• washing
avidin bead
enrichment:
• incubation
• washing
tryptic digest and differential labeling of peptifes
L M H
unique target protein peptide
L M H
L H M
H L M
m/z

Figure S8. Gel-free target identification strategy: Cells are grown, labeled with a photoreactive probe and irradiated with UV light. Then bacterial cells are lysed and a fluorescent and/or biotin tag is attached via click reaction. After enrichment with avidin beads the proteins are digested, treated with dimethyl labeling reagents, mixed and analyzed via mass spectrometry.

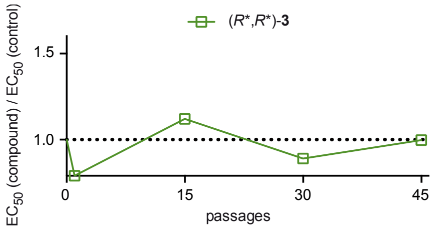

Figure S9. Long term resistance development assay with 16 µM (5.1 µg/mL) antihemolytic compound (R^*,R^*)-**3**. Relative EC$_{50}$: EC$_{50}$ of (R^*,R^*)-**3** on long-term compound treated bacteria / EC$_{50}$ of long-term DMSO control treated bacteria. One experiment is shown.

a

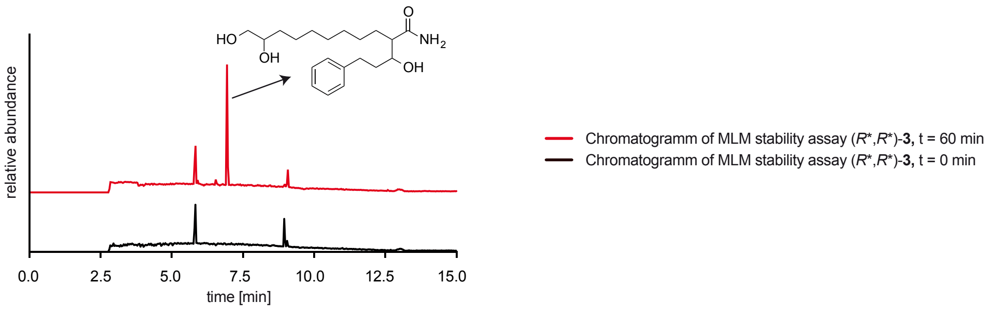
HO
OH
O
NH2
OH
relative abundance
0.0
2.5
5.0
7.5
10.0
12.5
15.0
time [min]
Chromatogramm of MLM stability assay (R*,R*)-3, t = 60 min
Chromatogramm of MLM stability assay (R*,R*)-3, t = 0 min

b

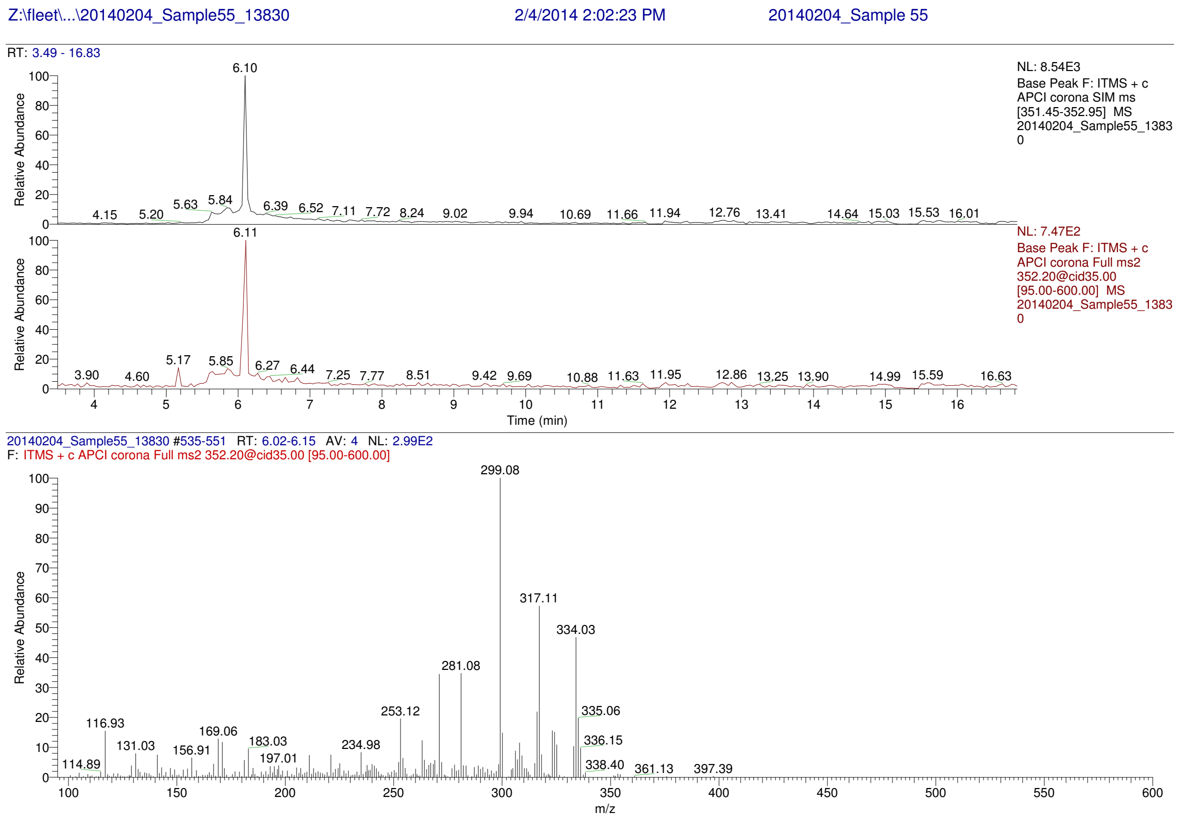
Z:\fleet\...\20140204_Sample55_13830
2/4/2014 2:02:23 PM
20140204_Sample 55
RT: 3.49 - 16.83
NL: 8.54E3
Base Peak F: ITMS + c APCI corona SIM ms [351.45-352.95] MS 20140204_Sample55_13830
Relative Abundance
100
80
60
40
20
0
6.10
4.15
5.20
5.63
5.84
6.39
6.52
7.11
7.72
8.24
9.02
9.94
10.69
11.66
11.94
12.76
13.41
14.64
15.03
15.53
16.01
NL: 7.47E2
Base Peak F: ITMS + c APCI corona Full ms2 352.20@cid35.00 [95.00-600.00] MS 20140204_Sample55_13830
6.11
3.90
4.60
5.17
5.85
6.27
6.44
7.25
7.77
8.51
9.42
9.69
10.88
11.63
11.95
12.86
13.25
13.90
14.99
15.59
16.63
4
5
6
7
8
9
10
11
12
13
14
15
16
Time (min)
20140204_Sample55_13830 #535-551 RT: 6.02-6.15 AV: 4 NL: 2.99E2
F: ITMS + c APCI corona Full ms2 352.20@cid35.00 [95.00-600.00]
Relative Abundance
100
90
80
70
60
50
40
30
20
10
0
299.08
317.11
334.03
281.08
253.12
335.06
336.15
338.40
361.13
397.39
234.98
197.01
183.03
169.06
156.91
131.03
116.93
114.89
100
150
200
250
300
350
400
450
500
550
600
m/z

c

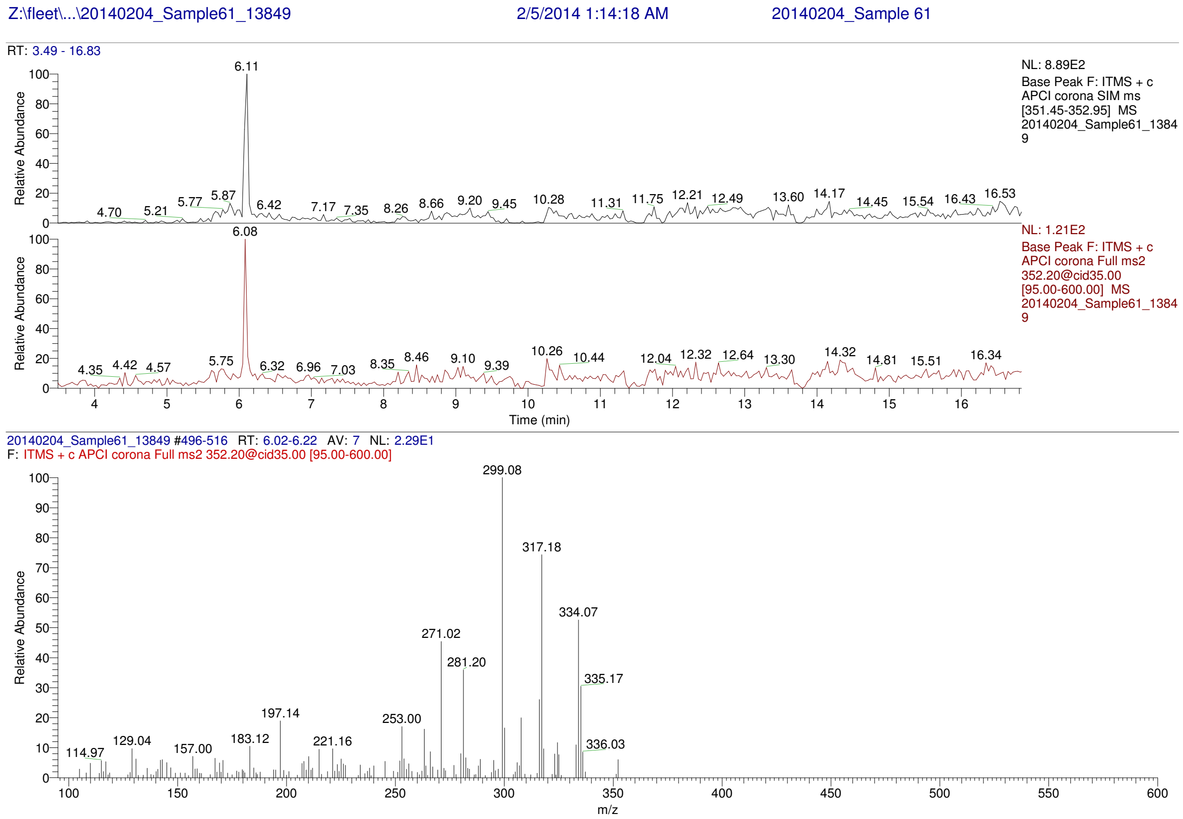

Figure S10. Metabolic stability. a) LC-MS Chromatogram of a phase-1 metabolic stability assay in microsomal preparations from mice at time points t = 0 and 60 min. The formation of one major metabolite is indicated. b) Microsomal preparation was incubated with (*R**,*R**)-**3** and precipitated with acetonitrile as described in materials and methods chapter 2.13. Subsequently, analysis by LC-MS revealed the presence of one major metabolite at retention time = 6.11 min which was further analyzed by CID fragmentation and displayed a characteristic fragmentation pattern of 6 major peaks. The correct molecular mass was determined by high-resolution mass spectrometry (HRMS-APCI) 452.2485 (m/z). The mass was predicted to correspond with 0.866 ppm mass accuracy to the formula $C_{20}H_{34}O_4N$, potentially corresponding to the dihydroxylation product of the terminal double bond with a calculated (m/z): 352.2482 [M+H]. c) Blanc microsomal preparation was quenched with acetonitrile as described before and spiked with the dihydroxylated derivative of (*R**,*R**)-**3** (**9**) which was synthetically prepared. Subsequent LC-MS analysis revealed the identical fragmentation pattern to the metabolite of (*R**,*R**)-**3** and therefore proved the identity of the metabolite.

MATERIALS AND METHODS

1 Synthesis

All reactions were carried out under argon in oven-dried glassware unless noted otherwise. All chemicals were of reagent grade or better and used without further purification. Chemicals and solvents were purchased from Sigma Aldrich. Solvents for chromatography and workup purposes were generally of reagent grade. In all reactions, temperatures were measured externally. ^{1}H NMR and ^{13}C spectra of small molecules were recorded on Bruker instruments (250 MHz, 360 MHz or 500 MHz) and referenced to the residual proton signal of the deuterated solvent. Carbon samples were referenced externally against the residual ^{13}C signal of $CDCl_3$. HR-MS-ESI spectra were recorded with a Thermo Scientific LTQ FT. HPLC purification was accomplished with a Waters 2545 quaternary gradient module, a XBridge™ prep C18 10 µm column (50×250 mm) and a Waters 2998 PDA detector.

4-(2-Methoxyethoxy)butanoic acid was synthesized from 2-(2-methoxyethoxy)ethyl iodide in close analogy to Taubitz et al. [2]

1.1 Synthesis of various substituted 3-hydroxyamides

Methyl 4-(2-methoxyethoxy)butanoate

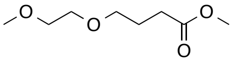

4-(2-Methoxyethoxy)butanoic acid (7.5 g, 46 mmol) was dissolved in MeOH (40 mL) at RT (room temperature) and 4 drops of H_2SO_4 were added to this solution. The reaction mixture was stirred for 6 h at RT. The reaction was quenched by $NaHCO_3$, and volatiles were distilled off under reduced pressure. EtOAc was added to the residue and the precipitate obtained was filtered off. The filtrate was concentrated under reduced pressure to give the desired product (5.3 g, 65 %). – ^{1}H NMR (250 MHz, $CDCl_3$) δ 3.66 (s, 3 H), 3.59–3.46 (m, 6 H), 3.37 (s, 3 H), 2.41 (t, J = 7.4 Hz, 2 H), 1.98 – 1.85 (m, 2 H).

S-Pyridin-2-yl 4-phenylbutanethioate.

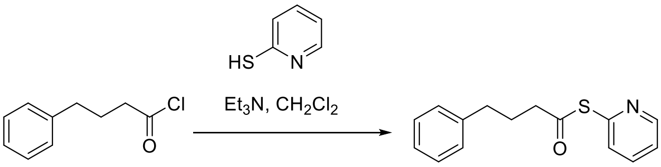

To a stirred solution of 2-pyridylmercaptane (6.6 g, 60 mmol) in CH_2Cl_2 (150 mL) was added 4-phenylbutanoyl chloride (10 g, 55 mmol) at 0 °C followed by Et_3N (18 mL). The solution was stirred for 3 h at RT, quenched with 1N HCl, phases were separated and the organic phase was washed with saturated $NaHCO_3$ solution and then dried over Na_2SO_4. Volatiles were removed under reduced pressure yielding a yellow oil that was purified by flash column chromatography. Yield: 13.6 g (96%). The spectral data are identical to the published ones.[2]

S-Pyridin-2-yl heptanethioate.

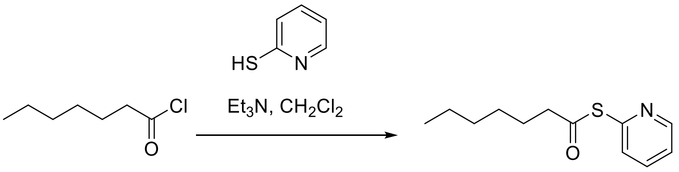

S-Pyridin-2-yl heptanethioate was obtained analogously to *S*-pyridin-2-yl 4-phenylbutanethioate starting from 2-pyridylmercaptane (8.9 g, 80 mmol), Et_3N (15 mL) and heptanoyl chloride (obtained from heptanoic acid (7.1 mL, 6.5 g, 50 mmol) oxalyl chloride (4.8 mL, 7.0 g, 55 mmol) and DMF (3 drops) in CH_2Cl_2 (150 mL)). The product was purified by column chromatography (eluent: hexane/EtOAc = 4/1). Yield: 9.7 g (87 %). – ^{1}H NMR (360 MHz, $CDCl_3$) δ 8.59–8.65 (m, 1 H), 7.69–7.78 (m, 1 H), 7.58–7.64 (m, 1 H), 7.24–7.31 (m, 1 H), 2.70 (t, J = 7 Hz, 2 H), 1.66–1.79 (m, 2 H), 1.22–1.44 (m, 6 H), 0.89 (t, *J* = 7 Hz, 3 H).– HRMS (ESI) calcd. for $C_{12}H_{18}NOS$ $[M+H]^+$ 224.1109, found 224.1103.

General procedure for the synthesis of ketene acetals (GP1).

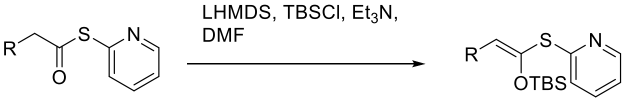

LHMDS (13 mL, 13 mmol, 1 M in THF) was placed in a flask cooled to -78 °C. DMF (1.7 mL) was added via syringe followed by Et_3N (3 mL, 21 mmol) and a solution of TBSCl (1.7 g, 11 mmol) in THF (7.5 mL) and thioester (10.8 mmol) in THF (20 mL). The solution was stirred 1 h at -78 °C and then let warm up to 0 °C over 1 h and quenched with H_2O. Phases were separated, the aqueous layer was extracted with EtOAc (3 x 20 mL) and the combined organic phases were dried over Na_2SO_4. The solvent was distilled off under reduced pressure and the residue was separated by column chromatography (eluent: hexane/EtOAc) to give a desired product.

(*E*)-2-((1-((tert-butyldimethylsilyl)oxy)undeca-1,10-dienyl)thio)pyridine

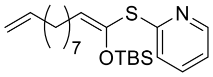

(*E*)-2-((1-((tert-butyldimethylsilyl)oxy)undeca-1,10-dienyl)thio)pyridine was obtained according to GP1 starting from LHMDS (13 mL, 13 mmol, 1 M in THF), DMF (1.7 mL), Et_3N (3 mL, 21 mmol), TBSCl (1.7 g, 11 mmol) and the corresponding thioester (3 g, 10.8 mmol) Yield: 3 g (71 %). Spectral data of the product are identical to those published in the literature.[3]

(*E*)-2-((1-((*tert*-butyldimethylsilyl)oxy)-4-phenylbut-1-enyl)thio)pyridine

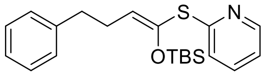

(*E*)-2-((1-((tert-butyldimethylsilyl)oxy)-4-phenylbut-1-enyl)thio)pyridine was obtained according to GP1 starting from LHMDS (20 mL, 20 mmol, 1 M in THF), DMF (2.6 mL), Et_3N (4.6 mL), TBSCl (3.0 g, 20 mmol) in THF (15 mL) and a solution of *S*-pyridin-2-yl 4-phenylbutanethioate (4.5 g, 17.5 mmol) in THF (30 mL). Yield: 1.2 g (18 %), R_f = 0.35 (hexane/EtOAc = 20/1). – ^{1}H NMR (360 MHz, *CDCl3*): δ 8.42–8.45 (m, 1 H), 7.49 (td, *J* = 8.9, 2.0 Hz, 1 H), 7.36–7.16 (m, 5 H), 7.09 (dt, *J* = 8.0, 0.7 Hz, 1 H), 7.00 (ddd, *J* = 4.8, 8.0, 0.7 Hz, 1 H), 5.43 (t, *J* = 7.3 Hz, 1 H), 2.77 (t, *J* = 7.3 Hz, 2 H), 2.56 (q, *J* = 7.3 Hz, 2 H), 0.89 (s, 9 H), 0.08 (s, 6 H) ppm. – ^{13}C NMR (91 MHz, *CDCl3*): δ 149.33, 141.58, 140.06, 136.50, 128.56, 128.32, 125.87, 122.73, 121.47, 119.59, 35.30, 28.32, 25.68, 18.09, -4.38. – HRMS (ESI) calcd. for $C_{21}H_{30}NOSSi$ $[M+H]^+$ 372.1817, found 372.1811.

(*E*)-2-((1-((*tert*-butyldimethylsilyl)oxy)-hept-1-enyl)thio)pyridine

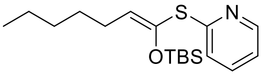

(*E*)-2-((1-((tert-butyldimethylsilyl)oxy)-hept-1-enyl)thio)pyridine was obtained according to GP1 starting from LHMDS (57 mL, 57 mmol, 1 M in THF), DMF (6 mL), Et_3N (10 mL), TBSCl (6.8 g, 45 mmol) in THF (30 mL) and a solution of *S*-pyridin-2-yl heptanethioate (8.4 g, 38 mmol) in THF (100 mL). Yield: 3.8 g (30 %). R_f = 0.31 (hexane/EtOAc = 20/1) – ^{1}H NMR (360 MHz, *CDCl₃*): δ 8.42 (d, *J* = 5 Hz, 1 H), 7.56 (td, *J* = 8, 2 Hz, 1 H), 7.35 (d, *J* = 8 Hz, 1 H), 7.01 (dd, *J* = 5, 8 Hz, 1 H), 5.41 (t, *J* = 7 Hz, 1 H), 2.20 (dt, *J* = 7, 7 Hz, 2 H), 1.24–1.46 (m, 6 H), 0.90–0.94 (m, 3 H), 0.89 (s, 9 H), 0.10 (s, 6 H) ppm. – ^{13}C NMR (91 MHz, *CDCl₃*): δ 160.6, 149.4, 139.3, 136.4, 124.1, 121.4, 119.6, 31.6, 28.8, 26.8, 25.7, 22.5, 18.1, 14.1, -4.4. – HRMS (ESI) calcd. for $C_{18}H_{32}NOSSi$ $[M+H]^+$ 338.1974, found 338.1961.

General procedure for the synthesis of trans-β-lactones (GP2).

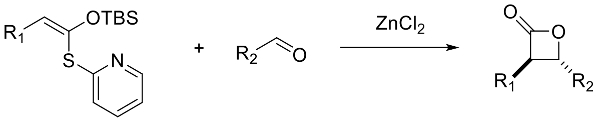

To the suspension of freshly fused $ZnCl_2$ (0.72 g, 5.4 mmol) in CH_2Cl_2 (18 mL) was added a solution of corresponding aldehyde (2.7 mmol) in CH_2Cl_2 (5 mL) followed by corresponding ketene acetal (3.8 mmol). The reaction mixture was stirred for 4 days. Then the reaction was quenched with H_2O and the organic phase was separated and dried over Na_2SO_4. The solvent was distilled off under reduced pressure and the residue was separated by column chromatography (eluent: hexane/EtOAc = 20/1), yielding the desired product.

(3*R**,4*R**)-3-(8-Nonenyl)-4-(2-phenylethyl)oxetan-2-one (**1**)

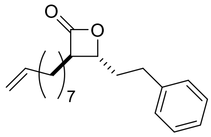

(3*R**,4*R**)-3-(8-Nonenyl)-4-(2-phenylethyl)oxetan-2-one was obtained according to GP2 starting from freshly fused $ZnCl_2$ (0.72 g, 5.4 mmol), 3-phenylpropanal (0.37 g, 2.7 mmol) in CH_2Cl_2 (5 mL) and (*E*)-2-((1-((*tert*-butyldimethylsilyl)oxy)undeca-1,10-dienyl)thio)pyridine (1.5 g, 3.8 mmol). Yield: 0.36 g (45 %). ^{1}H, ^{13}C – NMR and mass-spectra are identical to the previously published data.[3-4]

(3*R**,4*R**)-3-Pentyl-4-(2-phenylethyl)oxetan-2-one

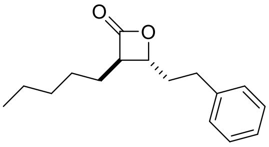

(3*R**,4*R**)-3-Pentyl-4-(2-phenylethyl)oxetan-2-one was obtained according to GP2 starting from freshly fused $ZnCl_2$ (2.1 g, 16 mmol), 3-phenylpropanal (1.1 g, 8 mmol) in CH_2Cl_2 (70 mL) and (*E*)-2-((1-((*tert*-butyldimethylsilyl)oxy)-hept-1-enyl)thio)pyridine (3.8 g, 11.3 mmol). Yield: 1.2 g (43 %). – ^{1}H NMR (360 MHz, *CDCl₃*): δ 7.20–7.36 (m, 5 H), 4.25 (ddd, *J* = 8, 4, 6 Hz, 1 H), 3.20 (ddd, *J* = 8, 7, 4 Hz, 1 H), 2.68–2.91 (m, 2 H), 2.03–2.26 (m, 2 H), 1.62–1.86 (m, 2 H), 1.24–1.50 (m, 6 H), 0.91 (t, *J* = 7 Hz, 3 H) ppm. – ^{13}C NMR (91 MHz, *CDCl₃*): δ 171.35, 140.19, 128.64, 128.34, 126.39, 77.13, 56.28, 36.15, 31.40, 31.35, 27.72, 26.58, 22.33, 13.93. – IR (film) *v* = 2954 cm^{-1}, 2929, 2858, 1815, 1496, 1455, 1114, 699.– HRMS (ESI) calcd. for $C_{16}H_{23}O_2$ [M+H]$^+$ 247.1698, found 247.1697.

(3*R**,4*R**)-3,4-Di(2-phenylethyl)oxetan-2-one

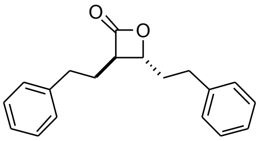

(3*R**,4*R**)-3,4-Di(2-phenylethyl)oxetan-2-one was obtained according to GP2 starting from freshly fused $ZnCl_2$ (0.6 g, 4.5 mmol), 3-phenylpropanal (0.4 g, 3 mmol) in CH_2Cl_2 (10 mL) and (*E*)-2-((1-((*tert*-butyldimethylsilyl)oxy)-4-phenylbut-1-enyl)thio)pyridine (1.7 g, 4.5 mmol). Yield: 120 mg (15 %). – ^{1}H NMR (360 MHz, *CDCl$_3$*): δ 7.40–7.12 (m, 10 H), 4.19 (ddd, *J* = 8.5, 4.9, 4.0 Hz, 1 H), 3.19 (ddd, *J* = 8.5, 6.9, 4.0 Hz, 1 H), 2.90–2.60 (m, 4 H), 2.25–1.90 (m, 4 H) ppm. – ^{13}C NMR (91 MHz, *CDCl$_3$*): δ 171.18, 140.14, 140.11, 128.65, 128.64, 128.43, 128.36, 126.48, 126.39, 77.43, 55.42, 35.95, 33.04, 31.34, 29.47. – IR (film) *v* = 2925 cm^{-1}, 1816, 1496, 1454, 1120, 837, 749. – HRMS (APCI) calcd. for $C_{19}H_{21}O_2$ [M+H]$^+$ 281.1541, found 281.1534.

(3*R**,4*R**)-4-(8-Nonenyl)-3-(2-phenylethyl)oxetan-2-one

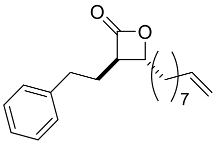

(3*R**,4*R**)-4-(8-Nonenyl)-3-(2-phenylethyl)oxetan-2-one was obtained according to GP2 starting from freshly fused $ZnCl_2$ (0.75 g, 5.6 mmol), 9-decenal (0.69 g, 4.5 mmol) in CH_2Cl_2 (15 mL) and (*E*)-2-((1-((tert-butyldimethylsilyl)oxy)-4-phenylbut-1-enyl)thio)pyridine (2.1 g, 5.6 mmol). Yield: 0.30 g (22 %). – ^{1}H NMR (360 MHz, *CDCl$_3$*): δ 7.13–7.36 (m, 5 H), 5.77–5.89 (m, 1 H), 4.93–5.05 (m, 2 H), 4.20 (ddd, *J* = 8, 4, 6 Hz, 1 H), 3.19 (ddd, *J* = 8, 7, 4 Hz, 1 H), 2.70–2.90 (m, 2 H), 2.00–2.26 (m, 4 H), 1.55–1.85 (m, 2 H), 1.24–1.45 (m, 10 H) ppm. – ^{13}C NMR (91 MHz, *CDCl$_3$*): δ 171.39, 140.24, 139.06, 128.63, 128.41, 126.45, 114.26, 78.38, 55.32, 34.25, 33.74, 33.07, 29.61, 29.21, 29.10, 28.92, 28.83, 24.99. – IR (film) *v* = 2926 cm^{-1}, 2858, 1816, 1497, 1455, 1115, 909, 700.– HRMS (APCI) calcd. for $C_{20}H_{29}O_2$ [M+H]$^+$ 301.2168, found 301.2163.

General procedure for the formation of aldol products (GP3)

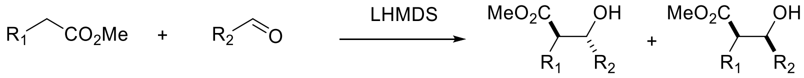

LHMDS (30 mL, 30 mmol, 1 M in THF) was placed in a flask under Ar and cooled to – 78 °C. A solution of the ester (26.3 mmol) in THF (15 mL) was added dropwise. The reaction was stirred for 40 min at – 78 °C and for 10 min at RT The reaction mixture was again cooled down to – 78 °C and the solution of the corresponding aldehyde (25 mmol) in THF (15 mL) was added dropwise. After 4 h at this temperature the reaction was quenched by addition of saturated NH_4Cl solution. The phases were separated and the aqueous layer was extracted with EtOAc three times. The combined organic phases were dried over Na_2SO_4, filtered and concentrated in vacuo. The products were isolated by column chromatography (eluent: hexane/EtOAc = 20/1).

Methyl 3-hydroxy-2-(non-8-enyl)-5-phenylpentanoate

Methyl 3-hydroxy-2-(non-8-enyl)-5-phenylpentanoate was obtained according to GP3 from LHMDS (30 mL, 30 mmol, 1 M solution in THF), methyl undec-10-enoate (5.2 g, 4.5 mmol) and 3-phenylpropanal (3.4 g, 25 mmol) as a mixture of two diastereomers which were separated by column chromatography (eluent: hexane/EtOAc = 20/1).

Diastereomeric aldol products can be differentiated by their ^{1}H-NMR spectra. (*R**,*R**)-products have a *H*C-3 signal at approx. 3.7 ppm whereas in case of (*R**,*S**)-diastereomers corresponding signals are situated at approx. 3.8 ppm. In order to verify their stereoconfiguration they were converted into corresponding diastereomeric 3-hydroxyamides. Comparison of their ^{1}H-NMR spectra with that of (*R**,*R**)-3-hydroxyamide **3** obtained from *trans*-β-lactone **1** allowed us to confirm the stereoconfiguration of aldol products.

Methyl (2*S**, 3*R**)-3-hydroxy-2-(non-8-enyl)-5-phenylpentanoate

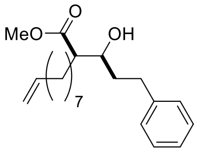

Yield: 3.5 g (42 %), R_f = 0.38 (hexane/EtOAc = 10/1). ^{1}H, ^{13}C – NMR and mass-spectra are identical to the previously published data.[1]

Methyl (2*R**, 3*R**)-3-hydroxy-2-(non-8-enyl)-5-phenylpentanoate

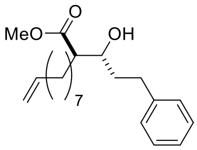

Yield: 0.75 g (9 %), R_f = 0.31 (hexane/EtOAc = 10/1). ^{1}H, ^{13}C – NMR and mass-spectra are identical to the previously published data.[1]

Methyl 3-hydroxy-2-(2-(2-methoxyethoxy)ethyl)-5-phenylpentanoate

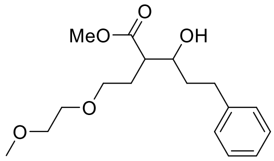

Methyl 3-hydroxy-2-(2-(2-methoxyethoxy)ethyl)-5-phenylpentanoate was obtained according to GP3 from LHMDS (22 mL, 22 mmol, 1 M solution in THF), methyl 4-(2-methoxyethoxy)butanoate (3.3 g, 18.9 mmol) and 3-phenylpropanal (2.6 g, 20 mmol) as a mixture of two diastereomers (55:45). Yield: 2.2 g (38 %), column chromatography (eluent: hexane/EtOAc = 1/1). – ^{1}H NMR (250 MHz, *CDCl₃*): δ 7.32–7.16 (m, 5 H), 3.93–3.82 (m, 0.45 H), 3.78–3.68 (m, 0.55 H), 3.70 (s, 1.35 H), 3.69 (s, 1.65), 3.60–3.44 (m, 6H), 3.372 (s, 1.65 H), 3.371 (s, 1.35), 2.95–2.78 (m, 1 H), 2.74–2.58 (m, 2 H), 2.10–1.70 (m, 4 H) ppm. – HRMS (ESI) calcd. for $C_{17}H_{27}O_5$ $[M+H]^+$ 311.1850, found 311.1859.

General procedure for hydrolysis of 3-hydroxyesters (GP4)

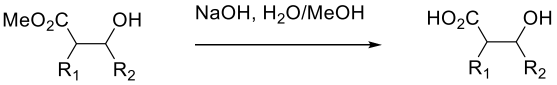

3-Hydroxyester (0.4 mmol) was dissolved in MeOH (12 mL) and aq. NaOH (4 mL, 4 mmol, 1 N) was added to this solution. The reaction mixture was stirred for 18 h at RT. MeOH was evaporated under reduced pressure and the residue was subsequently neutralized by addition of conc. HCl. The solvent was evaporated to dryness *in vacuo* and the solid residue was dissolved in EtOAc and dried over Na_2SO_4. The solution was filtered and the volatiles were evaporated under reduced pressure yielding the crude acid that was used further without further purification.

(2*S**, 3*R**)-3-Hydroxy-2-(non-8-enyl)-5-phenylpentanoic acid

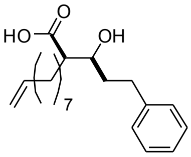

(2*S**, 3*R**)-3-Hydroxy-2-(non-8-enyl)-5-phenylpentanoic acid was obtained according to GP4 from methyl (2*S**, 3*R**)-3-hydroxy-2-(non-8-enyl)-5-phenylpentanoate (350 mg, 1.05 mmol) and NaOH (420 mg, 10.5 mmol) in a mixture of MeOH (24 mL) and H_2O (8 mL). The product was used without any further purification. Yield: 110 mg (33 %). – ^{1}H NMR (250 MHz, *CDCl₃*): δ 7.32–7.16 (m, 5 H), 5.81 (ddt, *J* = 16.9, 10.1, 6.7 Hz, 1 H), 5.04–4.88 (m, 2 H), 3.88 (dt, *J* = 8.5, 4.2 Hz, 1 H), 2.96–2.80 (m, 1 H), 2.75–2.60 (m, 1 H), 2.50 (dt, *J* = 9.1, 4.4 Hz, 1 H), 2.08–1.96 (m, 2 H), 1.92–1.48 (m, 4 H), 1.42 – 1.18 (m, 10 H) ppm.

(2*R**, 3*R**)-3-Hydroxy-2-(non-8-enyl)-5-phenylpentanoic acid (**2**)

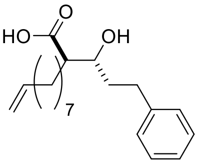

(2*R**, 3*R**)-3-Hydroxy-2-(non-8-enyl)-5-phenylpentanoic acid was obtained according to GP4 from methyl (2*R**, 3*R**)-3-hydroxy-2-(non-8-enyl)-5-phenylpentanoate (350 mg, 1.05 mmol) and NaOH (420 mg, 10.5 mmol) in a mixture of MeOH (24 mL) and H_2O (8 mL). The product was used without any further purification. Yield: 260 mg (78 %). – ^{1}H NMR (250 MHz, *CDCl₃*): δ 7.33–7.16 (m, 5 H), 5.81 (ddt, *J* = 16.9, 10.1, 6.7 Hz, 1 H), 5.04–4.88 (m, 2 H), 3.79–3.68 (m, 1 H), 2.94–2.78 (m, 1 H), 2.78–2.60 (m, 1 H), 2.54–2.40 (m, 1 H), 2.08–1.96 (m, 2 H), 1.92–1.48 (m, 4 H), 1.42 – 1.18 (m, 10 H) ppm.

3-Hydroxy-2-(2-(2-methoxyethoxy)ethyl)-5-phenylpentanoic acid

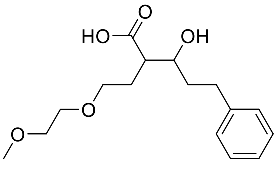

3-Hydroxy-2-(2-(2-methoxyethoxy)ethyl)-5-phenylpentanoic acid was obtained according to GP4 from methyl 3-hydroxy-2-(2-(2-methoxyethoxy)ethyl)-5-phenylpentanoate (2.2 g, 7.1 mmol) and NaOH (2.8 g, 71 mmol) in a mixture of MeOH (100 mL) and H_2O (35 mL). The product was used without any further purification. Yield: 2.0 g (99 %).

General procedure for amidation of 3-hydroxyacids (GP5)

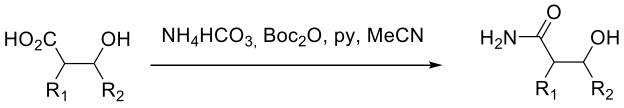

3-Hydroxyacid (1.2 mmol) was dissolved in CH_3CN (18 mL). Ammonium bicarbonate (284 mg, 3.6 mmol) and di-*tert*-butyl dicarbonate (872 mg, 4.0 mmol) were added followed by pyridine (0.3 mL). The resction mixture was stirred for 18 h, and the volatiles were removed in vacuo. The residue was separated by column chromatography (eluent: CH_2Cl_2/MeOH = 30/1) yielding the desired product. Products were additionally purified by preparative HPLC.

General Procedure for the preparation of 3-hydroxyamides from β-lactones (variant A, GP6A)

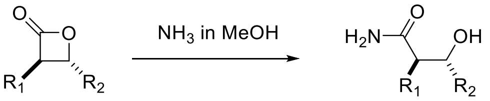

A solution of NH_3 (7 mL, 7 N in MeOH) was added to the corresponding *trans*-lactone (1.4 mmol). The reaction mixture was stirred for 18 h at RT Volatiles were removed under reduced pressure and the crude product was isolated by column chromatography (eluent: CH_2Cl_2 / MeOH = 30/1). Some products were additionally purified by preparative HPLC.

General Procedure for the preparation of 3-hydroxyamides from β-lactones (variant B, GP6B)

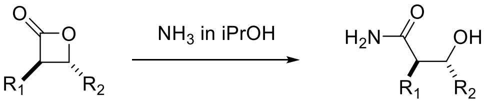

A solution of NH_3 (30 mL, 2 N in *i*PrOH) was added to the corresponding *trans*-β-lactone (3.1 mmol). The reaction mixture was stirred for 72 h at RT Volatiles were removed under reduced pressure and the crude product was isolated by column chromatography (eluent: CH_2Cl_2/MeOH = 30/1). Some products were additionally purified by preparative HPLC.

(2*R**,3*R**)-3-Hydroxy-2-(non-8-enyl)-5-phenylpentanamide ((*R**,*R**)-**3**)

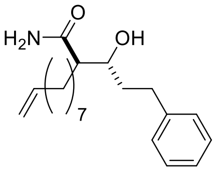

(2*R**,3*R**)-3-Hydroxy-2-(non-8-enyl)-4-phenylpentanamide was obtained according to GP6B from (3*R**,4*R**)-3-(8-nonenyl)-4-(2-phenylethyl)oxetan-2-one (1.8 g, 6 mmol) and ammonia (15 mL, 30 mmol, 2N solution in iPrOH). The product was additionally purified by preparative HPLC. Yield: 1.3 g (68 %). ^{1}H NMR (500 MHz, $CDCl_3$): δ 7.34–7.27 (m, 2 H), 7.23 – 7.16 (m, 3 H), 5.92 – 5.86 (br m, 2 H), 5.82 (ddt, *J* = 16.9, 10.1, 6.7 Hz, 1 H), 5.03 – 4.89 (m, 2H), 3.73–3.66 (m, 1H), 3.52 – 3.40 (br m, 1 H), 2.89 (ddd, *J* = 13.6, 8.8, 5.6 Hz, 1 H), 2.74–2.66 (m, 1 H), 2.16 (dt, *J* = 9.1, 5.0 Hz, 1H), 2.07 – 2.01 (m, 2H), 1.90 – 1.74 (m, 3H), 1.67 – 1.58 (m, 1H), 1.44 - 1.24 (m, 10H). ^{13}C NMR (125 MHz, $CDCl_3$): δ 178.11, 141.91, 139.18, 128.52, 128.46, 125.93, 114.22, 71.77, 51.64, 37.73, 33.80, 32.38, 30.40, 29.60, 29.33, 29.07, 28.89, 27.56. ESI-MS (m/z): 318.2425 [M+H], calcd for: $C_{20}H_{32}NO_2$: 318.2433.

(2*R**,3*S**)-3-Hydroxy-2-(non-8-enyl)-5-phenylpentanamide ((*R**,*S**)-**3**)

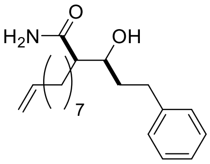

(2*R**,3*S**)-3-Hydroxy-2-(non-8-enyl)-4-phenylpentanamide was obtained according to GP5 from (2*R**,3*S**)-3-hydroxy-2-(non-8-enyl)-4-phenylpentanoic acid (110 mg, 0.35 mmol), NH_4HCO_3 (87 mg, 1.1 mmol), di-*tert*-butyl dicarbonate (330 mg, 1.5 mmol) and pyridine (0.1 mL) in acetonitrile (6 mL). The product was purified by column chromatography (eluent: CH_2Cl_2/MeOH = 30/1) and finally by preparative HPLC. Yield: 34 mg (31 %), R_f = 0.31 (CH_2Cl_2/MeOH = 30/1). ^{1}H NMR (360 MHz, $CDCl_3$): δ 7.35 – 7.15 (m, 5 H), 5.81 (ddt, *J* = 16.9, 10.1, 6.7 Hz, 1 H), 5.72 (s, 1H), 5.50 (s, 1 H), 5.05 – 4.90 (m, 2H), 3.87 (dt, *J* = 9.4, 3.3 Hz, 1H), 3.02 (s, 1 H), 2.88 (ddd, *J* = 13.8, 9.5, 5.3 Hz, 1H), 2.73–2.62 (m, 1H), 2.21 (dt, *J* = 10.2, 3.7 Hz, 1H), 2.09 – 2.01 (m, 2H), 1.99 - 1.82 (m, 1H), 1.80 – 1.67 (m, 2H), 1.58 – 1.45 (m, 1H), 1.45 - 1.20 (m, 10H). ^{13}C NMR (91 MHz, $CDCl_3$): δ 177.68, 141.71, 139.11, 128.47, 125.97, 114.16, 71.54, 51.34, 35.67, 35.36, 33.74, 32.43, 29.67, 29.28, 29.03, 28.87, 27.90, 26.34. ESI-MS (m/z): 318.2431 [M+H], calcd for: $C_{20}H_{32}NO_2$: 318.2433.

(2*R**,3*R**)-3-Hydroxy-2-(2-phenylethyl)-5-phenylpentanamide (**6**)

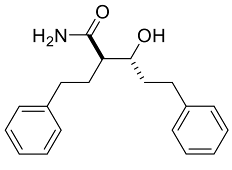

(2*R**,3*R**)-3-Hydroxy-2-(2-phenylethyl)-5-phenylpentanamide was synthesized according to GP6A starting from (3*R**,4*R**)-3,4-bis-(2-phenylethyl)-oxetan-2-one (57 mg, 0.2 mmol) and solution of NH_3 (4 mL, 7 N in MeOH). After purification by column chromatography the product was additionally purified by HPLC. Yield: 23 mg (39 %).

^{1}H NMR (360 MHz, $CDCl_3$): δ 7.32–7.17 (m, 10H), 5.61 (s, 1H), 5.42 (s, 1H), 3.77 – 3.69 (m, 1H), 3.13 (d, *J* = 7.5 Hz, 1H), 2.92 – 2.82 (m, 1H), 2.79 – 2.60 (m, 3H), 2.23 – 2.10 (m, 2H), 2.05 – 1.73 (m, 3H). ESI-MS (m/z): 298.1806 [M+H], calcd for: $C_{19}H_{24}NO_2$: 298.1807.

(2*R**,3*R**)-3-Hydroxy-2-(2-phenylethyl)-dodec-11-enamide (**4**)

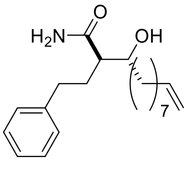

(2*R**,3*R**)-3-Hydroxy-2-(2-phenylethyl)-dodec-11-enamide was synthesized according to GP6A starting from (3*R**,4*R**)-4-(non-8-enyl)-3-(2-phenylethyl)oxetan-2-one (166 mg, 0.55 mmol) and solution of NH_3 (10 mL, 7 N in MeOH). After purification by column chromatography the product was additionally purified by HPLC. Yield: (59.2 mg, 34 %).

^{1}H NMR (360 MHz, $CDCl_3$): δ 7.37-7.16 (m, 5H), 5.89–5.76 (m, 1H), 5.57–5.51 (m, 1H), 5.04–4.92 (m, 2H), 3.74–3.66 (m, 1H), 2.97 (d, J = 6.0 Hz, 1H), 2.81–2.62 (m, 2H), 2.28–1.90 (m, 4H), 1.56–1.23 (m, 12H). ^{13}C NMR (91 MHz, $CDCl_3$): δ 177.36, 141.32, 139.15, 128.50, 128.39, 126.10, 114.15, 72.31, 50.69, 35.82, 33.77, 33.44, 31.83, 29.46, 29.39, 29.04, 28.89, 25.98. ESI-MS (m/z): 318.2439 [M+H], calcd for: $C_{20}H_{32}NO_2$: 318.2433.

3-Hydroxy-2-(2-(2-methoxyethoxy)ethyl)-5-phenylpentanamide (**7**)

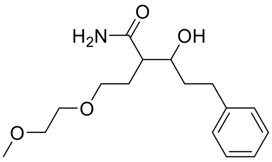

3-Hydroxy-2-(2-(2-methoxyethoxy)ethyl)-5-phenylpentanamide was obtained according to GP5 starting from 3-hydroxy-2-(2-(2-methoxyethoxy)ethyl)-5-phenylpentanoic acid (1.0 g, 3.4 mmol), NH_4HCO_3 (340 mg, 4.3 mmol), di-*tert*-butyl dicarbonate (981 mg, 4.5 mmol) and pyridine (0.2 mL) in acetonitrile (15 mL). The product was purified by column chromatography (eluent: CH_2Cl_2/MeOH = 30/1) and finally by preparative HPLC. Yield: 600 mg (60 %) as a mixture of 2 diastereomers.

^{1}H NMR (360 MHz, $CDCl_3$): δ 7.32–7.16 (m, 5H), 6.78–6.59 (m, 1H), 5.60–5.47 (m, 1H),4.12–4.04 (m, 0.5H), 4.02–3.95 (m, 0.5H), 3.70–3.40 (m, 7H), 3.385 (s, 1.5H), 3.381 (s, 1.5H), 2.96 – 2.83 (m, 1H), 2.77–2.52 (m, 2H), 2.15–1.61 (m, 4H). ^{13}C NMR (91 MHz, $CDCl_3$): δ 178.70, 178.21, 142.15, 142.04, 128.52, 128.51, 128.36, 128.34, 125.80, 125.76, 72.09, 71.79, 71.75, 70.66, 69.96, 69.93, 68.75, 68.46, 58.88, 58.87, 46.83, 46.29, 37.81, 35.72, 32.47, 32.35, 30.49, 25.73. ESI-MS (m/z): 296.1855 [M+H], calcd for: $C_{16}H_{26}NO_4$: 296.1862.

(2*R**,3*R**)-3-Hydroxy-2-pentyl-5-phenylpentanamide (**5**)

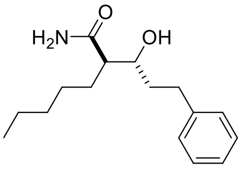

(2*R**,3*R**)-3-Hydroxy-2-pentyl-5-phenylpentanamide was synthesized according to GP6A starting from (3*R**,4*R**)-3-pentyl-4-(2-phenylethyl)oxetan-2-one (500 mg, 2.0 mmol) and solution of NH_3 (20 mL, 7 N in MeOH). After purification by column chromatography the product was additionally purified by HPLC. Yield: (270 mg, 51 %).

^{1}H NMR (250 MHz, $CDCl_3$): δ 7.34-7.16 (m, 5H), 5.78–5.65 (m, 1H), 5.60–5.45 (m, 1H), 3.69 (dt, *J* = 8.3, 4.1 Hz, 1H), 2.95–2.80 (m, 1H), 2.76 – 2.60 (m, 1H), 2.23 – 2.10 (m, 1 H), 1.92 – 1.70 (m, 3H), 1.68–1.52 (m, 1H), 1.42 – 1.22 (m, 6H), 0.88 (t, *J* = 6.8 Hz, 3H). ^{13}C NMR (91 MHz, $CDCl_3$): δ 178.95, 141.71, 128.47, 128.45, 125.97, 71.72, 51.77, 37.44, 32.26, 31.72, 30.26, 27.10, 22.44, 13.97. ESI-MS (m/z): 264.1952 [M+H], calcd for: $C_{16}H_{25}NO_2$: 264.1964.

(2*R**, 3*R**)-3-Hydroxy-2-(oxiran-2-ylheptyl)-5-phenylpentanamide

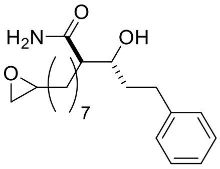

The solution of (2*R**,3*R**)-3-hydroxy-2-(non-8-enyl)-5-phenylpentanamide ((*R**,*R**)-**3**) (1.00 g, 3.15 mmol) in CH_2Cl_2 (80 mL) was cooled to 0 °C and then *m*CPBA (1.09 g, 6.30 mmol) was added in three portions over 15 min. The solution was stirred at r.t. for 36 h and the organic layer was washed with $Na_2S_2O_3$ (8 mL, 10 %), saturated $NaHCO_3$ (8 mL) and brine (2 × 8 mL) and then dried over Na_2SO_4. The solvent was removed *in vacuo* and the residue was purified by column chromatography (eluent: CH_2Cl_2/ MeOH = 20/1) to give the desired product as a white solid. Yield: 1.04 g, (99 %). R_f = 0.17 (CH_2Cl_2/MeOH = 20:1). ^{1}H NMR (360 MHz, $CDCl_3$): δ 7.31 – 7.17 (m, 5H), 5.90 – 5.86 (m, 2H), 3.72 – 3.66 (m, 1H), 3.46 – 3.40 (m, 1H), 2.93 – 2.83 (m, 2H), 2.76 – 2.65 (m, 2H), 2.49 – 2.46 (m, 1H), 2.20 – 2.15 (m, 1H), 1.88 – 1.72 (m, 3H), 1.60 – 1.31 (m, 13H). ^{13}C NMR (91 MHz, $CDCl_3$) δ 178.01, 141.88, 128.46, 128.41, 125.88, 71.73, 52.41, 51.60, 47.10, 37.70, 32.41, 32.35, 30.35, 29.44, 29.28, 27.45, 25.90. ESI-MS (*m/z*): 334.2373 $[M+H]^+$, calcd for $C_{20}H_{32}NO_3$: 334.2377.

(2*R**,3*R**)-3-Hydroxy-2-(8,9-dihydroxynonyl)-5-phenylpentanamide (**9**)

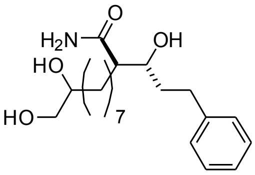

(2*R**, 3*R**)-3-Hydroxy-2-(oxiran-2-ylheptyl)-5-phenylpentanamide (200 mg, 0.6 mmol) was added to the solution of $NaHCO_3$ (200 mg, 2.4 mmol) in H_2O (15 mL) and *N*-methyl-2-pyrrolidon (NMP) (5 mL). The reaction mixture was stirred for 5 h at 130 °C (bath temperature) and cooled down to RT The reaction mixture was extracted with EtOAc (3 times) and combined organic layers were dried over Na_2SO_4. Solids were filtered off and the filtrate was evaporated. The residue was separated by column chromatography (eluent: CH_2Cl_2/MeOH = 10/1) to yield a product (80 mg, 38 %). R_f = 0.32 (CH_2Cl_2/MeOH = 10/1). ^{1}H NMR (360 MHz, CD_3OD): δ 7.29–7.12 (m, 5H), 3.70 – 3.62 (m, 1H), 3.61–3.53 (m, 1H), 3.51–3.38 (m, 2H), 3.35–3.30 (m, 1 H), 2.87–2.77 (m, 1H), 2.72–2.62 (m, 1H), 2.34–2.26 (m, 1H), 1.90–1.58 (m, 3H), 1.56–1.43 (m, 3H), 1.42–1.24 (m, 11H). ^{13}C NMR (91 MHz, CD_3OD) δ 178.94, 142.05, 128.06, 127.98, 125.39, 66.01, 51.97, 36.92, 33.02, 31.63, 29.31, 29.22, 29.21, 29.13, 27.13, 25.24. ESI-MS (*m/z*): 352.2490 $[M+H]^+$, calcd for $C_{20}H_{33}NO_4$: 352.2488.

1.2 Synthesis of the diastereomeric photoprobes

11-Trimethylsilyl)undec-10-ynoic acid

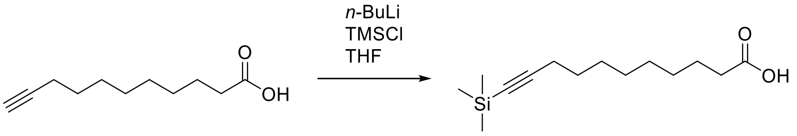

n-BuLi (26 mL, 65 mmol, 2.5 M in hexane) was added to the solution of undec-10-ynoic acid (5 g, 27 mmol) in THF (350 mL) at -78 °C. The mixture was stirred for 30 min at this temperature and freshly distilled TMSCl (10 mL, 8.6 g, 80 mmol) was added. The reaction mixture was stirred for 15 min at -78 °C and 1 h at RT The reaction was quenched by the addition of H_2O (100 mL). The mixture was extracted by CH_2Cl_2 (3×50 mL) and the combined organic phases were dried over Na_2SO_4, filtered and concentrated under reduced pressure. Subsequent purification by column chromatography (eluent: hexane/EtOAc = 3/1 to 2/1) yielded 6.8 g (99 %) of the desired product as a colorless oil. R_f = 0.42 (hexane/EtOAc = 3/1).

^{1}H NMR (250 MHz, $CDCl_3$) = δ 2.36 (t, *J* = 7.5 Hz, 2H), 2.21 (t, *J* = 7.1 Hz, 2H), 1.65 (m, 2H), 1.52 (m, 2H), 1.42 – 1.19 (m, 8H), 0.15 (s, 9H).

ESI-MS (m/z): 255.1774 [M+H], calcd.: $C_{14}H_{27}O_2Si^+$: 255.1775.

Methyl 11-(Trimethylsilyl)undec-10-ynoate

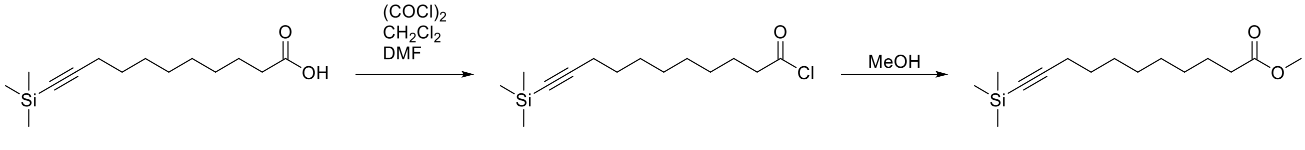

A solution of (11-trimethylsilyl)undec-10-ynoic acid (6.9 g, 27.1 mmol) in dry CH_2Cl_2 (25 mL) was cooled to 0 °C. DMF (5 drops) was added to this solution followed by oxalyl chloride (2.3 mL, 27.1 mmol). The reaction mixture was stirred for 4 h at 0 °C. The volatiles were removed under reduced pressure and dry methanol (30 mL) was added to the residue. The solution was stirred for 2 h at RT and the volatiles were removed under reduced pressure. Immediately after that the residue was purified by column chromatography (eluent: hexane/EtOAc = 20/1) yielding 6.2 g (85 %) of the product as a colorless oil.

^{1}H NMR (360 MHz, $CDCl_3$): δ 3.66 (s, 3H), 2.30 (t, J = 7.5 Hz, 2H), 2.25 – 2.13 (m, 2H), 1.67 – 1.57 (m, 2H), 1.57 – 1.45 (m, 2H), 1.42 – 1.25 (m, 8H), 0.14 (s, 9H). ESI-MS (m/z): 269.1931 [M+H], calcd.: $C_{15}H_{29}O_2Si^+$: 269.1931.

Synthesis of 3-(4-(2-phenyl-1,3-dioxolanyl)phenyl)propanol - Variant 1.

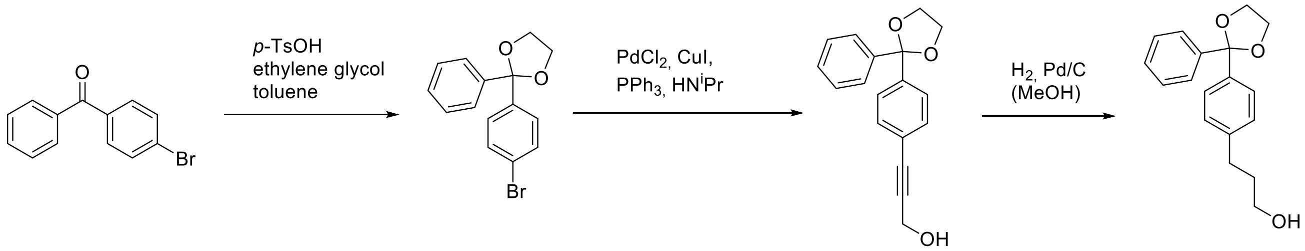

2-(4-Bromophenyl)-2-phenyl-1,3-dioxolane

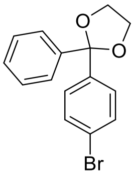

4-Bromobenzophenone (11.0 g, 42.1 mmol), pTosOH (0.25 g, 1.45 mmol) and ethylene glycol (12.0 mL, 174 mmol) were dissolved in benzene (200 mL). The reaction mixture was stirred for 40 h under reflux (bath temperature 160°C) with a Dean-Stark apparatus and cooled down to the RT The solution was washed with 1 M NaOH (100 mL) and H_2O (100 mL). The organic phase was dried over Na_2SO_4. The precipitate was filtered off and the filtrate was concentrated under reduced pressure. The raw product was purified by column chromatography (eluent: hexane/CH_2Cl_2 = 4/1 to 3/1), yielding 12.1 g (94 %) of a product as a white solid. Alternatively the product can be purified by recrystallization from ethanol.

^{1}H NMR (360 MHz, $CDCl_3$): δ 7.52 – 7.23 (m, 9H), 4.05 (m, 4H). ^{13}C NMR (91 MHz, $CDCl_3$): δ 141.78, 141.49, 131.42, 128.38, 128.16, 126.18, 122.38, 109.18, 77.36, 65.12. ESI-MS (m/z): 305.0173 [M+H], calcd.: $C_{15}H_{14}BrO_2^+$: 305.0172

2-(4-(3-Hydroxyprop-1-inyl)phenyl)-2-phenyl-1,3-dioxolane

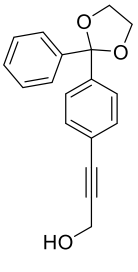

2-(4-Bromophenyl)-2-phenyl-1,3-dioxolane (12.0 g, 39.3 mmol) was dissolved in diisopropylamine (40 mL). $PdCl_2$ (140 mg, 0.79 mmol, 2 mol %), CuI (110 mg, 0.59 mmol, 1.5 mol %), PPh_3 (410 mg, 1.57 mmol) and propargyl alcohol (2.3 g, 41.3 mmol) were added and the reaction mixture was refluxed for 20 h at 95°C. The precipitate formed was filtered off and washed with Et_2O (200 mL). The filtrate was concentrated under reduced pressure and the residue was purified by column chromatography (eluent: hexane/EtOAc = 2/1 to 1.5/1) yielding the desired product (4.7 g, 43 %) as a brown oil.

^{1}H NMR (250 MHz, $CDCl_3$): δ 7.59 – 7.43 (m, 4H), 7.43 – 7.15 (m, 5H), 4.58 – 4.36 (m, 2H,), 4.06 (d, J = 2.1 Hz, 4H). ^{13}C NMR (63 MHz, $CDCl_3$): δ 142.67, 141.83, 131.66, 128.36, 126.34, 126.22, 122.43, 109.26, 87.59, 85.65, 77.06, 76.65, 65.11, 51.82. ESI-MS (m/z): 281.1173 [M+H], calcd.: $C_{18}H_{17}O_3^+$: 281.1172

3-(4-(2-Phenyl-1,3-dioxolan-2-yl)phenyl)propan-1-ol

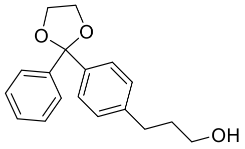

2-(4-(3-Hydroxyprop-1-inyl)phenyl)-2-phenyl-1,3-dioxolane (4.6 g, 16.4 mmol) was dissolved in dry MeOH (150 mL). Pd/C (2.0 g, 1.9 mmol) was added in the stream of Ar. The reaction mixture was stirred for 2 d under the H_2 atmosphere. Pd/C was filtered off through the silica pad and washed with MeOH (100 mL). The filtrate was concentrated under reduced pressure yielding the desired product (4.3 g, 92 %) as colorless oil.

^{1}H NMR (250 MHz, $CDCl_3$): δ 7.65 – 7.48 (m, 2H), 7.48 – 7.39 (m, 2H), 7.39 – 7.22 (m, 3H), 7.16 (d, *J* = 7.8 Hz, 2H), 4.16 – 3.94 (m, 4H), 3.65 (t, *J* = 6.5 Hz, 2H), 2.68 (dd, *J* = 8.7, 6.7 Hz, 2H), 1.98 – 1.75 (m, 2H). ESI-MS (m/z): 285.1485 [M+H], calcd.: $C_{18}H_{21}O_3^+$: 285.1485

Synthesis of 3-(4-(2-phenyl-1,3-dioxolanyl)phenyl)propanol - Variant 2.

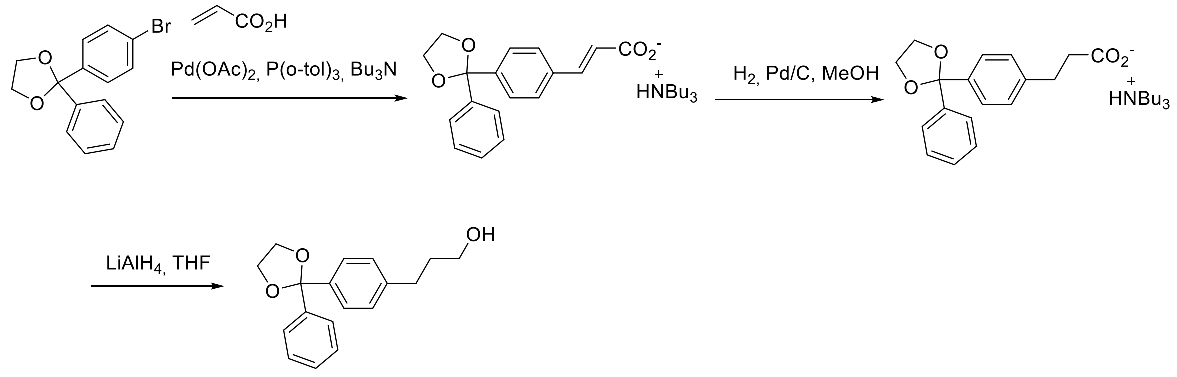

Tributylammonium 3-(4-(2-phenyl-1,3-dioxolan-2-yl)phenyl)propenoate

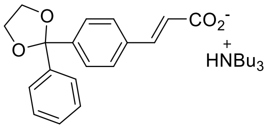

$Pd(OAc)_2$ (72 mg, 0.32 mmol, 2 mol%), tri(*o*-tolyl)phosphine (388.8 mg, 1.3 mmol) and 2-(4-bromophenyl)-2-phenyl-1,3-dioxolane (5 g, 16.4 mmol) were placed in the flask which was then evacuated and backfilled with argon 3 times. *o*-Xylene (3.2 mL), tributylamine (8 mL, 6.24 g, 33.7 mmol) and acrylic acid (1.22 mL, 1.28 g, 17.8 mmol) were added and the reaction mixture was stirred at 150 °C for 5 h. Then it was cooled down to RT, concentrated under reduced pressure and separated by column chromatography (hexane/EtOAc = 1/2, R_f = 0.43). The product was dried in high vacuum to get rid of the residual tributylamine and yielding 5.8 g (74 %) of a yellow oil.

^{1}H NMR (360 MHz, $CDCl_3$) = δ 7.62–7.27 (m, 10H), 6.50 (d, *J* = 15.9 Hz, 1H), 4.05 (s, 4H), 3.02 – 2.85 (m, 6H), 1.76 – 1.59 (m, 6H), 1.46–1.31 (h, 6H), 0.96 (t, *J* = 7.3 Hz, 9H)

^{13}C NMR (91 MHz,$CDCl_3$) = δ 172.45, 142.72, 141.88, 139.94, 135.76, 128.16, 128.10, 127.50, 126.44, 124.61, 109.24, 77.23, 64.90, 60.38, 51.58, 25.46, 20.33, 13.71.

3-(4-(2-Phenyl-1,3-dioxolan-2-yl)phenyl)propenoic acid: ESI-MS (m/z): 297.1120 [M+H], calcd.: $C_{18}H_{19}O_4^+$: 297.1127

Tributylammonium ion: ESI-MS (m/z): 186.2216 [M+H], calcd.: $C_{12}H_{28}N^+$: 186.2216

Tributylammonium 3-(4-(2-phenyl-1,3-dioxolan-2-yl)phenyl)propanoate

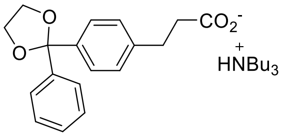

Pd/C (0.966 g, 9.36 mmol, 10 %) placed in the flask which was then evacuated and backfilled with argon 3 times. The solution of tributylammonium 3-(4-(2-phenyl-1,3-dioxolan-2-yl)phenyl)prop-2-enoate (8.8 g, 18.2 mmol) in MeOH (35 mL) was added and argon was replaced by hydrogen gas. The suspension was stirred for 16 h under hydrogen and subsequently filtered through Celite. The filtrated was concentrated under reduced pressure yielding the desired product (8.567 g, 97 %) as orange oil. According to the NMR spectrum the product was sufficiently pure and therefore was used for the next step without additional purification.

^{1}H NMR (250 MHz, $CDCl_3$) = δ 7.60 – 7.03 (m, 9H), 4.10–3.98 (m, 4H), 3.01–2.82 (m, 8H), 2.61–2.46 (dd, *J* = 9.4, 6.7 Hz, 2H), 1.78 – 1.57 (m, 6H), 1.46 – 1.24 (m, 6H), 1.04 – 0.88 (t, *J* = 7.3 Hz, 9H). 3-(4-(2-Phenyl-1,3-dioxolan-2-yl)phenyl)propanoic acid: ESI-MS (m/z): 299.1277 [M+H], calcd.: $C_{18}H_{19}O_4^+$: 299.1283

Tributylammonium ion: ESI-MS (m/z): 186.2216 [M+H], calcd.: $C_{12}H_{28}N^+$: 186.2216

3-(4-(2-Phenyl-1,3-dioxolan-2-yl)phenyl)propan-1-ol

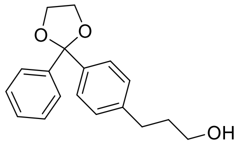

$LiAlH_4$ (0.6 g, 16 mmol) was slowly added under Ar to the solution of tributylammonium 3-(4-(2-phenyl-1,3-dioxolan-2-yl)phenyl)propanoate (4.2 g, 8.6 mmol) in THF (80 mL) at 0 °C and the resulting suspension was heated to 80 °C and stirred for 2 h at this temperature. Then the reaction mixture was cooled down to 0 °C and quenched by the dropwise addition of 0.1 M HCl (40 mL). The mixture was extracted with EtOAc (3x60 mL) and the combined organic phase was dried over Na_2SO_4. The solid was filtered off and the filtrate was concentrated under reduced pressure. The residue was purified by column chromatography (eluent: hexane/EtOAc = 1/1) yielding 1.2 g (50 %) of a product as white crystals. R_f = 0.57 (hexane/EtOAc = 1/1). The spectral data of the compound is identical to those of the sample obtained by another synthesis.

3-(4-(2-Phenyl-1,3-dioxolanyl)phenyl)propanal

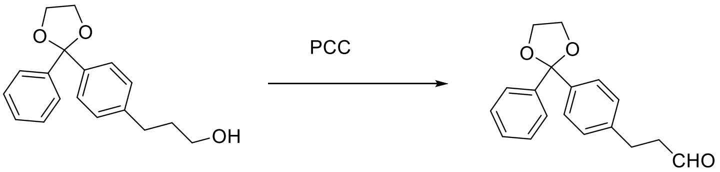

Pyridinium chlorochromat (4.9 g, 22.7 mmol) was added to the solution of 3-(4-(2-phenyl-1,3-dioxolanyl)phenyl)propan-1-ol (4.3 g, 15.1 mmol) in CH_2Cl_2 (50 mL). The reaction mixture was stirred for 5 h at RT Et_2O (100 mL) was added and the precipitate formed was filtered off through a pad of silica. The filtrate was concentrated under reduced pressure yielding 3.4 g (80 %) of the product as a green oil.

^{1}H NMR (360 MHz, CDCl$_3$): δ 9.80 (t, *J* = 1.4 Hz, 1H), 7.54 – 7.46 (m, 2H), 7.46 – 7.38 (m, 2H), 7.37 – 7.27 (m, 3H), 7.21 – 7.08 (m, 2H), 4.11 – 3.96 (m, 4H), 3.00 – 2.85 (m, 2H), 2.78 – 2.70 (m, 2H). ^{13}C NMR (91 MHz, CDCl$_3$): δ 201.56, 140.33, 128.28, 128.23, 128.18, 126.60, 126.56, 126.51, 126.26, 77.36, 65.04, 45.30, 27.94.

Synthesis of both diastereomers of 5-(4-benzoylphenyl)-3-hydroxy-2-(8-nonynyl)-pentanoic acid

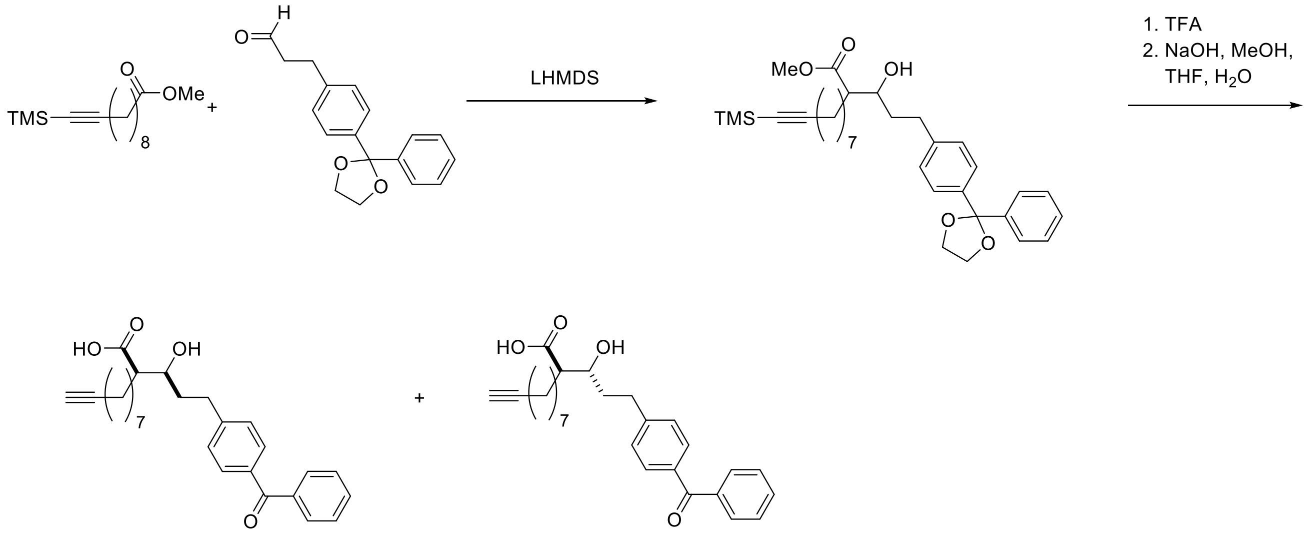

Methyl 2-Hydroxy-3-(9-trimethylsilyl-8-nonynyl)-5-(4-(2-phenyl-1,3-dioxolan-2-yl)phenyl)-pentanoate

LHMDS (8 mL, 1 M in THF, 8 mmol) was slowly added to the solution of methyl 11-(trimethylsilyl)undec-10-ynoate (1.8 g, 6.6 mmol) in dry THF (12 mL) at -78°C under Ar. The mixture was stirred for 50 min at this temperature. A solution of 3-(4-(2-phenyl-1,3-dioxolanyl)phenyl)propanal (1.8 g, 6.4 mmol) in dry THF (12 mL) was slowly added to the reaction mixture and the reaction was stirred for 1 h at -78°C and for 2 h at 0°C. The reaction was quenched by the addition of H$_2$O. The mixture obtained was extracted with EtOAc. The combined organic phases were dried over Na$_2$SO$_4$ and concentrated under reduced pressure. The crude product was purified by column chromatography (eluent: hexane/EtOAc = 5/1 to 1/1) yielding 970 mg (28 %) of methyl 2-hydroxy-3-(9-trimethylsilyl-8-nonynyl)-5-(4-(2-phenyl-1,3-dioxolan-2-yl)phenyl)-pentanoate as a colorless oil. R_f = 0.33 (hexane/EtOAc = 5/1). ^{1}H NMR (250 MHz, CDCl$_3$): δ 7.51 (ddp, *J* = 6.6, 2.8, 1.2 Hz, 2H), 7.43 (dd, *J* = 8.1, 4.6 Hz, 2H), 7.39 - 7.23 (m, 3H), 7.15 (d, *J* = 8.0 Hz, 2H), 4.06 (d, *J* = 1.9 Hz, 4H), 3.88 - 3.73 (m, 1H), 3.70 (s, 3H), 3.00 - 2.36 (m, 4H), 2.21 (t, *J* = 7.0 Hz, 1H), 1.83 - 1.41 (m, 4H), 1.41 - 1.14 (m, 8H), 0.15 (s, 9H). ^{13}C NMR (63 MHz, CDCl$_3$): δ 128.38, 128.27, 128.14, 126.60, 126.42, 126.30, 76.65, 65.02, 28.72, 19.98, 0.34. ESI-MS (m/z): 551.3176 [M+H], calcd for $C_{33}H_{47}O_5Si$: 551.3187

5-(4-Benzoylphenyl)-3-hydroxy-2-(8-nonynyl)-pentanoic acid

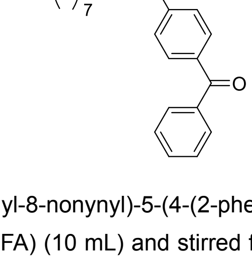

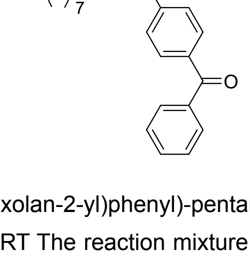

Methyl 3-hydroxy-2-(9-trimethylsilyl-8-nonynyl)-5-(4-(2-phenyl-1,3-dioxolan-2-yl)phenyl)-pentanoate (960 mg, 1.76 mmol) was dissolved in trifluoroacetic acid (TFA) (10 mL) and stirred for 20 h at RT The reaction mixture was poured in H$_2$O (100 mL) and extracted with CH_2Cl_2 (3 x 100 mL). The combined organic phases were dried over Na_2SO_4, concentrated under reduced pressure and the product obtained was used for the next reaction without any further purification, R_f = 0.14 (hexane/EtOAc = 5/1). This product was dissolved in THF (100 mL) and added to the solution of NaOH (1.0 g, 25.0 mmol) in H_2O (10 mL) and MeOH (40 mL). The reaction mixture was stirred for 4 h at RT MeOH and THF were distilled off under reduced pressure and the residue was neutralized by addition of conc. HCl. The mixture was extracted with CH_2Cl_2 (2 x 100 mL) and EtOAc (100 mL). The combined organic phases were dried over Na_2SO_4 and concentrated under reduced pressure. Diastereomers of the product were separated by column chromatography (eluent: hexane/EtOAc = 1/1) yielding 170 mg (23 %) of (*R**, *S**)-diastereomer (R_f = 0.44, hexane/EtOAc = 1/1) and 92 mg (12 %) of (*R**, *R**)-diastereomer (R_f = 0.11, hexane/EtOAc = 1/1).

(*R**, *S**)-5-(4-Benzoylphenyl)-3-hydroxy-2-(8-nonynyl)-pentanoic acid: ^1H NMR (250 MHz, $CDCl_3$): δ 7.84 - 7.72 (m, 4H), 7.63 - 7.53 (m, 1H), 7.52–7.42 (m, 2H), 7.32 (d, *J* = 8.3 Hz, 2H), 3.88 (dt, *J* = 9.3, 3.6 Hz, 1H), 3.05 – 2.90 (m, 1 H), 2.85 – 2.65 (m, 1 H), 2.52 (dt, *J* = 9.8, 4.3 Hz, 1H), 2.17 (td, *J* = 7.0, 2.6 Hz, 2H), 1.93 (t, *J* = 2.6 Hz, 1H), 1.90 - 1.65 (m, 3H), 1.65 - 1.40 (m, 3H), 1.43 - 1.23 (m, 8H).

ESI-MS (m/z): 421.2375 [M+H], calcd for: $C_{27}H_{33}O_4$: 421.2373

(*R**, *R**)-5-(4-Benzoylphenyl)-3-hydroxy-2-(8-nonynyl)-pentanoic acid: ^1H NMR (250 MHz, $CDCl_3$): δ 7.82 - 7.70 (m, 4H), 7.63 - 7.55 (m, 1H), 7.53 – 7.42 (m, 2H), 7.32 (d, J = 8.3 Hz, 2H), 3.74 (dt, J = 8.1, 4.9 Hz, 1H), 3.03 – 2.70 (m, 2H), 2.50 (dt, *J* = 8.6, 5.2 Hz, 1H), 2.17 (td, *J* = 7.0, 2.7 Hz, 2H), 1.93 (t, *J* = 2.7 Hz, 1H), 1.90 - 1.44 (m, 6H), 1.42 - 1.19 (m, 8H).

(*R**,*R**)-5-(4-Benzoylphenyl)-3-hydroxy-2-(8-nonynyl)-pentanamide ((*R**,*R**)-**8**)

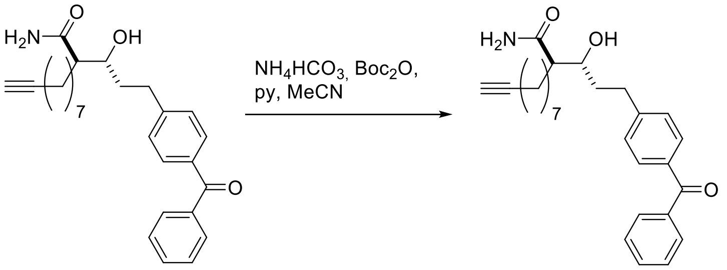

(*R**,*R**)-5-(4-Benzoylphenyl)-3-hydroxy-2-(8-nonynyl)-pentanamide was synthesized according to GP5. Di-*tert*-butyl dicarbonate (180 mg, 1.3 mmol), NH_4HCO_3 (103 mg, 1.3 mmol) and pyridine (100 µL) were added to the solution of (*R**, *R**)-5-(4-benzoylphenyl)-3-hydroxy-2-(8-nonynyl)-pentanoic acid (180 mg, 0.43 mmol) in acetonitril (10 mL). The reaction mixture was stirred for 14 h at RT Volatiles were distilled off under reduced pressure and the residue was purified by column chromatography (eluent: hexane/EtOAc = 1/1 to 0/1), yielding 40 mg (22 %) of the product as a light yellow solid. R_f = 0.19 (hexane/EtOAc = 1/1).

^1H NMR (500 MHz, $CDCl_3$): δ 7.82 - 7.74 (m, 4H), 7.63 - 7.58 (m, 1H), 7.52–7.47 (m, 2H), 7.33 (d, *J* = 8.3 Hz, 2H), 5.77 (s, 1H), 5.50 (s, 1H), 3.74–3.67 (m, 1H), 3.32 (d, *J* = 7.9 Hz, 1H), 2.99 (ddd, *J* = 13.4, 8.6, 5.1 Hz, 1H), 2.80 (ddd, *J* = 13.4, 7.0, 9.4 Hz, 1H), 2.23 – 2.15 (m, 1H), 2.19 (td, *J* = 7.1, 2.6 Hz, 2H), 1.95 (t, *J* = 2.6 Hz, 1H), 1.94 - 1.78 (m, 3H), 1.68 – 1.62 (m, 1H), 1.56 – 1.48 (m, 2H), 1.42 - 1.26 (m, 8H). ^{13}C NMR (125 MHz, $CDCl_3$): δ 196.54, 177.70, 147.17, 137.81, 135.37, 132.31, 130.49, 129.99, 128.46, 128.27, 84.71, 71.61, 68.17, 51.50, 37.47, 32.44, 30.46, 29.48, 28.91, 28.63, 28.39, 27.51, 18.37.

ESI-MS (m/z): 420.2537 [M+H], calcd for $C_{27}H_{34}NO_3+$: 420.2533

(*R**,*S**)-5-(4-Benzoylphenyl)-3-hydroxy-2-(8-nonynyl)-pentanamide ((*R**,*S**)-**8**)

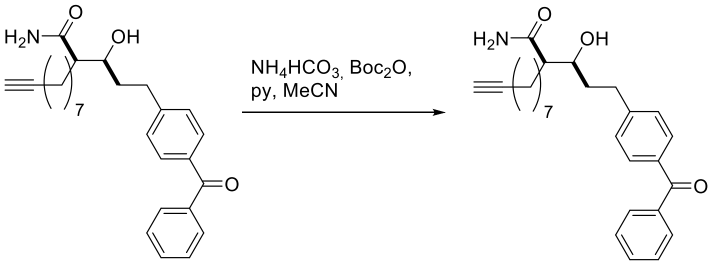

(*R**,*S**)-5-(4-Benzoylphenyl)-3-hydroxy-2-(8-nonynyl)-pentanamide was obtained according to GP5 from di-*tert*-butyl dicarbonate (150 mg, 0.65 mmol), NH_4HCO_3 (50 mg, 0.65 mmol), pyridine (50 µL) and (*R**, *R**)-5-(4-benzoylphenyl)-3-hydroxy-2-(8-nonynyl)-pentanoic acid (92 mg, 0.22 mmol) in acetonitril (10 mL). Yield: 20 mg (22 %) of the product as a light yellow solid.^{1}H NMR (360 MHz, $CDCl_3$): δ 7.82 - 7.74 (m, 4H), 7.63 - 7.58 (m, 1H), 7.52–7.47 (m, 2H), 7.33 (d, *J* = 8.3 Hz, 2H), 5.72 (s, 1H), 5.47 (s, 1H), 3.88 (dq, *J* = 9.8, 3.3 Hz, 1H), 3.18 (d, *J* = 3.3 Hz, 1H), 2.97 (ddd, *J* = 13.7, 8.8, 5.1 Hz, 1H), 2.76 (ddd, *J* = 13.7, 7.0, 9.4 Hz,1H), 2.25 – 2.21 (m, 1H), 2.19 (td, *J* = 7.1, 2.6 Hz, 2H), 1.95 (t, *J* = 2.6 Hz, 1H), 1.94 - 1.87 (m, 1H), 1.82 - 1.70 (m, 2 H), 1.59 – 1.48 (m, 3H), 1.46 - 1.22 (m, 8H). ^{13}C NMR (125 MHz, $CDCl_3$): δ 196.53, 177.61, 147.00, 137.79, 135.42, 132.31, 130.49, 130.00, 128.47, 128.27, 84.71, 71.28, 68.17, 51.33, 35.44, 32.46, 29.60, 28.92, 28.64, 28.40, 27.88, 26.34, 18.37.

ESI-MS (m/z): 420.2537 [M+H], calcd for $C_{27}H_{34}NO_3^+$: 420.2533.

2. *In vitro* experiments

2.1 Bacteria

S. aureus strains and media

Commercially available strains were obtained from the following suppliers: Institute Pasteur, France (NCTC 8325, Mu 50), American Type Culture Collection, USA (USA 300 BAA-1717); NARSA library (Network on Antimicrobial Resistance in *Staphylococcus aureus*); University of Nebraska Medical Center (USA 300 Lac and corresponding transposon mutants (TN mut.)). Clinical Isolates were a kind gift from Prof. Markus Gerhard at the Institute of Medical Microbiology and Immunology, Technische Universität München.

Bacterial growth media: B-medium (LB-Broth 20 g/L, K_2HPO_4 1 g/L); BHB-medium (Brain Heart Infusion 17.5 g/L, Na_2HPO_4 2.5 g/L, Glucose 2 g/L, Tryptic peptone 5 g/L, NaCl 5 g/L)

Correlation of CFUs and OD_{600} of bacterial cultures / bacterial growth curves

For determining bacterial numbers in liquid cultures, growth curves for used strains were established. Therefore, bacteria from glycerol stocks or overnight (ON) cultures were inoculated in B-medium (1:100). OD_{600} values were measured every 20-30 min until an OD_{600} value > 1 was determined. At each time point 150 µL of bacterial suspension were transferred to a 1.5 mL microcentrifuge tube. Bacterial suspensions were serially diluted by 1:10 and 20 µL of the following dilutions were plated on agar plates: 1:10^4, 1:10^5, 1:10^6, 1:10^7. Plates were incubated ON at 37°C and colonies were counted using plates with a minimum of 80 and a maximum of 200 colonies. For the correlation of CFUs and OD_{600} values equations were fitted to the measured data.

Defined growth conditions

5 mL of B-medium were inoculated with 50 µL ON culture (1:100) and incubated by shaking at 37 °C (200 rpm). After 1.5-2.5 h the culture reached an OD_{600} between 0.4 and 0.6. Bacteria were diluted in B-medium to get a concentration of 3.4×10^4 bacteria per mL according to previously recorded growth curves. Diluted bacterial cultures were aliquoted into plastic culture tubes (1 mL

in each tube) and DMSO (10 µL) or compound in DMSO (10 µL) was added. Bacterial cultures were grown in polystyrol culture tubes with tightly closed lids at 200 rpm for 20 h at 37°C.

2.2. ClpP peptidase activity assay

Inhibition of recombinant *S. aureus* ClpP peptidase activity was determined by cleavage of the fluorogenic model substrate N-succinyl-Leu-Tyr-7-amidomethylcoumarin (SLY-AMC, Bachem Holding AG) as described previously.[4-5] Experiments were conducted in 100 µL activity buffer (100 mM NaCl, 100 mM HEPES, pH 7.0). IC_{50} values were calculated from curve fittings by Originlab OriginPro 9.0 and GraphPad Prism 6.0c.

2.3 Minimal inhibitory concentration (MIC) and hemolysis assay

Bacteria were cultured as described in 2.1 in presence of test compound or DMSO-only as positive control, respectively. After 20 h at 200 rpm and 37°C 100 µL of the cultures were diluted 1:10, transferred to a microtiter plate and measured at 600 nm with a plate reader (TECAN, Infinite M200pro). The MIC was defined as the concentration of a compound sufficient to fully inhibit bacterial growth. The remaining undiluted bacterial cultures were pelleted for 10 min at 6.200 xG, 100 µL of the supernatant were transferred to a microtiter plate (in triplicates per culture), incubated with 50 µL of diluted sheep blood solution (10 % v/v in PBS, heparinized sheep blood washed 5x in PBS, Elocin lab, Germany) and measured in a 1 min interval at 600 nm, at 37°C with a plate reader (TECAN, Infinite M200pro). Incubation of 100 µL growth medium with 50 µL diluted sheep blood solution (10 % v/v in PBS) was used as a negative control. Bacterial supernatant from DMSO control samples (no inhibition of hemolysis) with 50 µL diluted sheep blood solution was used as a positive control. Quantification was achieved via calibration curve: a 1:2 dilution series of bacterial supernatant from DMSO control samples with growth medium was incubated with diluted sheep blood solution. As a readout parameter from the assay the area under the curve (absorbance at at 600 nm vs. time) was used. When different strains were compared (clinical isolates, transposon mutant strains) the OD_{600} values at the timepoint with the highest dynamic range were used.

2.4 Affinity-based protein profiling with photoprobes (AfBPP)

Bacteria were cultured under defined growth conditions according to chapter 2.1 for 20 h. Cultures were collected in a 50 mL falcon tube and centrifuged at 6200 xG for 5 min at 4°C. The supernatant was disposed and the pellet was resuspended in PBS to reach OD_{600} = 40. 1 mL of this suspension and 10 µL of photo probe in DMSO (or just DMSO as a control) were mixed and the tube was briefly mixed by vortexing. After 30 min incubation at RT in the dark the tube was mixed by vortexing again and incubated for another 30 min at RT in the dark. The suspension was transferred into a transparent 6 well plate and irradiated for 15 min with UV light (UV low-pressure mercury-vapor fluorescent lamp, Philips TL-D 18W BLB). During irradiation a cool pack was placed under the 6 well plate. The irradiated bacterial suspension was transferred to a 1.5 mL microcentrifuge tube. After centrifugation (6200 xG, 2 min, 4°C) the supernatant was removed and the pellets were stored ON at -80°C.

Pellets were resuspended in 1 mL PBS (4°C) and transferred to a 'Precellys Glass/Ceramic Kit SK38 2.0 mL' tube. Tubes were cooled on ice for about 5 min or longer and cells were lysed with the Precellys Homogeniser using two times lysis program 3 (5400 rpm, run number: 1, run time: 20 sec, pause: 5 sec). After each lysis run the tubes were cooled on ice for 5 min. The ball mill tubes were centrifuged (16200 xG, 10 min, 4°C) and 800 µL of supernatant were transferred to new 1.5 mL microcentrifuge tubes and treated with 43 µL gel-based AfBPP Mix (3 µL TFL (Trifuctional linker (TFL) with rhodamine, biotin and azide groups[6]: 5(6)-(1-[5-(4-Azido-benzoylamino)-1-carbamoyl-pentylcarbamoyl]-5-(6-biotinoylamino-hexanoylamino)-pentyl-carbamoyl)-tetramethylrhodamin; 10 mM in DMSO), 10 µL fresh TCEP (3,3',3''-phosphinetriyltripropanoic acid; 50 mM in ddH_2O), 30 µL TBTA Ligand (tris((1-benzyl-1H-1,2,3-triazol-5-yl)methyl)amine; 1.667 mM in 80 % tBuOH and 20 % DMSO)) or with 60 µL gel-free AfBPP Mix (20 µL Biotin-PEG_3-N_3 (Jena Bioscience, CLK-AZ104P4-100; 10 mM in DMSO), 10 µL fresh TCEP (50 mM in ddH_2O), 30 µL TBTA Ligand (1.667 mM in 80 % tBuOH and 20 % DMSO)). The final concentrations for gel-based experiments were: 35.6 µM TFL, 593 µM TCEP and 59.3 µM TBTA Ligand; and for gel-free experiments: 233 µM Biotin-PEG_3-N_3, 581 µM TCEP and 58.2 µM TBTA Ligand. The lysates were mixed by vortexing and 10 µL $CuSO_4$ solution (50 mM in ddH_2O) were added. The lysates were mixed by vortexing again and incubated for 1h at RT in the dark. After the click-reaction with the AfBPP mix, the lysates were transferred to 15 mL falcon tubes and 4 mL of cold acetone (-80°C, MS grade) were added. Proteins were precipitated ON at -80°C.

The precipitated proteins were thawed on ice, pelletized (16900 xG, 15 min, 4°C) and supernatant was disposed. Falcon tubes were stored on ice during the following washing procedure: The proteins were washed two times with 1 mL cold methanol (-80°C). Resuspension was achieved by sonication (15 sec at 10 % intensity) and proteins were pelletized via centrifugation (16900 xG, 10 min, 4°C). Only MS grade water was used for the following procedures. After two washing steps supernatant was disposed and the pellet resuspended in 500 µL 0.2 % SDS in PBS at RT by sonication (15 sec at 10 % intensity). Avidin beads were thawed on ice and resuspended by carefully inverting. Then 50 µL of bead suspension were transferred into Protein LoBind Eppendorf tubes using wide bore pipette tips and washed three times with 1 mL 0.2 % SDS in PBS (resuspension: carefully inverting 10 times, pelleting: 400 xG, 2 min, RT). 500 µL protein solution from the 15 mL falcon tubes were transferred to the Protein LoBind Eppendorf tubes with washed avidin beads and incubated under continuous inverting (20 rpm, 1 h, RT). Beads were washed 3 times with 1 mL 0.2 % SDS in PBS, 2 times with 1 mL 6 M urea in water and 3 times with 1 mL PBS (resuspension: carefully inverting 20 times, pelleting: 400 xG, 2 min, RT).

2.4.1 Gel-based AfBPP

The procedure as described under 2.4 was followed. The beads were resuspended with 50 µL 2x Laemmli Sample Buffer and mixed in a thermomixer (300 rpm, 6 min, 96°C). Then beads were centrifuged (9600 xG, 2 min, RT) and the supernatant was analyzed via SDS PAGE (10 % agarose gel (PEQLAB Biotechnologie GmbH, Erlangen, PerfectBlue Dual Gel System, gels were prepared according to the manual), 3.5 h, 300 V, 8 µL fluorescent protein standard) and fluorescence imaging (GE Healthcare, ImageQuant LAS-4000). Fluorescent bands were excised with a scalpel. For every band a new scalpel blade was used. Each band was cut into cubes and the gel pieces were stored in 0.5 mL microcentrifuge tubes at -20°C. The excision of the bands and the following washing, reduction and alkylation steps were conducted wearing lab coat, gloves, bouffant cap and a hygiene mask to prevent keratin contamination of the samples. All solutions containing ammoniumbicarbonate (ABC) were prepared freshly at the day of usage. For all following steps, water and acetonitrile of HPLC-MS grade were used. Washing steps were performed by adding washing solution to cut gel pieces, followed by an incubation step at RT under shaking at 550 rpm. Gel pieces were first washed with 100 µL H_2O for 15 min, then with 200 µL acetonitrile (ACN)/50 mM ABC in H_2O (1:1) for 15 min and finally with 100 µL ACN for 10 min. 100 µL of 50 mM ABC in H_2O were added, the microcentrifuge tubes were mixed at 550 rpm for 5 min and then additional 100 µL of ACN were added without removing the supernatant. After shaking for 15 min at 550 rpm the supernatant was removed from the gel pieces and a final washing step with 100 µL ACN was conducted (10 min). The gel pieces were dried in a centrifugal evaporator at 30°C and 5 mbar for 15 min. Reduction of disulfide bonds was done with 100 µL 10 mM dithiothreitol (DTT) in 50 mM ABC (fresh solution) at 56°C and 550 rpm for 45 min. Supernatant was removed and the reduced disulfide bonds were alkylated using 100 µL 55 mM iodoacetamide (IAA) in 50 mM ABC (fresh solution). The reaction was conducted in the dark at RT and 550 rpm for 30 min. After removing the supernatant gel pieces were washed three times with 100 µL ACN/50 mM ABC in H_2O (1:1) for 15 min and then once with 100 µL ACN for 10 min. Supernatant was removed and the gel pieces were dried in a centrifugal evaporator at 30°C and 5 mbar for 15 min. The gel pieces were covered with 150 µL trypsin solution (1 µL sequencing grade modified trypsin (0.5 µg/µL) in 100 µL 25 mM ABC) and incubated ON at 300 rpm and 37°C in a shaker. The supernatant was transferred to a new 1.5 mL low protein absorbance Eppendorf tube (Protein LoBind) that was stored at RT (trypsin digest solution). Extraction was done by adding 100 µL 25 mM ABC to the gel pieces, followed by sonication for 15 min, adding additional 100 µL ACN and another sonication step for 15 min. The supernatant was transferred into the trypsin digest solution. Then 100 µL 5 % formic acid (in H_2O) were added and after sonication for 15 min additional 100 µL ACN were added. After sonication for 15 min the supernatant was transferred to the trypsin digest solution and 100 µL ACN were added (sonication for 15 min, transfer of the supernatant into the trypsin digest solution). The 1.5 mL low protein absorbance Eppendorf tubes with the trypsin digest solution were placed in a centrifugal evaporator and solvents were removed at 40°C and 5 mbar (more than 4h). The microcentrifuge tubes with the dried peptides could be stored at -20°C.

Prior to HPLC-MS measurements peptides were dissolved in 20 µL 1 % formic acid by sonication for 10 min and passed through an equilibrated VWR 0.45 µm centrifugal filter (2 min, 16200 xG). Equilibration was done by centrifuging the filter with 2 times 500 µL H_2O, 1 x 500 µL 0.05 M NaOH and 2 x 500 µL 1 % formic acid, each at 16200 xG for 1 min. Samples were analyzed via HPLC-MS/MS, Thermo Fischer LTQ Orbitrap XL (Thermo Fisher Scientific Inc., Waltham, Massachusetts, USA) with a UltiMate 3000 nano HPLC system (Dionex, Sunnyvale, California, USA) using a Acclaim C18 PepMap100 75 µm ID x 2 cm trap and Acclaim C18 PepMap RSLC, 75 µM ID x 15 cm separation columns (0.1 % FA, 5 % DMSO, gradient 46 min from 4 % ACN to 30 % ACN, then 11 min to 50 % ACN, 3 min to 65 % ACN and 1 min to 80 % ACN). The mass spectrometer was operated in data dependent mode. Precursors were measured in the orbitrap at a resolution of 60000 and an ion target of 1E6 in a scan range from 350 m/z to 1400 m/z. Preview mode for FTMS master scans was enabled. Charge states higher than 1 and a minimum signal threshold of 1000 counts were accepted for fragmentation. 5 most intensive precursors were selected for fragmentation using collision induced dissociation (CID) with a normalized collision energy of 35 %. Fragments were measured in the ion trap with an ion target of 1E4. Measurements were done with a Thermo Xcalibur^{TM} mass spectrometry data system version 2.1.0 SP1 build 1160. Assignment of the measured peptides to proteins was done with Proteome Discoverer 1.3.0.339 (Thermo Fisher Scientific, Massachusetts, USA) software: Precursor mass tolerance: 10 ppm; Fragment mass tolerance: 0.8 Da. Default settings were used except for the following: Mass precision: 2 ppm; Precursor ions area detector for quantification; Spectrum selection: lowest charge state: 2, highest charge state: 4, max. precursor mass: 5000 Da, mass analyzer: ITMS, FTMS, activation type: CID, HCD, ionization source: nanospray, polarity mode: +; Sequest: Protein database: Uniprot taxon identifier (strain): 93061 (NCTC 8325) download: 8.5.2014, enzyme name: trypsin (full), dynamic N-terminal modification: acetyl / +42.011 (any N-terminus), dynamic modification: oxidation / +15.995 Da (M), static modification: carbamindomethyl / +57.021 Da (C); Peptide validation: FDR min 5 %.

2.4.2 Gel-free AfBPP and dimethyl labeling

The procedure described under 2.4 was followed. The beads were resuspended with 200 µl denaturation buffer (7 M urea, 2 M thiourea in 20 mM pH 7.5 HEPES buffer). Dithiothreitol (DTT, 1 M, 0.2 µL) was added, the tubes were mixed by vortexing shortly and incubated in a thermomixer (450 rpm, 45 min, RT). Then 2-Iodoacetamide (IAA, 550 mM, 2 µL) was added, the tubes were mixed by vortexing shortly and incubated in a thermomixer (450 rpm, 30 min, RT, in the dark). Remaining IAA was quenched by the addition of dithiothreitol (DTT, 1 M, 0.28 µL). The tubes were shortly mixed by vortexing and incubated in a thermomixer (450 rpm, 30 min, RT). LysC (0.5 µg/µL) was thawed on ice and 1 µL was added to each microcentrifuge tube, the tubes were shortly mixed by vortexing and incubated in a thermomixer (450 rpm, 4 h, RT, in the dark). TEAB solution (600 µL, 50 mM in water) and then typsin (1.5 µL, 0.5 µg/µL in 50 mM acetic acid) were added to each tube with a short vortexing step after each addition. The microcentrifuge tubes were incubated in a thermomixer (450 rpm, 13-15 h, 37°C). The digest was stopped by adding 4 µL formic acid (FA) and vortexing. After centrifugation (100 xG, 1 min, RT) the supernatant was transferred to a new Protein LoBind Eppendorf tube. FA (50 µL, aqueous 0.1 % solution) was added to the beads and after vortexing and centrifugation (100 xG, 1 min, RT) the supernatant was added to the supernatant collected before. Again FA (50 µL, aqueous 0.1 % solution) was added to the beads and after vortexing and centrifugation (16200 xG, 3 min, RT) the supernatant was transferred to the combined supernatants. 50 mg SepPak C18 columns were equilibrated by gravity flow with 1 mL acetonitrile, 0.5 mL elution buffer (80 % ACN, 0.5 % FA) and 1 mL wash 1 (aqueous 0.1 % TFA solution). Subsequently the samples were loaded by gravity flow and washed with 1 mL wash 1 (aqueous 0.1 % TFA solution) and 0.5 mL wash 2 (aqueous 0.5 % FA solution). Elution into new 2.0 mL Protein LoBind Eppendorf tubes was performed by the addition of 250 µL elution buffer by gravity flow followed by 250 µL elution buffer by vacuum flow until all liquid was eluted from the column. The eluates (total volume should be about 1.2 mL for each sample) were lyophilized and reconstituted in 100 µL TEAB buffer (100 mM TEAB, 0.36 % FA, pH = 6) by pipetting up and down, vortexing and sonication (10 sec) with short centrifugation steps after each reconstitution step. Then 8 µL of fresh isotope labeling solution (light: 2 % CH_2O, 0.3 M $NaBH_3CN$, medium: 2 % CD_2O, 0.3 M $NaBH_3CN$, heavy: 2 % $^{13}CD_2O$, 0.3 M $NaBD_3CN$) were added and the tubes were mixed by vortexing, centrifuged briefly and incubated in a thermoshaker (450 rpm, 1 h, 25°C). Samples were cooled on ice for 3 min, quenched with 16 µL chilled 1 % ammonia solution and 8 µL chilled 5 % FA solution with brief vortexing and centrifugation steps after each addition. Differentially labeled peptide solutions were mixed in a new Protein LoBind Eppendorf tube, lyophilized and stored at -20°C. Before MS measurement the samples were dissolved in 30 µL 1 % FA by pipetting up and down, vortexing and sonication for 15 min (brief centrifugation after each step). VWR 0.45 µm centrifugal filter were equilibrated with two times 500 µL water, 500 µL 0.05 N NaOH and two times 500 µL 1 % FA (centrifugation of the filters: 16200 xG, 1 min, RT). The peptide solutions were filtered through the equilibrated filters (centrifugation: 16200 xG, 2 min, RT) and analyzed via HPLC-MS/MS as described in chapter 2.4.1 with a longer HPLC gradient (0.1 % FA, 5 % DMSO, gradient 112 min from 4 % ACN to 35 % ACN and then 4 min to 80 % ACN).

Peptide and protein identifications were performed using MaxQuant 1.3.0.5 software with Andromeda as search engine using following parameters: Carbamidomethylation of cysteines as fixed and oxidation of methionine as well as acetylation of N-termini as dynamic modifications, trypsin/P as the proteolytic enzyme, 4.5 ppm for precursor mass tolerance (main search ppm) and 0.5 Da for fragment mass tolerance (ITMS MS/MS tolerance). Searches were done against the Uniprot database for *S. aureus* NCTC 8325 (taxon identifier: 93061, downloaded on 8.5.2014) and USA 300 (taxon identifier: 367830, downloaded on 8.5.2014). Quantification was performed using dimethyl labeling with the following settings: light: DimethLys0, DimethNter0; medium: DimethLys4, DimethNter4 and heavy: DimethLys8, DimethNter8. Variable modifications were included for quantification. The I = L and requantify options were used. Identification was done with at least 2 unique peptides and quantification only with unique peptides.

2.4.3 Gel-based AfBPP without biotin enrichment

Bacteria were cultured according to chapter 2.1 without addition of compounds or DMSO in individual tubes. Bacterial 20 h cultures were collected in a 50 mL falcon tube and centrifuged at 6200 xG for 5 min at 4°C. The supernatant was disposed and the pellet was resuspended with PBS to get a suspension with OD_{600} = 40. To 198 µL of this suspension in a microcentrifuge tube 2 µL of photo probe solution in DMSO (or just DMSO as a control) were added and the tube was briefly mixed by vortexing. After 30 min incubation at RT in the dark the microcentrifuge tube was again mixed by vortexing and incubated for another 30 min at RT in the dark. The suspension was transferred into a transparent 24 well plate and irradiated for 15 min with UV light (UV low-pressure mercury-vapor fluorescent lamp, Philips TL-D 18W BLB). During irradiation a cool pack was placed under the 6 well plate. The irradiated bacterial suspension was transferred to a 1.5 mL microcentrifuge tube. After centrifugation (6200 xG, 2 min, 4°C) the supernatant was removed and the pellets were stored ON at -80°C.

Pellets were resuspended in 150 µL PBS (4°C) and transferred to a 'Precellys Glass Kit VK05S 0.5 mL' tube. Tubes were cooled on ice for about 5 min or longer and cells were lysed with the Precellys Homogeniser using two times lysis program 3 (5400 rpm, run number: 1, run time: 20 sec, pause: 5 sec). After each lysis run the tubes were cooled on ice for 5 min. The ball mill tubes were centrifuged (16200 xG, 10 min, 4°C) and 86 µL of supernatant were transferred to new 1.5 mL microcentrifuge tubes and treated with 10 µL gel-based AfBPP Mix (2 µL RhN_3 (Tetramethylrhodamine (TAMRA) Azide (Tetramethylrhodamine 5-Carboxamido-(6-Azidohexanyl)), 5-isomer (life technologies, T10182); 5 mM in DMSO), 2 µL fresh TCEP (50 mM in ddH_2O), 6 µL TBTA Ligand (1.667 mM in 80 % tBuOH and 20 % DMSO)). The final concentrations were: 104 µM RhN_3, 1.04 mM TCEP and 104 µM TBTA Ligand. The lysates were mixed by vortexing and 2 µL $CuSO_4$ solution (50 mM in ddH_2O) were added. The lysates were again mixed by vortexing and incubated for 1h at RT in the dark. Then 80 µL 2x Laemmli Sample Buffer were added, samples were mixed in a thermomixer (300 rpm, 3 min, 96°C) and analyzed via SDS PAGE (10 % agarose gel (PEQLAB Biotechnologie GmbH, Erlangen, PerfectBlue Dual Gel System, gels were prepared according to the manual), 3.5 h, 300 V, 8 µL fluorescent protein standard) and fluorescence imaging (GE Healthcare, ImageQuant LAS-4000).

2.5 Western blot analysis

Western blot analysis was performed with each 10µl of sterile filtered supernatants of compound- or DMSO-treated bacterial cultures. Protein SDS-PAGE gels were prepared with the Mini-PROTEAN Tetra Cell system (Bio-Rad) according to manufacturer's instructions using 12 % Mini Protean TGX gels (456-1043) from Bio-Rad. Blotting was performed with the Tetra Blotting Module (Bio-Rad) according to manufacturer's instructions using PVDF membranes. PVDF membranes were blocked in 5% skim milk in TBS-0.1% Tween20. Rabbit polyclonal anti-*Staphylococcus* alpha Hemolysin primary antibody (Abcam ab50536) was diluted 1:4000 in 5% skim milk in TBS-0.1% Tween20 an incubated at 4°C overnight for optimal binding and the goat antibody anti-Rabbit IgG (H+L) Poly-HRP Secondary Antibody (Thermo Fisher Scientific 32260) was used 1:10000 for detection with ECL .

2.6 Enterotoxin ELISA

Enterotoxin determination was performed with sterile filtered supernatants of compound- or DMSO-treated bacterial culture samples prepared according to chapter 2.1 and a Ridascreen set A,B,C,D,E immunoassay from R-Biopharm (R4101) (8). Supernatants (35 µL) were transferred to the supplied ELISA stripes for enterotoxins A-E including both positive and negative controls. After an incubation time for 1 h at 37°C supernatant was removed and 300 µL supplied washing buffer were added and removed again. This step was repeated 5 times. Subsequently, 100 µL of conjugate 1 (biotin-conjugated anti-SET antibody mix) was added to each well and incubated for 1h at 37°C. 5 washing steps with 300 µL washing buffer were performed. Then, 100 µL conjugate 2 (streptavidin-POD) was added per well and incubated for 30 min at 37°C. 5 washing steps with 300 µL washing buffer were performed. Then, 100 µl of substrate/chromophore solution was added to each well and the plate was incubated for 15 min in the dark. 100 µL stop reagent was added and gently mixed. Test wells were analyzed by measuring absorbance at 450 nm with absorbance at 630 nm as a reference.

2.7 Toxic shock syndrome toxin 1 (TSST-1) ELISA

The ELISA assay is based on Freed et al. (1982) [7], Yarwood et al. (2000) [8] and Tal-Gan et al. (2013) [9]. All standard reagents were purchased from Sigma-Aldrich and used according to enclosed instructions. Antibodies (prim. LTI101, sek. LTC101) and recombinant TSST-1 protein (rTT606) were purchased from Toxin Technology and ABTS substrate solution from Thermo Fisher Scientific (37615). 96-well polystyrene microtiter plates (Starlab) were coated by incubation with 100 µL rabbit anti-TSST-1 serum solution per well (serum diluted 1:100 in 0.05 M $NaHCO_3$, pH 9.6) and then incubated ON at 4°C. The wells of the microtiter plate were washed 3x with 200 µL PBS-T (PBS + 0.05 % Tween 20). To block the plate, 100 µL FCS solution (1 % fetal calf serum in PBS-T) were added and the plate was incubated for 15 min at RT. The wells were washed again 3x with 200 µL PBS-T. TSST-1 ELISA was performed with sterile filtered supernatants of compound or DMSO control treated bacterial culture samples (*S. aureus* Mu 50) prepared according to chapter 2.1. 100 µL of each supernatant (or suitable dilutions in B-medium) were added to the microtiter plate in triplicates. TSST-1 standards with known concentrations in B-medium were included. After incubation for 2 h at RT, the wells were washed 3x with 200 µL PBS-T and afterwards 100 µL anti-TSST-1 IgG horseradish peroxidase conjugate (conjugate diluted 1:300 in PBS-T) were added and the plate was incubated for 1 h at RT. The wells were washed 5x with 200 µL PBS-T and then 100 µL of 2,2'-azinobis(3-ehtylbenzthiazoline-sulfonic acid) solution (ABTS solution) were added. The absorbance at 405 nm was measured every 2.5 min with a plate reader. Remaining TSST-1 in percent was plotted against the logarithmic concentration of (*R**,*R**)-**3**. Logistic regression was then used to determine the corresponding EC_{50} value.

2.8 MTT protection assay

The aim was to measure cytotoxic effects of secreted, bacterial toxins in culture supernatants on the human alveolar epithelial cell line A549 cell line [10]. 5000-7000 cells per well were plated into a 96 well plate and cultivated in DMEM supplemented with 10 % FCS and 5 mM L-Glutamine at 37°C, 5 % CO_2 ON in order to reach approximately 50-70 % confluency. 100µl of sterile-filtered supernatants of compound- or DMSO-treated NCTC 8325 cultures, prepared according to chapter 2.1, were added onto the cell culture plates (in triplicates). Treated cells were incubated for 4 h at 37°C, 5 % CO_2. Supernatants from vehicle (DMSO) treated cultures and blank B-Medium served as controls. 20 µl MTT stock solution in PBS (5 mg/mL) were added and placed on a shaking table (300 rpm for 5 min) to thoroughly mix the MTT with the medium. After incubation (37°C, 5 % CO_2) for 2 h the medium was removed. Formazan (MTT metabolic product) was resuspended in 200 µl DMSO and placed on a shaking table (300 rpm for 5 min) to thoroughly mix the formazan with the solvent. Optical density was measured at 570 nm and background at 630 nm was subtracted. Metabolic activity of A549 cells treated with blank bacterial culture medium (B-medium) was set to 100 %. The metabolic activity of A549 treated with bacterial culture supernatants with DMSO or (*R*,R**)-**3** was expressed relative to the B-medium control. Mean values of three biological replicates ± SD were determined.

2.9 Long term compound resistance development assay

For investigation of *S. aureus* 8325 resistance development the following assay was applied. For each passage, 1 mL of B-medium was inoculated to 3.4 x 10^4 colony forming units per mL in 15 mL polystyrene culture tubes followed by addition of compound solution or the respective DMSO or 0.1 N NaOH control. Colony forming units were determined by optical density measurement at 600 nm and *S. aureus* 8325 growth curves. The cultures were then incubated 1 day shaking at 200 rpm and 37 °C. Hemolysis assay was performed as described above (chapter 2.3). Growth inhibition was determined via OD_{600} measurement after ON growth (chapter 2.3). Hemolysis and growth inhibition assay were performed in parallel based on ON cultures from glycerol stocks. A relative EC_{50} was determined: EC_{50} of compound treated bacteria / EC_{50} of control treated bacteria (DMSO control for (*R**,*R**)-**3** or 0.1 N NaOH control for ofloxacin [11]). EC_{50} for (*R**,*R**)-**3** was determined via hemolysis assay and EC_{50} for ofloxacin via growth inhibition assay. Hemolysis and growth inhibition assay were performed in parallel based on ON cultures from glycerol stocks prepared at passage 1, 4, 8 and 12 cultures (Figure 5) or 1, 15, 30 and 45 (Supporting Information, Figure S10).

2.10 RNA Sequencing

Bacteria were cultured according to chapter 2.1 in a 15 mL culture with 100 µM (31.7 µg/mL) (*R**,*R**)-3. Isolation of the RNA from 1x10^9 bacteria/sample was done with Precellys Bacterial/Fungal RNA Kit (12-7611-01) including a DNAse I digest. RNA was eluted with 43 µL RNAse free ddH_2O. The samples were stored at -80°C. Terminator 5'-phosphate-dependent exonuclease (TEX) (Epicentre #TER51020) treatment, library construction, sequencing, read mapping, coverage plot construction and data analysis were done according to Dugar et al. [12]. The pairwise expression comparison based on these gene quantifications was done with READemption's subcommand "deseq" with relies on DESeq version 1.12.1. Genes with a log2 fold-change of > 1 or < 1 and p value < 0.05 were considered as differentially expressed. 48 genes were up- and 149 genes were downregulated. Functional annotation based on official gene symbols (SAOUHSC) was done with the Database for Annotation, Visualization and Integrated Discovery (DAVID) using default settings for functional annotation clustering.[13, 14] Virulence genes were identified searching the DAVID functional annotation table for the terms: virulence, pathogenesis, cell killing and cytolysis.

The raw, de-multiplexed reads have been deposited in the National Center for Biotechnology Information's Gene Expression Omnibus (GEO)[15] and are accessible via the GEO accession GSE64747 (http://www.ncbi.nlm.nih.gov/geo/query/acc.cgi?acc=GSE64747).

2.11 Phage transduction

Transposon mutations were transferred from USA 300 Lac into NCTC 8325 strain using phage transduction.[16] The USA 300 Lac mutant strain from the NARSA library [17] was grown with erythromycin (1:1000; 10 mg/mL in EtOH stock solution) in 20 mL B broth at 37°C and 200 rpm ON. Subsequently, 100 µL of 1 M $CaCl_2$ were added. 300 µL of culture were heated in 15 mL falcon tubes for 2 min in a 52°C water bath to inactivate restriction enzymes. Phage lysate containing page ϕ11 was diluted 1:10 and 1:100 in LB broth with 5 mM $CaCl_2$ and 100 µL of the dilutions were added to the heated bacterial culture samples and mixed by vortexing. Additionally, control samples without phages and without bacteria were prepared. After 2.5 h incubation at RT 4 mL of 55°C soft agar I (LB broth, 0.6% agar, 5 mM $CaCl_2$) were added and the mixtures were poured onto LB agar plates. After incubation of the plates ON at 37°C the soft agar layers were swept of and transferred into 50 mL falcon tubes, mixed by vortexing and centrifuged for 20 min at 5000 xG. Supernatants were passed through 0.45 nm sterile filters and stored at 4°C.

The NCTC 8325 recipient strain was grown in 10 mL B broth at 37°C and 200 rpm ON and 50 µL of 1 M $CaCl_2$ was added. 300 µL of culture were heated in 15 mL falcon tubes for 2 min in a 52°C water bath to inactivate restriction enzymes. Phage supernatant obtained before was diluted 1:10 and 1:100 in LB broth with 5 mM $CaCl_2$ and 100 µL of the dilutions were added to the heated bacterial culture samples and mixed by vortexing. Additionally, control samples without phage supernatant and without bacteria were prepared. After 30 min incubation at RT 4 mL of 55°C soft agar II (LB broth, 0.6% agar, 20 mM Na_3−Citrate) were added and the mixtures were poured onto LB agar plates. After incubation of the plates for 2-4 days at 37°C TN mutant colonies (in NCTC 8325 background) could be picked.

2.12 Plasma stability

The compound stability in plasma was determined by addition of 100 µM compound of interest to 250 µl of undiluted plasma at 37°C. Human and mouse plasma were purchased lyophilized from Sigma (P9275, P9523) and reconstituted according to the manufacturer's protocol. Final assay concentration of DMSO from compound stocks was 1 %. Procaine-HCL purchased from Sigma-Aldrich (P9879) was used as positive control. Directly after test compound addition the reaction mixture was shortly mixed by vortexing and the first sample of 25 µl was withdrawn. Every sample was quenched immediately by the addition 30 µl of pre-chilled acetonitrile. The reaction mixture was incubated at 37°C with gentle shaking at 600 rpm. For every test compound additional 25 µl samples were taken at several time-points (5, 10, 20, 30, 60, 120, 240 min), quenched as described and stored at -20°C. For analysis by LC-MS all samples were thawed and centrifuged for 5 min at 13000 rpm. The supernatants were filtered through modified nylon centrifugal filters (0.45 µM) and transferred to LS-MS glass vials. Quantitative LC-MS analysis was performed by LCQ-Fleet Ion Trap Mass Spectrometer equipped with an APCI ion source and a DionexHPLC system using a Waters Xbridge BEH130 C18 column (5 µM 4.6 x 100 mm). Data analysis was performed by Thermo Scientific™ Xcalibur™ software. Shortly, ion peaks from single ion monitoring mass detection were integrated. Peak areas at 0 min were set to 100 % and peak decline with time was expressed relative to 100 % at t = 0 min.

2.13 Metabolic stability *in vitro*

The metabolic stability of compounds towards liver enzymes through phase-1 metabolism was determined in both human and mouse microsomes purchased from Sigma-Aldrich (M9441, M0317). Compounds were diluted in DMSO to a final concentration of 1 or 10 mM. These stocks were used as 100x stocks for the final assay (assay concentration was 10-100 µM). In a 96-well plate 98.8 µl of 0.1 M phosphate buffer were distributed per well. Then, 12.5 µl of a 30 mM stock NADPH were added to all wells except for negative controls which obtained 0.1 M phosphate buffer instead. Each test compound was tested in three wells. Two wells were tested for metabolization in the presence of NADPH and the third well served as negative control without the cofactor. 1.25 µl of 100x compound stock were added to each of these wells. Subsequently, the 96-well plate was incubated at 37°C for 5 min with gentle agitation (300 rpm). Meanwhile, the microsomal suspension was thawed on ice and diluted to 5 mg/mL in 0.1 M phosphate buffer pH 7.4. The metabolic reaction started by the addition of 12.5 µl of microsomes in each well of the test plate. Immediately after microsomal addition the reaction was mixed thoroughly by pipetting and the first sample was withdrawn (50 µl) and quenched with 50 µl ice-cold acetonitrile. Quenched samples were stored at -20°C until further processing. The reaction plate was incubated at 37°C and gentle agitation. At t = 60 min the second reaction sample was withdrawn and quenched and stored at -20°C if not processed directly. For analysis by LC-MS all samples were thawn and centrifuged for 5 min at 13000 rpm. The supernatants were filtered through modified nylon centrifugal filters (0.45 µM) and transferred to LS-MS glass vials. Quantitative LC-MS analysis was performed by LCQ-Fleet Ion Trap or LTQ-FT (HRMS) mass spectrometer equipped with an APCI ion source and a DionexHPLC system using a Waters Xbridge BEH130 C18 column (5 µM 4.6 x 100 mm). Data analysis was performed by Thermo Scientific™ Xcalibur™ software. Shortly, ion peaks from single ion monitoring mass detection were integrated. Peak areas at 0 min were set to 100 % and the remaining fraction of test compound was determined.

3 *In vivo* experiments

All animal experiments were approved by the Regierung von Oberbayern (Germany), and conducted according to this approval (license number: 55.2-1/54-2531-114/10) and to the German Law for Animal Protection (Deutsches Tierschutzgesetz).

3.1 Pharmakokinetics i.v. and i.p.

In order to determine pharmacokinetic properties, test compounds were formulated in an appropriate vehicle. For intravenous (i.v.) injections (*R**,*R**)-**3** was solubilized in 10 % Cremophor EL (C5135 from Sigma-Aldrich) + 20 % EtOH in PBS at an envisaged concentration of 4.8 mg/ml (15 mM) at 55°C for 1 h and ultrasonication. Subsequently, the injection solution was sterile filtered (pore size 0.22 µm) and the precise concentration and compound stability was determined by analytical HPLC (determined concentration was 4.2 mg/ml). 100 µl of injection solution were administered into the tail vein of Balb/cOlaHsd mice. In order to determine pharmakokinetics parameter upon intraperitoneal injection (i.p.) (*R**,*R**)-**3** was solubilized in DMSO 10 % in sterile corn oil (C8267 from Sigma-Aldrich) to give a concentration of 31.7 mg/ml (100 mM). For both types of administration routes the group size was 4 mice (n = 4) using 3 groups and an alternating blood withdrawal scheme in order to obtain 8 time points in total at 0, 5, 15, 30, 60, 120, 180, 300 min (& 24 hours only for i.p. administration). At the beginning of the experiment every mouse obtained an amount 100 µl either i.v. or i.p. corresponding to a dose of 0.48 mg (24 mg per kg body weight) or 3.17 mg (159 mg per kg body weight), respectively. At each time point 50-100 µl blood per animal were collected either submandibularly or by cardiac puncture directly into the collection tube (Mini collect 0.8 mL, Li-Heparin with gel, Greiner BioOne). Each tube was inverted 3 times immediately after collection and spun down using a table top mini centrifuge until plasma separation was completed (2-3 min). Plasma was transferred into a new Eppendorf tube and snap frozen on dry ice and further stored at -20°C for no longer than 1 week. For analysis by LC-MS all samples were thawed and quenched by acetonitrile protein precipitation (1:1 v/v), then centrifuged for 5 min at 13000 rpm. The supernatants were filtered through modified nylon centrifugal filters (0.45 µM) and transferred to LC-MS glass vials. For absolute quantification a standard of serial dilutions was prepared in heat-inactivated fetal calf serum and prepared for LC-MS accordingly. Quantitative LC-MS analysis was performed by LCQ-Fleet Ion Trap or LTQ-FT (HRMS) mass spectrometer equipped with an APCI ion source and a Dionex HPLC system using a Waters Xbridge BEH130 C18 column (5 µM 4.6 x 100 mm). Data analysis was performed by Thermo Scientific™ Xcalibur™ software. Using the external standards the absolute plasma concentrations were determined. The average compound concentrations in mg/L (C_p) were plotted against time [h]. Using average compound concentrations for each time point the area under the curve (AUC) [h mg/L] was determined via the trapezoid rule with the remaining area estimated as the value of the final C_p point divided by the k_{el} value. The values for rate constant k_{el}, k_{abs} and for C_p^0 (C_p at time = 0) were determined by linear fitting of ln(C_p) over time plots. Absorption and elimination phase were fitted separately. The point of time where the maximum i.p. C_p level was reached was calculated from the rate constants by the following equation:

$$t_{\max} = \frac{\ln k_{el} - \ln k_{abs}}{k_{el} - k_{abs}}$$

Half life ($t_{1/2}$), clearance (CL) and volume of distribution (V_d) were determined by the following equations (D_0 = applied dose):

$$t_{1/2} = \frac{\ln(2)}{k} \qquad CL = \frac{D_0}{AUC} \qquad V_d = \frac{CL}{k_{el}}$$

3.2 Mouse skin abscess model for efficacy testing

In order to prepare the inoculum for animal infection, *S. aureus* USA 300 BAA1717 was cultured in BHB-medium to the mid-exponential phase of growth in BHB medium, washed three times in PBS, and diluted in PBS to the concentration of 2.2x10^6 CFU/µl and stored on ice. Next, female Crl:SKH1-Hr^{hr} mice (6–8 weeks old; Charles River) were anesthetized by intraperitoneal injection of a saline solution containing fentanyl (0.05 mg/kg), midazolam (5 mg/kg), and medetomidine (0.5 mg/kg). The backs of the animals were disinfected with 70 % ethanol, and a suspension of 60 µL with 1.3x10^8 CFU in PBS was inoculated subcutaneously. Subsequent to infection, anesthesia was terminated by subcutaneous injection of a saline solution containing buprenorphine (0.1 mg/kg), atipamezol (2.5 mg/kg), and flumazenil (0.5 mg/kg) into the neck region. Treatment of mice was performed by intraperitoneal injection of 100 µL of vehicle (10 % DMSO in corn oil, C8267 from Sigma-Aldrich) or 100 µL of compound (*R**,*R**)-**3** (100 mM (*R**,*R**)-**3** dissolved in 10 % DMSO in corn oil) respectively (dose: 3.17 mg (159 mg/kg). Treatment was performed at following time points: 1 h pre-infection, 5 h post-infection and 17 h post-infection. Mice were weighed before infection. Weight and abscess area were monitored for 10 days. The length (*L*) and width (*W*) of abscesses were determined using a caliper. The size of the abscesses was then calculated with the standard formula for area: $A = [\pi/2] \times L \times W$. Abscess areas from vehicle-treated animals at day 1 were set to 100 %.

REFERENCES

[1] M. Gersch, F. Gut, V. S. Korotkov, J. Lehmann, T. Bottcher, M. Rusch, C. Hedberg, H. Waldmann, G. Klebe and S. A. Sieber, *Angew. Chem., Int. Ed.* **2013**, *52*, 3009-3014.

[2] J. Taubitz and U. Lüning, *Eur. J. Org. Chem.* **2008**, *2008*, 5922-5927.

[3] E. Zeiler, V. S. Korotkov, K. Lorenz-Baath, T. Bottcher, S. A. Sieber, *Bioorganic & medicinal chemistry* **2012**, *20*, 583-591.

[4] T. Bottcher and S. A. Sieber, *ChemBioChem* **2009**, *10*, 663-666.

[5] M. R. Maurizi, M. W. Thompson, S. K. Singh and S. H. Kim, *Methods Enzymol.* **1994**, *244*, 314-331.

[6] J. Eirich, J. L. Burkhart, A. Ullrich, G. C. Rudolf, A. Vollmar, S. Zahler, U. Kazmaier and S. A. Sieber, *Mol. BioSyst.* **2012**, *8*, 2067-2075.

[7] R. C. Freed, M. L. Evenson, R. F. Reiser and M. S. Bergdoll, *Appl. Environ. Microbiol.* **1982**, *44*, 1349-1355.

[8] J. M. Yarwood and P. M. Schlievert, *J. Clin. Microbiol.* **2000**, *38*, 1797-1803.

[9] Y. Tal-Gan, D. M. Stacy, M. K. Foegen, D. W. Koenig and H. E. Blackwell, *J. Am. Chem. Soc.* **2013**, *135*, 7869-7882.

[10] M. Luo, J. Qiu, Y. Zhang, J. Wang, J. Dong, H. Li, B. Leng, Q. Zhang, X. Dai, X. Niu, S. Zhao and X. Deng, *J. Microbiol. Biotechnol.* **2012**, *22*, 1170-1176.

[11] L. L. Ling, T. Schneider, A. J. Peoples, A. L. Spoering, I. Engels, B. P. Conlon, A. Mueller, T. F. Schaberle, D. E. Hughes, S. Epstein, M. Jones, L. Lazarides, V. A. Steadman, D. R. Cohen, C. R. Felix, K. A. Fetterman, W. P. Millett, A. G. Nitti, A. M. Zullo, C. Chen and K. Lewis, *Nature* **2015**, *517*, 455-459.

[12] G. Dugar, A. Herbig, K. U. Forstner, N. Heidrich, R. Reinhardt, K. Nieselt and C. M. Sharma, *PLoS Genet.* **2013**, *9*, e1003495.

[13] D. W. Huang, B. T. Sherman and R. A. Lempicki, *Nat. Protoc.* **2008**, *4*, 44-57.

[14] D. W. Huang, B. T. Sherman and R. A. Lempicki, *Nucleic Acids Res.* **2009**, *37*, 1-13.

[15] R. Edgar, M. Domrachev and A. E. Lash, *Nucleic Acids Res.*, 2002, **30**, 207-210.

[16] L. Rudin, J. E. Sjostrom, M. Lindberg and L. Philipson, *J. Bacteriol.* **1974**, *118*, 155-164.

[17] NARSA, Network on Antimicrobial Resistance in Staphylococcus aureus: Chantilly, Virginia; Vol. **2014**.

APPENDIX, NMR SPECTRA

(*Z*)-2-((1-((*tert*-butyldimethylsilyl)oxy)-hept-1-enyl)thio)pyridine

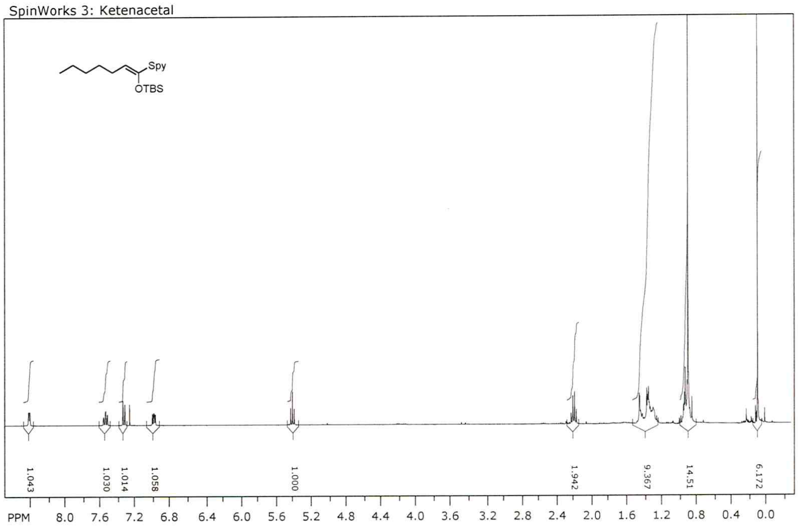

```
file: D:\Spektren\vk568\10\fid   expt: <zg30>                  freq. of 0 ppm: 360.130000 MHz
transmitter freq.: 360.132224 MHz                              processed size: 32768 complex points
time domain size: 65536 points                                 LB: 0.000    GF: 0.0000
width: 7440.48 Hz = 20.6604 ppm = 0.113533 Hz/pt               Hz/cm: 129.574    ppm/cm: 0.35980
number of scans: 16
```

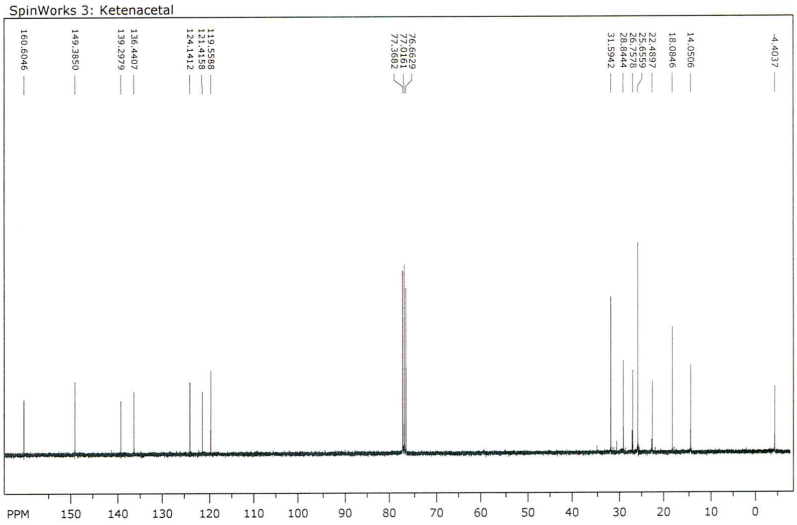

```
file: D:\Spektren\vk568\11\fid   expt: <zgpg30>                freq. of 0 ppm: 90.554761 MHz
transmitter freq.: 90.563816 MHz                               processed size: 32768 complex points
time domain size: 65536 points                                 LB: 0.000    GF: 0.0000
width: 21645.02 Hz = 239.0030 ppm = 0.330277 Hz/pt             Hz/cm: 625.491    ppm/cm: 6.90664
number of scans: 1024
```

(3R^*,4R^*)-3-Pentyl-4-(2-phenylethyl)oxetan-2-one

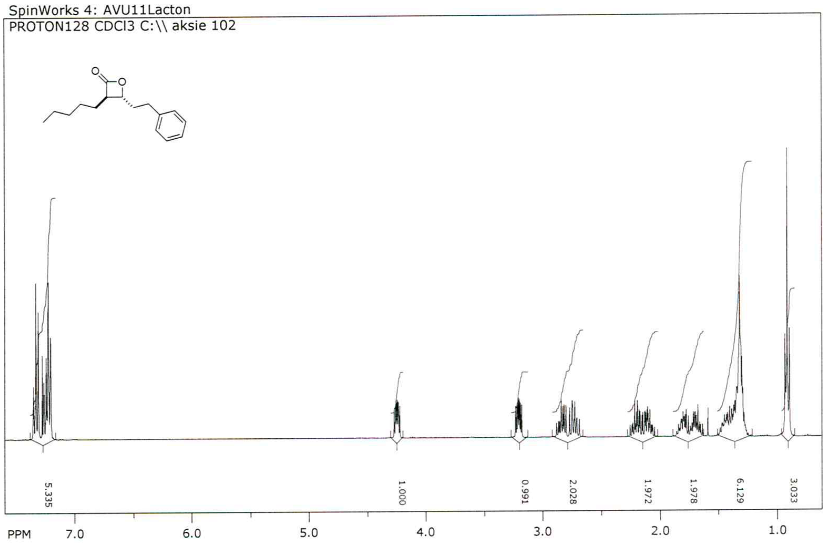

file: D:\Spektren\vk571rein\10\fid   expt: <zg30>
transmitter freq.: 360.132224 MHz
time domain size: 65536 points
width: 7440.48 Hz = 20.6604 ppm = 0.113533 Hz/pt
number of scans: 128

freq. of 0 ppm: 360.130000 MHz
processed size: 32768 complex points
LB: 0.000   GF: 0.0000

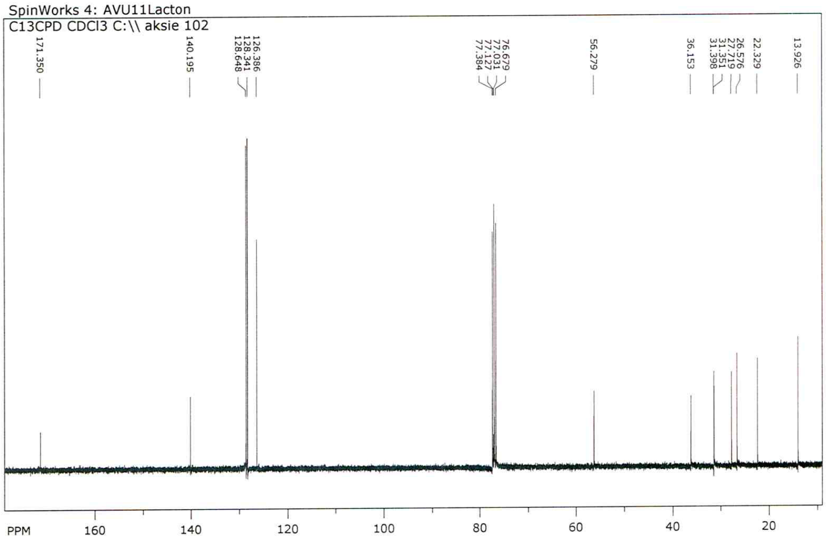

file: D:\Spektren\vk571rein\11\fid   expt: <zgpg30>
transmitter freq.: 90.563816 MHz
time domain size: 65536 points
width: 21645.02 Hz = 239.0030 ppm = 0.330277 Hz/pt
number of scans: 1024

freq. of 0 ppm: 90.554761 MHz
processed size: 32768 complex points
LB: 0.000   GF: 0.0000

(2*S**, 3*R**)-3-Hydroxy-2-(non-8-enyl)-5-phenylpentanoic acid

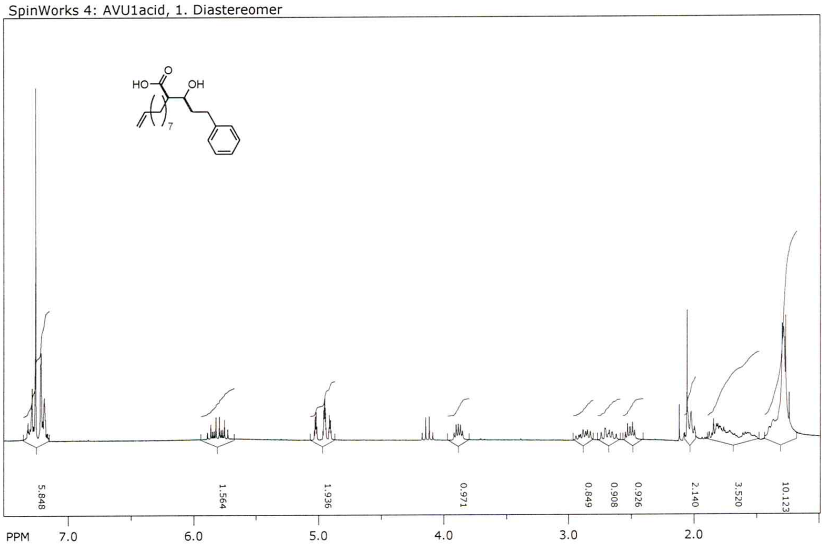

```
file: D:\Spektren\vk579-1\10\fid   expt: <zg30>
transmitter freq.: 250.131545 MHz
time domain size: 65536 points
width: 5175.98 Hz = 20.6930 ppm = 0.078979 Hz/pt
number of scans: 128
```

```
freq. of 0 ppm: 250.130000 MHz
processed size: 32768 complex points
LB: 0.000    GF: 0.0000
```

(2*R**, 3*R**)-3-Hydroxy-2-(non-8-enyl)-5-phenylpentanoic acid

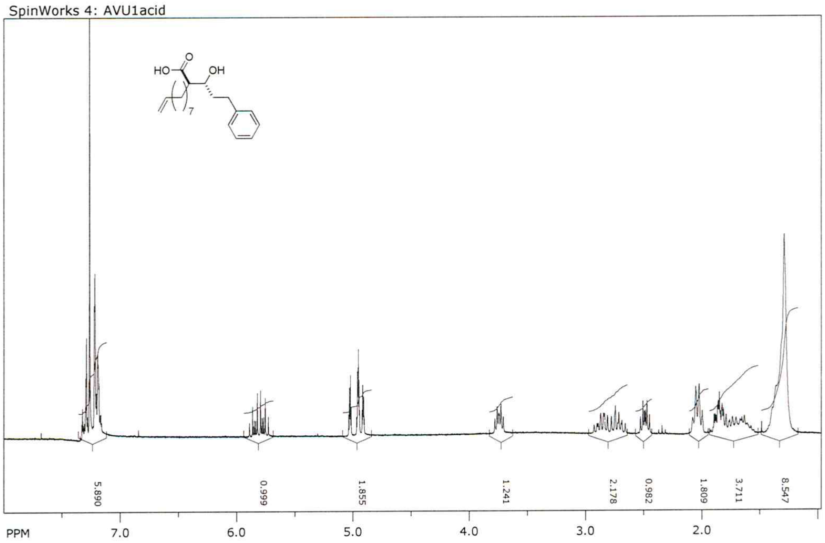

```
file: D:\Spektren\vk585rein\10\fid   expt: <zg30>
transmitter freq.: 250.131545 MHz
time domain size: 65536 points
width: 5175.98 Hz = 20.6930 ppm = 0.078979 Hz/pt
number of scans: 128
```

```
freq. of 0 ppm: 250.130000 MHz
processed size: 32768 complex points
LB: 0.000    GF: 0.0000
```

(2*R**,3*R**)-3-Hydroxy-2-pentyl-5-phenylpentanamide

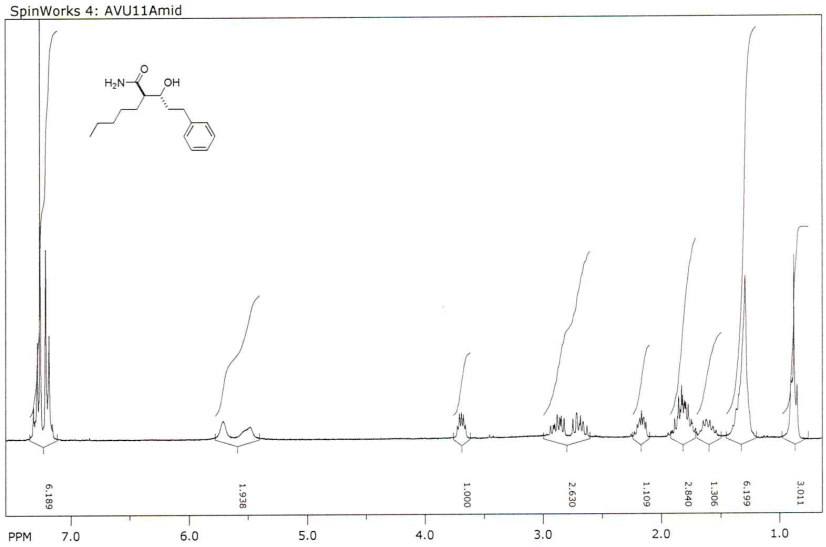

file: D:\Spektren\vk572\10\fid expt: <zg30>
transmitter freq.: 250.131545 MHz
time domain size: 65536 points
width: 5175.98 Hz = 20.6930 ppm = 0.078979 Hz/pt
number of scans: 128

freq. of 0 ppm: 250.130000 MHz
processed size: 32768 complex points
LB: 0.000 GF: 0.0000

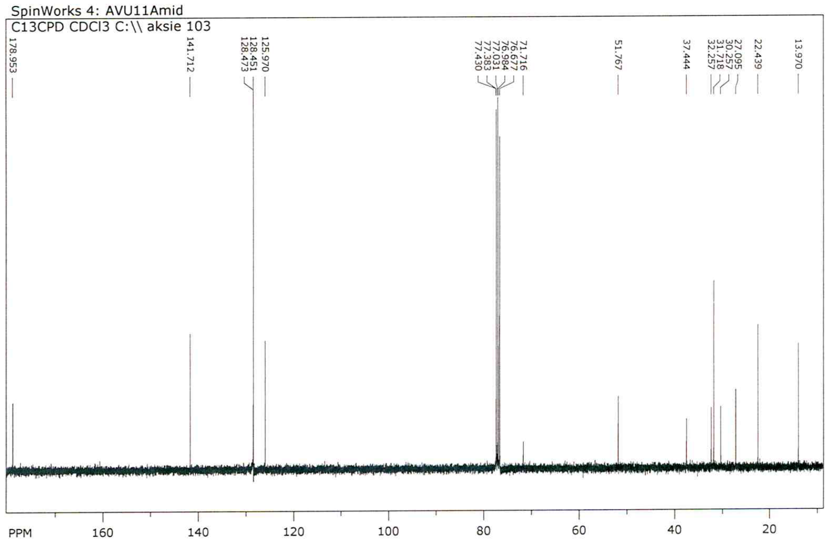

file: D:\Spektren\vk572\11\fid expt: <zgpg30>
transmitter freq.: 90.563816 MHz
time domain size: 65536 points
width: 21645.02 Hz = 239.0030 ppm = 0.330277 Hz/pt
number of scans: 1024

freq. of 0 ppm: 90.554761 MHz
processed size: 32768 complex points
LB: 0.000 GF: 0.0000

(2*R**,3*S**)-3-Hydroxy-2-(non-8-enyl)-5-phenylpentanamide

SpinWorks 3: PROTON128 CDCl3 C:\\ aksie 5

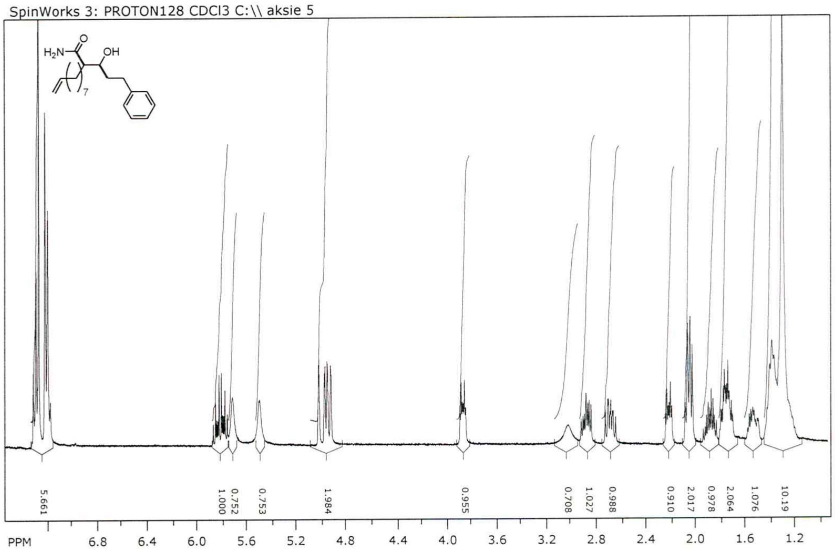

file: D:\Spektren\vk580\20\fid   expt: <zg30>
transmitter freq.: 360.132224 MHz
time domain size: 65536 points
width: 7440.48 Hz = 20.6604 ppm = 0.113533 Hz/pt
number of scans: 128

freq. of 0 ppm: 360.130000 MHz
processed size: 32768 complex points
LB: 0.000   GF: 0.0000
Hz/cm: 95.341   ppm/cm: 0.26474

SpinWorks 4: (R,S)-AVU1Amid
C13CPD CDCl3 C:\\ aksie 79

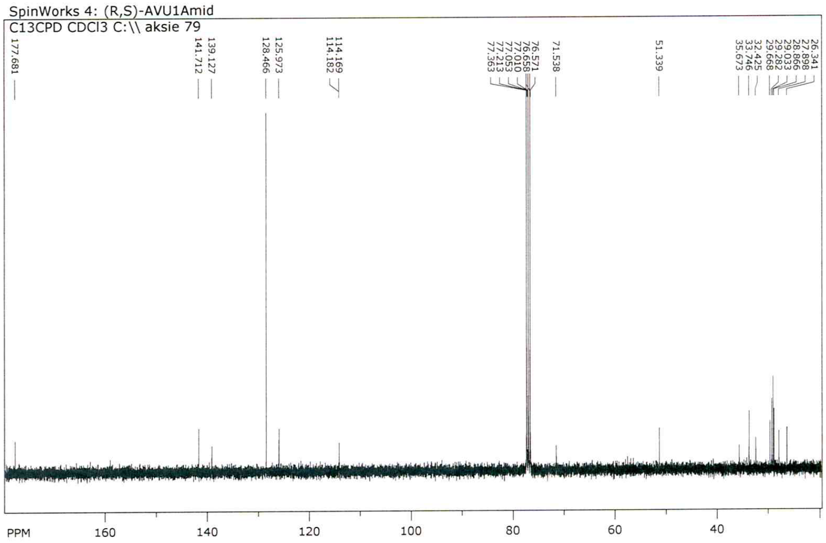

file: D:\Spektren\vk580\30\fid   expt: <zgpg30>
transmitter freq.: 90.563816 MHz
time domain size: 65536 points
width: 21645.02 Hz = 239.0030 ppm = 0.330277 Hz/pt
number of scans: 1024

freq. of 0 ppm: 90.554761 MHz
processed size: 32768 complex points
LB: 0.000   GF: 0.0000

(2*R**,3*R**)-3-Hydroxy-2-(non-8-enyl)-5-phenylpentanamide

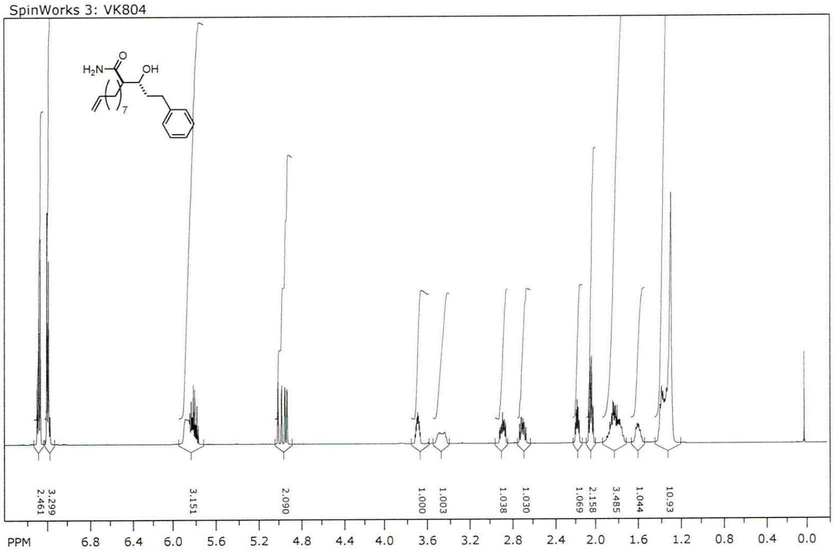

file: D:\Spektren\VK804\10\fid expt: <zg30>
transmitter freq.: 500.363002 MHz
time domain size: 65536 points
width: 9014.42 Hz = 18.0158 ppm = 0.137549 Hz/pt
number of scans: 128

freq. of 0 ppm: 500.360000 MHz
processed size: 65536 complex points
LB: 0.000 GF: 0.0000
Hz/cm: 156.412 ppm/cm: 0.31260

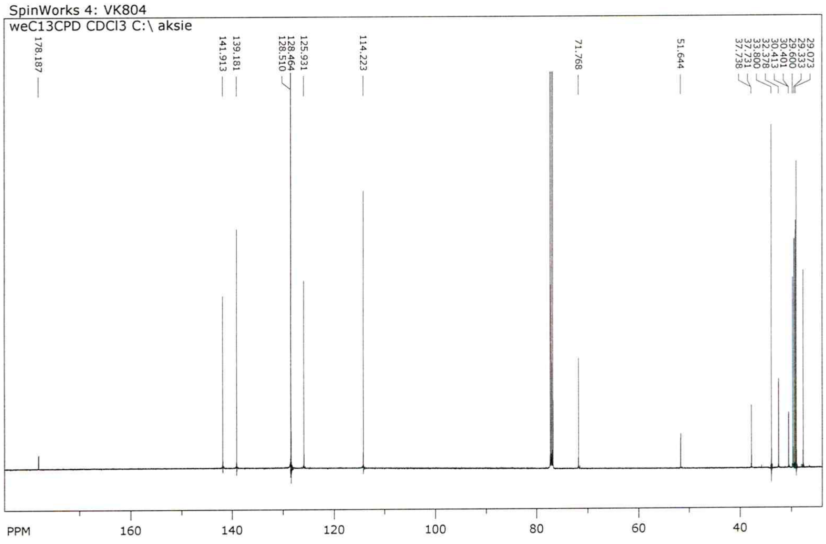

file: D:\Spektren\VK804\11\fid expt: <zgpg30>
transmitter freq.: 125.829462 MHz
time domain size: 65536 points
width: 32894.74 Hz = 261.4232 ppm = 0.501934 Hz/pt
number of scans: 1024

freq. of 0 ppm: 125.815622 MHz
processed size: 131072 complex points
LB: 0.000 GF: 0.0000

(*R**,*S**)-5-(4-Benzoylphenyl)-3-hydroxy-2-(8-noninyl)-pentanamide

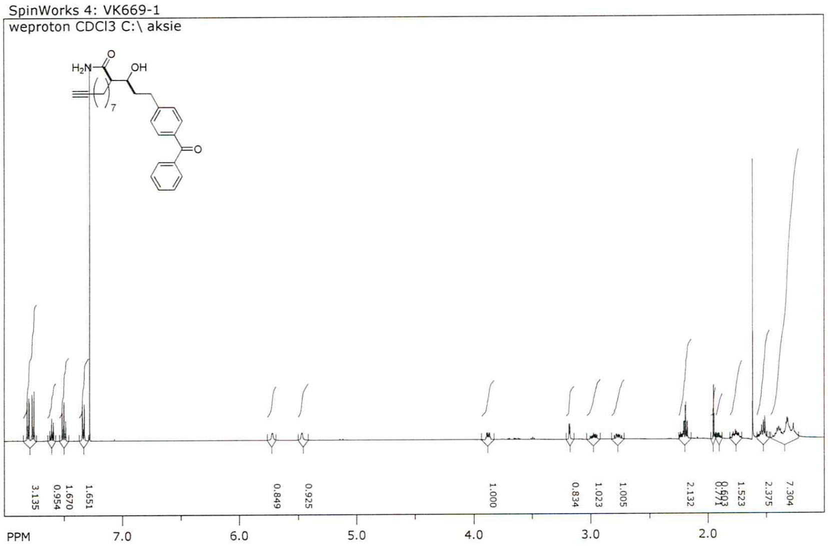

file: D:\Spektren\VK669-1\10\fid   expt: <zg30>
transmitter freq.: 500.363002 MHz
time domain size: 65536 points
width: 9014.42 Hz = 18.0158 ppm = 0.137549 Hz/pt
number of scans: 128

freq. of 0 ppm: 500.360000 MHz
processed size: 65536 complex points
LB: 0.000   GF: 0.0000

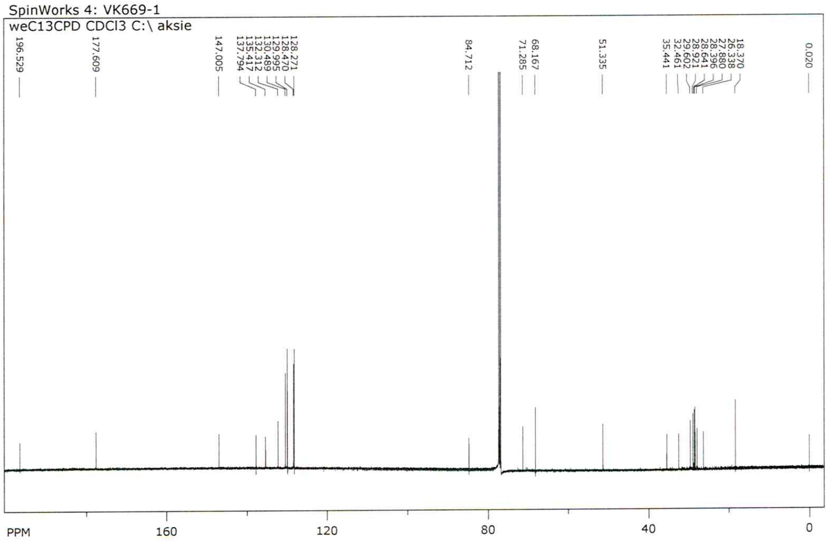

file: D:\Spektren\VK669-1\11\fid   expt: <zgpg30>
transmitter freq.: 125.829462 MHz
time domain size: 65536 points
width: 32894.74 Hz = 261.4232 ppm = 0.501934 Hz/pt
number of scans: 512

freq. of 0 ppm: 125.815622 MHz
processed size: 131072 complex points
LB: 0.000   GF: 0.0000

(*R**,*R**)-5-(4-Benzoylphenyl)-3-hydroxy-2-(8-noninyl)-pentanamide

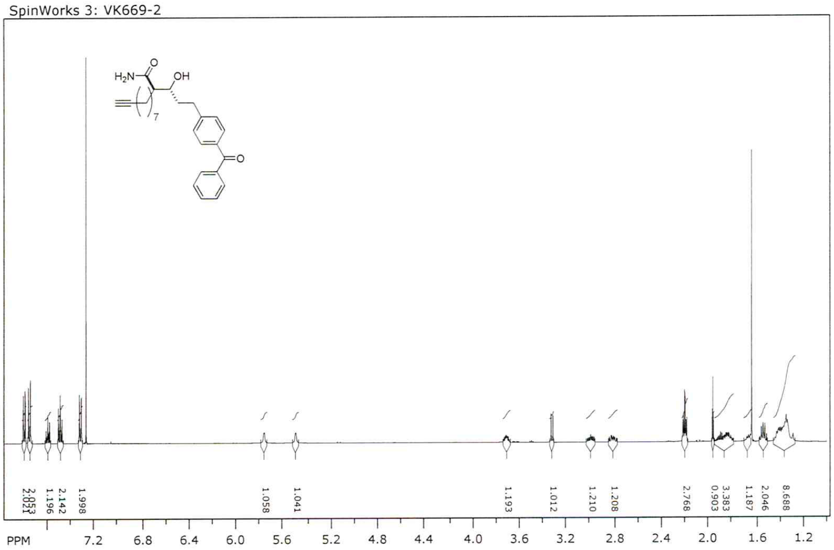

file: D:\Spektren\VK669-2\10\fid expt: <zg30>
transmitter freq.: 500.363002 MHz
time domain size: 65536 points
width: 9014.42 Hz = 18.0158 ppm = 0.137549 Hz/pt
number of scans: 128

freq. of 0 ppm: 500.360000 MHz
processed size: 65536 complex points
LB: 0.000 GF: 0.0000
Hz/cm: 139.888 ppm/cm: 0.27957

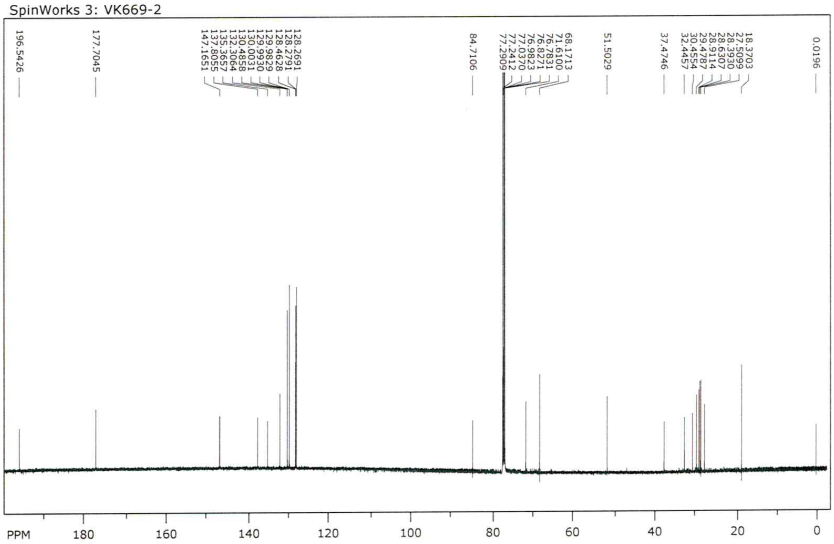

file: D:\Spektren\VK669-2\11\fid expt: <zgpg30>
transmitter freq.: 125.829462 MHz
time domain size: 65536 points
width: 32894.74 Hz = 261.4232 ppm = 0.501934 Hz/pt
number of scans: 512

freq. of 0 ppm: 125.815622 MHz
processed size: 131072 complex points
LB: 0.000 GF: 0.0000
Hz/cm: 1021.537 ppm/cm: 8.11842

HUMAN LYSOSOMAL ACID LIPASE INHIBITOR LALISTAT IMPAIRS MYCOBACTERIUM TUBERCULOSIS GROWTH BY TARGETING BACTERIAL HYDROLASES

Published in Medicinal Chemical Communications **2016**, by Johannes Lehmann,* Jan Vomacka,* Knud Esser,* Matthew Nodwell, Katharina Kolbe, Patrick Rämer, Ulrike Protzer, Norbert Reiling and Stephan A. Sieber.

*contributed equally

Reproduced from J. Lehmann, J. Vomacka, K. Esser, M. Nodwell, K. Kolbe, P. Rämer, U. Protzer, N. Reiling and S. A. Sieber, *Med. Chem. Commun.*, **2016**, DOI: 10.1039/C6MD00231E with permission from The Royal Society of Chemistry.

SUMMARY

Lalistat inhibits growth of *Mycobacterium tuberculosis* in bacterial culture as well as in infected macrophages. Target identification by quantitative proteomics revealed a cluster of 20 hydrolytic proteins including members of the lipase family. Lipases are essential for *M. tuberculosis* fatty acid production and energy storage thus representing promising antibiotic targets.

This summary is the abstract accompanying the publication.

AUTHOR CONTRIBUTIONS

S.A. Sieber, K. Esser, M. Nodwell, N. Reiling and U. Protzer conceived and supervised the project. J. Lehmann and M. Nodwell synthesized all chemical compounds. K. Kolbe, J. Lehmann, P. Rämer and N. Reiling performed all biological experiments with bacterial cultures. Target identification and validation was done by J. Vomacka, K. Kolbe and J. Lehmann. J. Vomacka, K. Esser, J. Lehmann, S.A. Sieber and N. Reiling wrote the manuscript.

Published on 21 July 2016. Downloaded by Cornell University Library on 21/07/2016 16:20:15.

MedChemComm

RESEARCH ARTICLE

View Article Online
View Journal

Cite this: DOI: 10.1039/c6md00231e

Human lysosomal acid lipase inhibitor lalistat impairs *Mycobacterium tuberculosis* growth by targeting bacterial hydrolases†‡

J. Lehmann,§[a] J. Vomacka,§[a] K. Esser,§[b] M. Nodwell,[a] K. Kolbe,[c] P. Rämer,[d] U. Protzer,[be] N. Reiling*[c] and S. A. Sieber*[a]

Received 26th April 2016,
Accepted 12th July 2016

DOI: 10.1039/c6md00231e

www.rsc.org/medchemcomm

Lalistat inhibits growth of *Mycobacterium tuberculosis* in bacterial culture as well as in infected macrophages. Target identification by quantitative proteomics revealed a cluster of 20 hydrolytic proteins including members of the lipase family. Lipases are essential for *M. tuberculosis* fatty acid production and energy storage thus representing promising antibiotic targets.

Tuberculosis (TB) is one of the world's most prevalent diseases responsible for the largest fraction of infection related casualties.[1] The disease is caused by *Mycobacterium tuberculosis* a pathogen difficult to treat by standard antibiotics requiring therapies with a combination of drugs such as isoniazid, rifampicin, ethambutol and pyrazinamide. Moreover, in recent years a strong increase in multidrug-resistant (MDR) TB cases (resistant to at least isoniazid and rifampicin) was observed. It is estimated that around 9% of MDR TB samples were also extensively drug-resistant (XDR) TB, *i.e.*, resistant to isoniazid and rifampin and to at least one representative of each class of the most effective second-line drugs (*i.e.*, fluoroquinolones and the injectable drugs kanamycin, amikacin, or capreomycin).[1] This augments the challenge of treatment and requires new and more efficient drug development strategies. However, these are challenged by a limited number of exploited targets and impaired uptake of small molecule drugs by the highly impermeable mycobacterial cell wall.[2]

M. tuberculosis is transmitted by aerosol and is initially taken up by alveolar macrophages, which phagocytose but do not kill the bacterium. Most infected individuals can immunologically control the disease. It is assumed that one-third of the world's population is latently infected. The bacteria adapt and survive in diverse environmental niches *in vivo*, *e.g.* in solid granulomas, a characteristic feature of latent TB infection.[3] It is presumed that *M. tuberculosis* resides in these regions in a slow growing or non-replicating, phenotypically drug resistant dormant-like state, due to limited availability and supply of oxygen and nutrients.[3,4] During infection experiments it has been shown that *M. tuberculosis* accumulates triacylglycerols (TAGs) within intracellular inclusion bodies.[5–7] The hydrolysis of TAGs to free fatty acids is an essential prerequisite for *M. tuberculosis* growth and survival requiring diverse lipases and hydrolases.[6,8–10] During infection the liberation of fatty acids represents an important energy source[11] triggered by the availability of lipids in the host cell.[12] Moreover, it is believed that these fatty acids are crucial for bacteria to enter and maintain the dormant state by the production of foamy lung macrophages during latent infection.[9,13] Accordingly, the *M. tuberculosis* genome encodes numerous hydrolytic enzymes involved in lipid metabolism.[14] Among those, the lip gene family consist of 24 lipid/ester hydrolases termed Lip C to Z which share a conserved active site as well as alpha/beta hydrolase fold.[6,15] Specifically targeting the bacterial lipid metabolism, could represent a viable strategy to address *M. tuberculosis*[10] and open a new opportunity to shorten the currently required long-term TB therapy, when given simultaneously with known first and second line antibiotics.[16] Thus focusing on known mammalian lipase inhibitors such as lalistat (La-0)[17] and orlistat[18] could represent a novel therapeutic strategy inhibiting TAG metabolism. Despite their prominent role only little is known about the exact function of lipid hydrolysing enzymes in mycobacteria. Orlistat was previously shown to reduce viability and mycolic acid biosynthesis for numerous mycobacterial strains.[19] In depth target analysis *via* activity based protein

---

[a] *Department of Chemistry, Technische Universität München, Lichtenbergstraße 4, 85748 Garching, Germany. E-mail: stephan.sieber@tum.de*
[b] *Institut für Virologie, Technische Universität München/Helmholtz Zentrum München, Trogerstraße 30, 81675 München, Germany*
[c] *Forschungszentrum Borstel, Leibniz-Zentrum für Medizin und Biowissenschaften, FG Mikrobielle Grenzflächenbiologie, Parkallee 22, 23845 Borstel, Germany. E-mail: nreiling@fz-borstel.de*
[d] *Institut für Medizinische Mikrobiologie, Immunologie und Hygiene, Technische Universität München, Trogerstraße 30, 81675 München, Germany*
[e] *German Center for Infection Research (DZIF), Munich partner site, Germany*

† The authors declare no competing interests.

‡ Electronic supplementary information (ESI) available. See DOI: 10.1039/c6md00231e

§ These authors equally contributed to this work.

Published on 21 July 2016. Downloaded by Cornell University Library on 21/07/2016 16:20:15.

profiling (ABPP)[20] with an alkynylated orlistat probe in *M. bovis* BCG revealed binding of multiple enzymes belonging to the Lip family. Orlistat or related hydrolase inhibitors that address the mycobacterial lipid metabolism thus represent attractive starting points for medicinal chemistry.[21,22]

We here show, that lalistat exhibits an inhibitory effect on *M. tuberculosis* reproduction and further investigated its mode of action by *in situ* target identification *via* ABPP. Several bacterial lipases were identified suggesting inhibition of TAG hydrolysis as the mode of action.

Lipases are important metabolic enzymes for many prokaryotic and eukaryotic organisms. Several compounds have been developed to inhibit eukaryotic hydrolases specifically *e.g.* for the treatment of obesity.[23,24] The beta-lactone orlistat represents a broad lipase inhibitor acting on a wide range of triglyceride- and cholesterol ester hydrolysing mammalian enzymes.[25,26] In addition, La-0 is a thiadiazole carbamate (Fig. 2A) developed as a specific inhibitor of the lysosomal acid lipase (LAL).[27] This enzyme is located in cellular late endosomes hydrolysing cholesterol esters and triglycerides from incoming lipoproteins.[24] Lalistat, similarly to orlistat, binds to the active site serine of lipases covalently and thereby inhibits enzyme activity.[27,28] Given the structural and electronic properties of La-0 we anticipated binding to diverse lipases which may deviate from the orlistat target spectrum and complement mechanistic insights. We thus inspected if lalistat impairs viability of *M. tuberculosis* by several independent approaches.

First, minimal inhibitory concentrations (MICs) were determined by addition of La-0 to diluted cultures of *M. tuberculosis* H37Rv and utilizing the resazurin assay.[29–31] The compound exhibited a MIC of 25–50 μM (Fig. S1‡) exceeding the potency of previously studied orlistat $\sim$30 μM.[19] Currently applied standard therapeutics such as rifampicin and isoniazid exhibit MIC values in the range of 0.04 to 1.0 μM.[32] *M. tuberculosis* infection is treated by a combination of up to four different drugs; we therefore tested mixtures of La-0 and various (myco-)bacterial drugs on two-dimensional MIC plates. Remarkably, a strong effect was obtained for the combined application of lalistat and vancomycin resulting in a MIC drop of factor 4 for lalistat and 16 for vancomycin (Fig. 1A). Using the fractional inhibitory concentration index (FICI)[33,34] a co-operative effect could be concluded as both molecules interfere with the composition and assembly of the cell wall. Furthermore, growth of green fluorescent protein (GFP) expressing *M. tuberculosis* H37Rv was monitored for 7 days in presence of either La-0 or rifampicin (control) as described by Michelucci *et al.*[35] Interestingly, growth inhibition was observed for lalistat down to a concentration of 4 μM (Fig. 1B). Finally, the effect of La-0 on intracellular growth of *M. tuberculosis* in human macrophage host cells was determined. To this end we infected human monocyte derived macrophages with strain *M. tuberculosis* H37Rv (multiplicity of infection 1:1) for 4 h and subsequently cultured the cells for 7 days with various concentrations of La-0 and DMSO (control). Cells were then lysed and CFUs were determined as described previously.[36] Again lalistat substantially reduced bacterial load by 55% compared to the untreated control suggesting that the compound can even address intracellular bacteria (Fig. 1C). These results point towards an essential mechanism addressed by lalistat and given its specificity for lipases a link to essential metabolic processes was subsequently evaluated by *in situ* target identification.

To analyse the mode of action we identified lalistat protein targets in live *M. tuberculosis* cells *via* ABPP. For this technology a chemical probe bearing an alkyne tag (La-1) was synthesized following established protocols (Fig. 2A).[27] In brief, a piperidine moiety was introduced in commercially available 3,4-dichloro-1,2,5-thiadiazole, replacing one of the chlorine substituents while the other was subsequently converted into an hydroxyl-function using potassium hydroxide (Scheme 1). The newly synthesized hydroxy-heterocycle was utilized as a common precursor for lalistat (La-0) and its alkynylated probe (La-1) using piperidyl chloroformate or 4-ethylylpiperidine chloroformate, respectively, to form the essential carbamate functionality.

Satisfyingly, La-1 retained activity and reduced *M. tuberculosis* growth comparable to the parent molecule La-0 (Fig. S1‡).

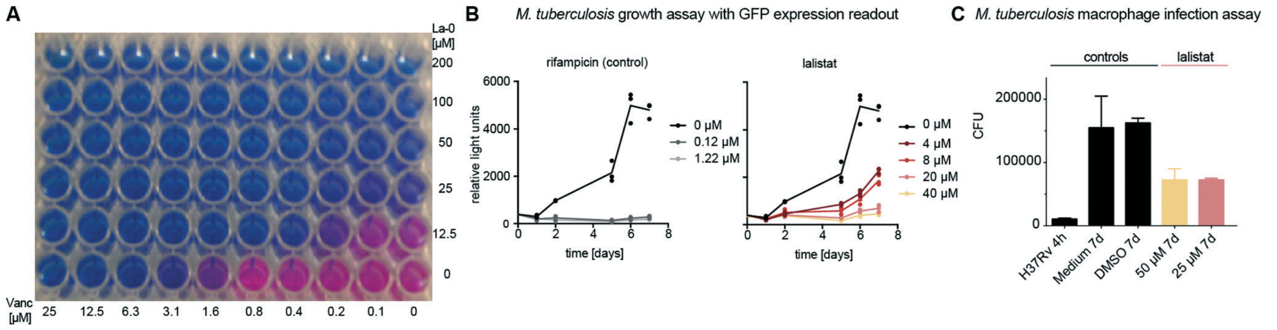

Fig. 1 Lalistat inhibits *M. tuberculosis* growth. (A) Two-dimensional MIC determination. Lanes: La-0 dose-down. Rows: vancomycin dose-down. (B) Inhibition of GFP-expressing *M. tuberculosis* H37Rv with rifampicin (left) and lalistat (right). All experiments were performed together with the same DMSO control (identical in both graphs). (C) Colony forming units (cfu) of *M. tuberculosis* H37Rv recovered from human macrophages in presence and absence of inhibitors. Shown is one representative experiment out of two performed, each consisting of three (B) and two (C) technical replicates.

Published on 21 July 2016. Downloaded by Cornell University Library on 21/07/2016 16:20:15.

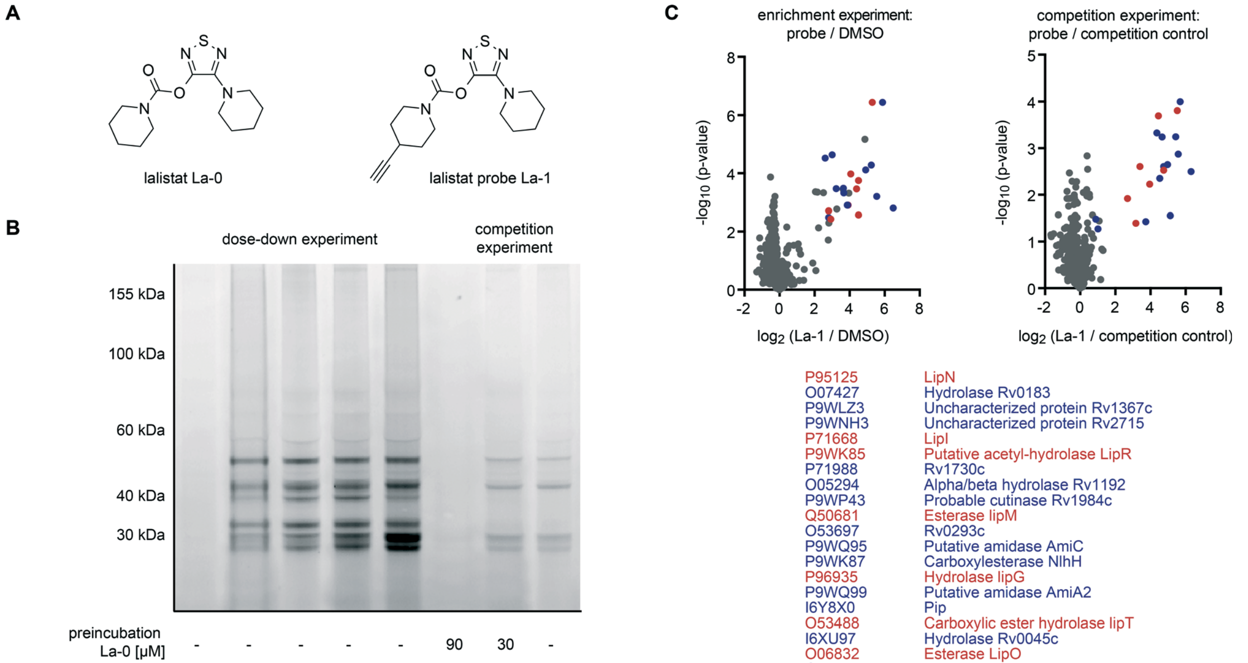

P95125	LipN
O07427	Hydrolase Rv0183
P9WLZ3	Uncharacterized protein Rv1367c
P9WNH3	Uncharacterized protein Rv2715
P71668	LipI
P9WK85	Putative acetyl-hydrolase LipR
P71988	Rv1730c
O05294	Alpha/beta hydrolase Rv1192
P9WP43	Probable cutinase Rv1984c
Q50681	Esterase lipM
O53697	Rv0293c
P9WQ95	Putative amidase AmiC
P9WK87	Carboxylesterase NlhH
P96935	Hydrolase lipG
P9WQ99	Putative amidase AmiA2
I6Y8X0	Pip
O53488	Carboxylic ester hydrolase lipT
I6XU97	Hydrolase Rv0045c
O06832	Esterase LipO
O05293	Alpha/beta hydrolase Rv1191

Fig. 2 *In vivo* target identification of lalistat in *M. tuberculosis* H37Rv *via* chemical proteomics. (A) Structure of lalistat and the corresponding probe. (B) Concentration dependent labelling and competition experiment visualized *via* SDS-PAGE and fluorescent scanning. (C) Enrichment (6 biological replicates) and competition (4 biological replicates) target identification (ABPP) volcano plot representations and corresponding list of common hits (blue and red). Proteins of the Lip family are marked in red, all others in blue.

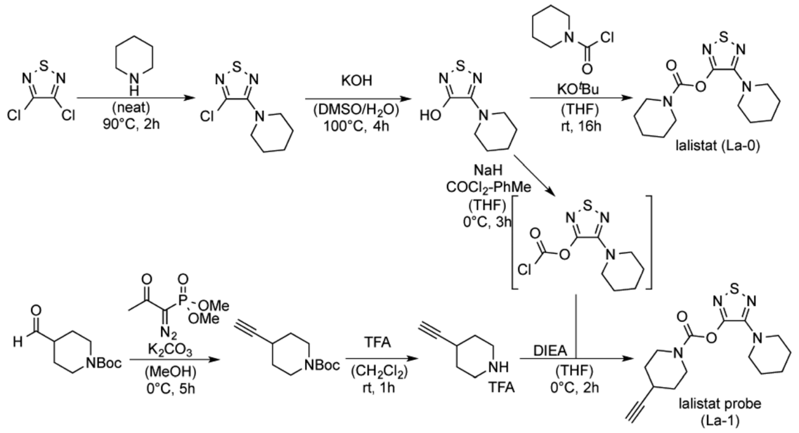

Scheme 1 Synthesis of lalistat (La-0) and lalistat probe (La-1). DMSO: dimethylsulfoxide, THF: tetrahydrofuran, Boc: *tert*-butyloxycarbonyl-, TFA: trifluoroacetic acid, DIEA: *N*,*N*-diisopropylethylamine.

Next, target identification experiments were conducted. *M. tuberculosis* cells were grown to log phase and incubated with La-1 or DMSO as a control. After cell lysis a rhodamine tag was attached to the alkyne moiety of La-1 *via* bioorthogonal click-reaction[37–39] to visualize target proteins on SDS-PAGE gel by fluorescence scanning. Protein labelling at different probe concentrations are displayed in Fig. 2B. Interestingly, proteins around a molecular size of 30 kDa showed increased fluorescent signal response with raising probe concentration while others (~50 kDa) only marginally changed intensity. A concentration between 30 µM and 60 µM was sufficient to achieve saturated labelling. We thus proceeded with gel-free proteomics and performed labeling studies with 30 µM La-1 in *M. tuberculosis* H37Rv to unravel the identities of target proteins. For these studies a biotin tag served as a handle to enrich labeled proteins on avidin beads (Fig. S2‡). After on-bead digestion primary amines were modified by heavy, medium and light isotopes using dimethyl labeling (DL).[40] Labelling ratios of probe *versus* DMSO were normalized, *z*-score and $\log_2(x)$ transformed. Target proteins with a high

Published on 21 July 2016. Downloaded by Cornell University Library on 21/07/2016 16:20:15.

enrichment and statistical significance (see ESI‡ for details) are located in the upper right area of the enrichment volcano plot in Fig. 2C. To validate these enriched hits we performed competition experiments where cells were pre-incubated with La-0 (60 μM) and subsequently treated with 30 μM La-1 probe (Fig. 2C). Strikingly, spectra of enrichment and competition experiments include 7 Lip enzymes (LipN, -I, -R, -M, -G, -T and -O) that selectively react with lalistat.

A comparison of lalistat hits with results of previous orlistat proteome labeling studies in *M. bovis* (BCG)[21] revealed Lip M, O, N, I and G as shared targets. Interestingly, while Lip R and T were selectively captured by orlistat-like probes suggesting a complementary target profile by both lipase inhibitors due to their different physico-chemical properties. It is thus intriguing to speculate that the shared preference for a common set of Lip enzymes may contribute to the growth inhibitory effects of both compounds.

LipR as one of the most strongly enriched hits by La-1, was exemplary confirmed as target by a heterologous expression and subsequent labeling with the probe. A strong fluorescent band indicated specific binding (Fig. 3). Beside members of the Lip family we identified six additional enzymes with lipolytic activity: Rv0183, a highly conserved monoalcylglycerol lipase,[41,42] Rv1984 (ref. 43 and 44) a cutinase preferentially active against monoacylglycerols, as well as the uncharacterized proteins Rv2715, Rv1192, Rv1399c (characterized esterase)[45] and Rv0045c[46–48] which are suggested to participate in lipid hydrolysis in mycobacterial metabolism.

We also detected few putative non-lipolytic enzymes bound by lalistat: Rv1367 and Rv1730, both possibly involved in cell wall biosynthesis, as well as amidases (Rv2888c and Rv2363), iminopeptidase (Rv0840c) and two proteins of unknown function (Rv0293c, Rv1191). To date it is not clear whether mycobacterial lipases hydrolysing short-chain substrates, like LipR, would participate in non-lipolytic metabolic processes because it remains unknown whether they have additional phospholipase, thioesterase or protease activity.[49]

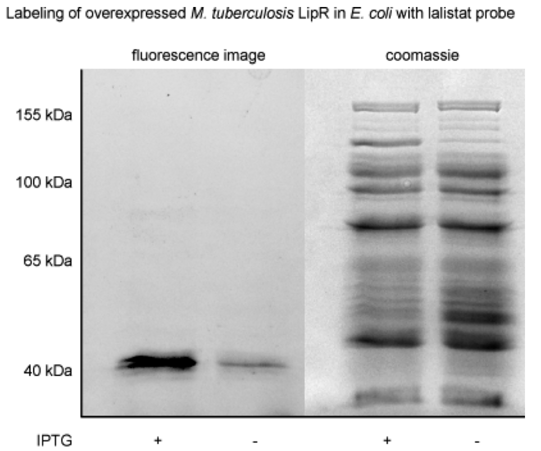
Labeling of overexpressed M. tuberculosis LipR in E. coli with lalistat probe
fluorescence image
coomassie
155 kDa
100 kDa
65 kDa
40 kDa
IPTG
+
-
+
-

Fig. 3 Validation of protein target LipR. LipR was overexpressed in *E. coli* and labelled with lalistat probe La-1. Rhodamine-azide was attached *via* click reaction after cell lysis. The experiment was conducted with and without induction by IPTG (indicated with "+" and "–", respectively).

Conclusions

Taken together, the specificity of lalistat for a suite of mycobacterial lipases is intriguing. Given the importance of these enzymes for *M. tuberculosis* viability during infection they may represent promising drug targets. Future studies need to further dissect and characterize the exact function and mechanism of these enzymes in order to design customized inhibitors suited to interfere with essential metabolic processes specifically in the bacteria. Here, orlistat and lalistat probes represent interesting chemical tools that allow simultaneous and selective detection of lipase activities in living mycobacteria. With regard to the paucity of potent antimycobacterial inhibitors future tuberculosis treatment approaches could largely benefit form adding these compounds into treatment regimens. They could also pave the way for the development of more specific drugs targeting mycobacterial lipases. Their use in combination with known antimycobacterial agents may offer an urgently needed opportunity to improve and shorten TB therapy.

Acknowledgements

The work was funded by the Deutsche Forschungsgemeinschaft (DFG) SI1096/6-1 to SAS. JL was supported by the Studienstiftung des deutschen Volkes. NR was funded by a grant of the DFG Excellence Cluster EXC306 "Inflammation at Interfaces". KK was supported by a doctoral fellowship of the Verband der Deutschen Chemischen Industrie e.V. (VCH). We gratefully acknowledge Lisa Niwinski and Carolin Golin (FZ Borstel), Mona Wolff and Katja Bäuml (TUM) for excellent technical support. We thank Eric Rubin for helpful advice and support.

Notes and references

1 WHO, *Global tuberculosis report*, 2015.
2 A. Koul, E. Arnoult, N. Lounis, J. Guillemont and K. Andries, *Nature*, 2011, **469**, 483–490.
3 M. Gengenbacher and S. H. Kaufmann, *FEMS Microbiol. Rev.*, 2012, **36**, 514–532.
4 D. G. Russell, B. C. VanderVen, W. Lee, R. B. Abramovitch, M. J. Kim, S. Homolka, S. Niemann and K. H. Rohde, *Cell Host Microbe*, 2010, **8**, 68–76.
5 N. J. Garton, M. Gilleron, T. Brando, H. H. Dan, S. Giguere, G. Puzo, J. F. Prescott and I. C. Sutcliffe, *J. Biol. Chem.*, 2002, **277**, 31722–31733.
6 G. Singh, G. Singh, D. Jadeja and J. Kaur, *Crit. Rev. Microbiol.*, 2010, **36**, 259–269.
7 H. Christensen, N. J. Garton, R. W. Horobin, D. E. Minnikin and M. R. Barer, *Mol. Microbiol.*, 1999, **31**, 1561–1572.
8 WHO, *Tuberculosis fact sheet*, 2010, p. 104.
9 J. Daniel, H. Maamar, C. Deb, T. D. Sirakova and P. E. Kolattukudy, *PLoS Pathog.*, 2011, 7, e1002093.

Published on 21 July 2016. Downloaded by Cornell University Library on 21/07/2016 16:20:15.

10 C. Deb, C. M. Lee, V. S. Dubey, J. Daniel, B. Abomoelak, T. D. Sirakova, S. Pawar, L. Rogers and P. E. Kolattukudy, *PLoS One*, 2009, **4**, e6077.

11 H. Bloch and W. Segal, *J. Bacteriol.*, 1956, **72**, 132–141.

12 D. G. Russell, P. J. Cardona, M. J. Kim, S. Allain and F. Altare, *Nat. Immunol.*, 2009, **10**, 943–948.

13 P. Peyron, J. Vaubourgeix, Y. Poquet, F. Levillain, C. Botanch, F. Bardou, M. Daffe, J. F. Emile, B. Marchou, P. J. Cardona, C. de Chastellier and F. Altare, *PLoS Pathog.*, 2008, **4**, e1000204.

14 S. T. Cole, R. Brosch, J. Parkhill, T. Garnier, C. Churcher, D. Harris, S. V. Gordon, K. Eiglmeier, S. Gas, C. E. Barry 3rd, F. Tekaia, K. Badcock, D. Basham, D. Brown, T. Chillingworth, R. Connor, R. Davies, K. Devlin, T. Feltwell, S. Gentles, N. Hamlin, S. Holroyd, T. Hornsby, K. Jagels, A. Krogh, J. McLean, S. Moule, L. Murphy, K. Oliver, J. Osborne, M. A. Quail, M. A. Rajandream, J. Rogers, S. Rutter, K. Seeger, J. Skelton, R. Squares, S. Squares, J. E. Sulston, K. Taylor, S. Whitehead and B. G. Barrell, *Nature*, 1998, **393**, 537–544.

15 L. Dedieu, C. Serveau-Avesque, L. Kremer and S. Canaan, *Biochimie*, 2013, **95**, 66–73.

16 C. Dye, S. Scheele, P. Dolin, V. Pathania and M. C. Raviglione, *JAMA, J. Am. Med. Assoc.*, 1999, **282**, 677–686.

17 J. Hamilton, I. Jones, R. Srivastava and P. Galloway, *Clin. Chim. Acta*, 2012, **413**, 1207–1210.

18 P. Y. Yang, K. Liu, M. H. Ngai, M. J. Lear, M. R. Wenk and S. Q. Yao, *J. Am. Chem. Soc.*, 2010, **132**, 656–666.

19 L. Kremer, C. de Chastellier, G. Dobson, K. J. Gibson, P. Bifani, S. Balor, J. P. Gorvel, C. Locht, D. E. Minnikin and G. S. Besra, *Mol. Microbiol.*, 2005, **57**, 1113–1126.

20 M. J. Evans and B. F. Cravatt, *Chem. Rev.*, 2006, **106**, 3279–3301.

21 M. S. Ravindran, S. P. Rao, X. Cheng, A. Shukla, A. Cazenave-Gassiot, S. Q. Yao and M. R. Wenk, *Mol. Cell Proteomics*, 2014, **13**, 435–448.

22 M. Fonovic and M. Bogyo, *Expert Rev. Proteomics*, 2008, **5**, 721–730.

23 L.-N. Zhang, J. Vincelette, D. Chen, R. D. Gless, S.-K. Anandan, G. M. Rubanyi, H. K. Webb, D. E. MacIntyre and Y.-X. Wang, *Eur. J. Pharmacol.*, 2011, **654**, 68–74.

24 A. Iyer, D. P. Fairlie, J. B. Prins, B. D. Hammock and L. Brown, *Nat. Rev. Endocrinol.*, 2010, **6**, 71–82.

25 B. Borgstrom, *Biochim. Biophys. Acta*, 1988, **962**, 308–316.

26 E. K. Weibel, P. Hadvary, E. Hochuli, E. Kupfer and H. Lengsfeld, *J. Antibiot.*, 1987, **40**, 1081–1085.

27 A. I. Rosenbaum, C. C. Cosner, C. J. Mariani, F. R. Maxfield, O. Wiest and P. Helquist, *J. Med. Chem.*, 2010, **53**, 5281–5289.

28 P. Hadvary, W. Sidler, W. Meister, W. Vetter and H. Wolfer, *J. Biol. Chem.*, 1991, **266**, 2021–2027.

29 R. S. Reis, I. Neves Jr., S. L. Lourenco, L. S. Fonseca and M. C. Lourenco, *J. Clin. Microbiol.*, 2004, **42**, 2247–2248.

30 S. Sungkanuparph, R. Pracharktam, A. Thakkinstian, B. Buabut and W. Kiatatchasai, *J. Med. Assoc. Thai*, 2002, **85**, 820–824.

31 J. C. Palomino, A. Martin, M. Camacho, H. Guerra, J. Swings and F. Portaels, *Antimicrob. Agents Chemother.*, 2002, **46**, 2720–2722.

32 R. J. Wallace Jr., D. R. Nash, L. C. Steele and V. Steingrube, *J. Clin. Microbiol.*, 1986, **24**, 976–981.

33 K. R. Caleffi-Ferracioli, F. G. Maltempe, V. L. Siqueira and R. F. Cardoso, *Tuberculosis*, 2013, **93**, 660–663.

34 D. F. Bruhn, M. S. Scherman, J. Liu, D. Scherbakov, B. Meibohm, E. C. Bottger, A. J. Lenaerts and R. E. Lee, *Sci. Rep.*, 2015, **5**, 13985.

35 A. Michelucci, T. Cordes, J. Ghelfi, A. Pailot, N. Reiling, O. Goldmann, T. Binz, A. Wegner, A. Tallam, A. Rausell, M. Buttini, C. L. Linster, E. Medina, R. Balling and K. Hiller, *Proc. Natl. Acad. Sci. U. S. A.*, 2013, **110**, 7820–7825.

36 N. Reiling, S. Homolka, K. Walter, J. Brandenburg, L. Niwinski, M. Ernst, C. Herzmann, C. Lange, R. Diel, S. Ehlers and S. Niemann, *mBio*, 2013, **4**(4), e00250-13.

37 R. Huisgen, *Proc. Chem. Soc.*, 1961, 357–396.

38 V. V. Rostovtsev, J. G. Green, V. V. Fokin and K. B. Sharpless, *Angew. Chem., Int. Ed.*, 2002, **41**, 2596–2599.

39 C. W. Tornøe, C. Christensen and M. Meldal, *J. Org. Chem.*, 2002, **67**, 3057–3064.

40 J. L. Hsu, S. Y. Huang, N. H. Chow and S. H. Chen, *Anal. Chem.*, 2003, **75**, 6843–6852.

41 P. Saravanan, V. K. Dubey and S. Patra, *Chem. Biol. Drug Des.*, 2012, **79**, 1056–1062.

42 K. Cotes, R. Dhouib, I. Douchet, H. Chahinian, A. de Caro, F. Carriere and S. Canaan, *Biochem. J.*, 2007, **408**, 417–427.

43 L. Dedieu, C. Serveau-Avesque and S. Canaan, *PLoS One*, 2013, **8**, e66913.

44 M. Schue, D. Maurin, R. Dhouib, J. C. Bakala N'Goma, V. Delorme, G. Lambeau, F. Carriere and S. Canaan, *FASEB J.*, 2010, **24**, 1893–1903.

45 S. Canaan, D. Maurin, H. Chahinian, B. Pouilly, C. Durousseau, F. Frassinetti, L. Scappuccini-Calvo, C. Cambillau and Y. Bourne, *Eur. J. Biochem.*, 2004, **271**, 3953–3961.

46 X. Zheng, J. Guo, L. Xu, H. Li, D. Zhang, K. Zhang, F. Sun, T. Wen, S. Liu and H. Pang, *PLoS One*, 2011, **6**, e20506.

47 C. P. Savas, A. Gehring, R. J. Johnson and G. Hoops, *FASEB J.*, 2013, **27**, 559.2.

48 J. Guo, X. Zheng, L. Xu, Z. Liu, K. Xu, S. Li, T. Wen, S. Liu and H. Pang, *PLoS One*, 2010, 5.

49 V. Delorme, S. V. Diomande, L. Dedieu, J. F. Cavalier, F. Carriere, L. Kremer, J. Leclaire, F. Fotiadu and S. Canaan, *PLoS One*, 2012, 7, e46493.

Electronic Supplementary Material (ESI) for MedChemComm.
This journal is © The Royal Society of Chemistry 2016

Supplementary information (SI)

1 Supplementary figures

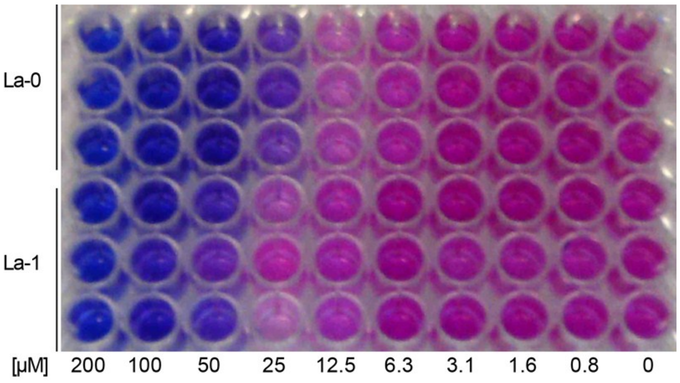
La-0
La-1
[µM]
200
100
50
25
12.5
6.3
3.1
1.6
0.8
0

Fig. S1 MIC determination of La-0 and La-1 in *M. tuberculosis* H37Rv. Purple: dead cells. Pink: alive cells.

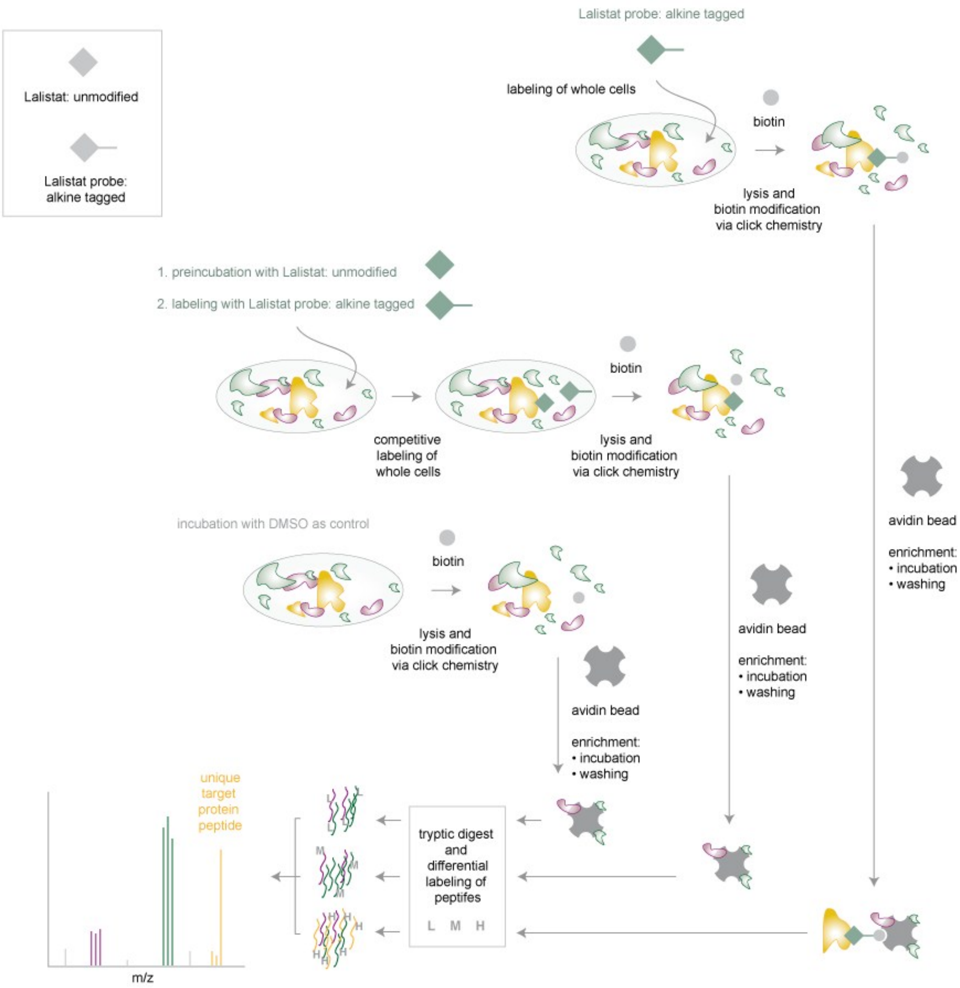
Lalistat: unmodified
Lalistat probe: alkine tagged
Lalistat probe: alkine tagged
labeling of whole cells
biotin
lysis and biotin modification via click chemistry
1. preincubation with Lalistat: unmodified
2. labeling with Lalistat probe: alkine tagged
competitive labeling of whole cells
biotin
lysis and biotin modification via click chemistry
avidin bead
enrichment:
• incubation
• washing
incubation with DMSO as control
biotin
lysis and biotin modification via click chemistry
avidin bead
enrichment:
• incubation
• washing
avidin bead
enrichment:
• incubation
• washing
unique target protein peptide
tryptic digest and differential labeling of peptifes
L M H
M
M
H
H
H
H
m/z

Fig. S2 Activity based protein profiling (ABPP) workflow for quantitative, gel-free proteomics including DMSO control and competition control.

2 Materials and methods

2.1 Synthesis

2.1.1 Synthesis of 4-(Piperidin-1-yl)-1,2,5-thiodiazol-3-yl piperidine-1-carboxylate (La-0)

La-0 was prepared according to Rosenbaum et al.[1]

2.1.2 Synthesis of 4-(Piperidin-1-yl)-1,2,5-thiadiazol-3-yl 4-ethynylpiperidine-1-carboxylate (La-1)

4-(Piperidin-1-yl)-1,2,5-thiadiazol-3-ol (76.7 mg, 0.41 mmol) was prepared according to Rosenbaum et al. [1] and dissolved in THF (10 mL). NaH (16.4 mg, 60% in mineral oil, 0.41 mmol) was added and the resulting suspension was stirred until full dissolution indicating complete deprotonation. A phosgene solution (234 µL, 20% in toluene, 1.75 M, 0.41 mmol) was added and the resulting solution was stirred at rt for 10 min. 4-Ethynylpiperidine-TFA salt (144 mg, 0.70 mmol), prepared as described by Braisted et al.[2], and DIPEA (120 µL, 0.70 mmol) were combined in THF (2 mL) and stirred for 5 min. This solution was added to the *in situ* formed chloroformate solution and stirred at rt for 20 min. The reaction was stopped by addition of 1 M HCl (10 mL) and diluted with EtOAc (25 mL). After separation of phases the organic layer was washed three times with saturated NaHCO3 solution, dried over $MgSO_4$ and concentrated *in vacuo*. The product was purified by RP-HPLC as the HCl salt to yield as a clear oil.

RP-HPLC (analytical setup, method: gradient 2% B → 98% B over 10 min): t_R = 8.73 min.

^{1}H-NMR (360 MHz, $CDCl_3$): δ [ppm] = 3.89-3.73 (m, 2 H), 3.59-3.43 (m, 2 H), 3.42-3.35 (m, 4 H), 2.73 (tq, J = 3.7, 7.0 Hz, 1 H), 2.15 (d, J = 2.4 Hz, 1 H), 1.95-1.83 (m, 2 H), 1.78-1.68 (m, 2 H), 1.67-1.57 (m, 6 H).

^{13}C-NMR (91 MHz, $CDCl_3$): δ [ppm] = 153.8, 150.9, 146.6, 85.5, 70.5, 49.1, 43.2, 42.8, 31.4, 20.9, 26.4, 25.5, 24.3.

HRMS (ESI): calc. for $C_{15}H_{25}N_2O_2$ $[M+H]^+$: 321.1380; found: 321.1372.

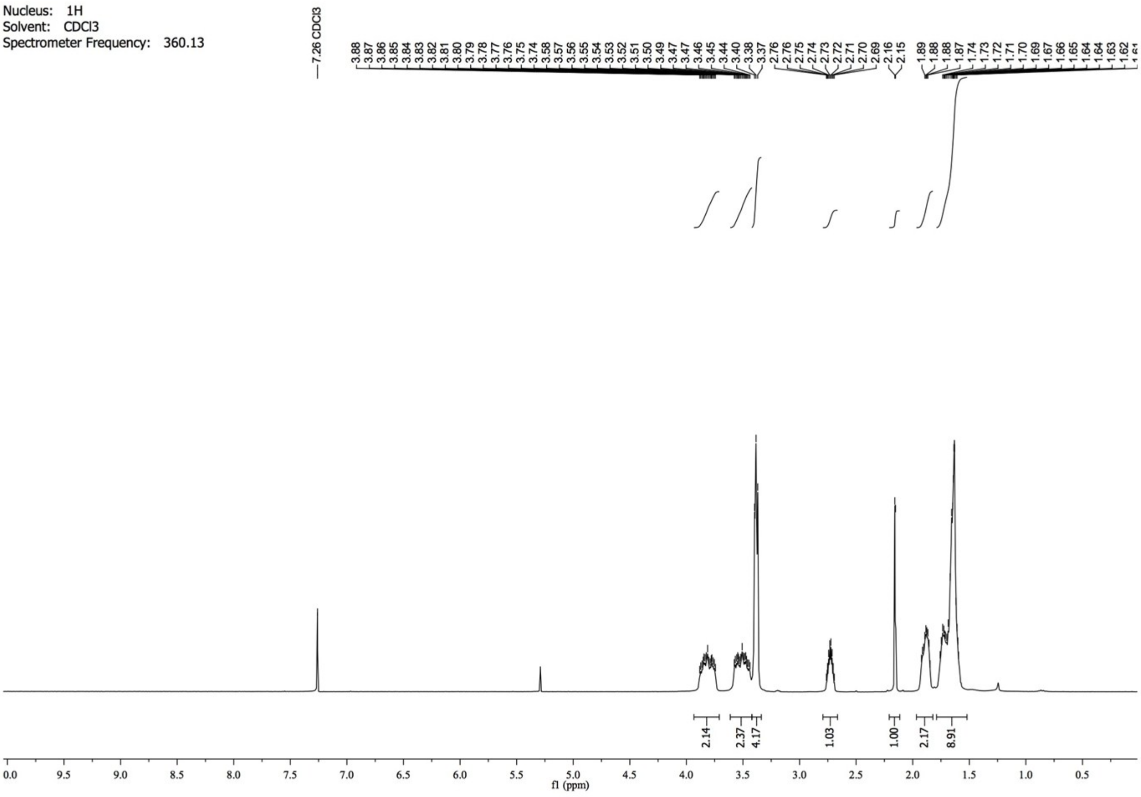
Nucleus: 1H
Solvent: CDCl3
Spectrometer Frequency: 360.13
7.26 CDCl3
3.88
3.87
3.86
3.85
3.84
3.83
3.82
3.81
3.80
3.79
3.78
3.77
3.76
3.75
3.74
3.58
3.57
3.56
3.55
3.54
3.53
3.52
3.51
3.50
3.49
3.47
3.46
3.45
3.44
3.40
3.38
3.37
2.76
2.76
2.75
2.74
2.73
2.72
2.71
2.70
2.69
2.16
2.15
1.89
1.88
1.88
1.87
1.74
1.73
1.72
1.71
1.70
1.69
1.67
1.66
1.65
1.64
1.64
1.63
1.62
2.14
2.37
4.17
1.03
1.00
2.17
8.91
10.0
9.5
9.0
8.5
8.0
7.5
7.0
6.5
6.0
5.5
5.0
4.5
4.0
3.5
3.0
2.5
2.0
1.5
1.0
0.5
f1 (ppm)

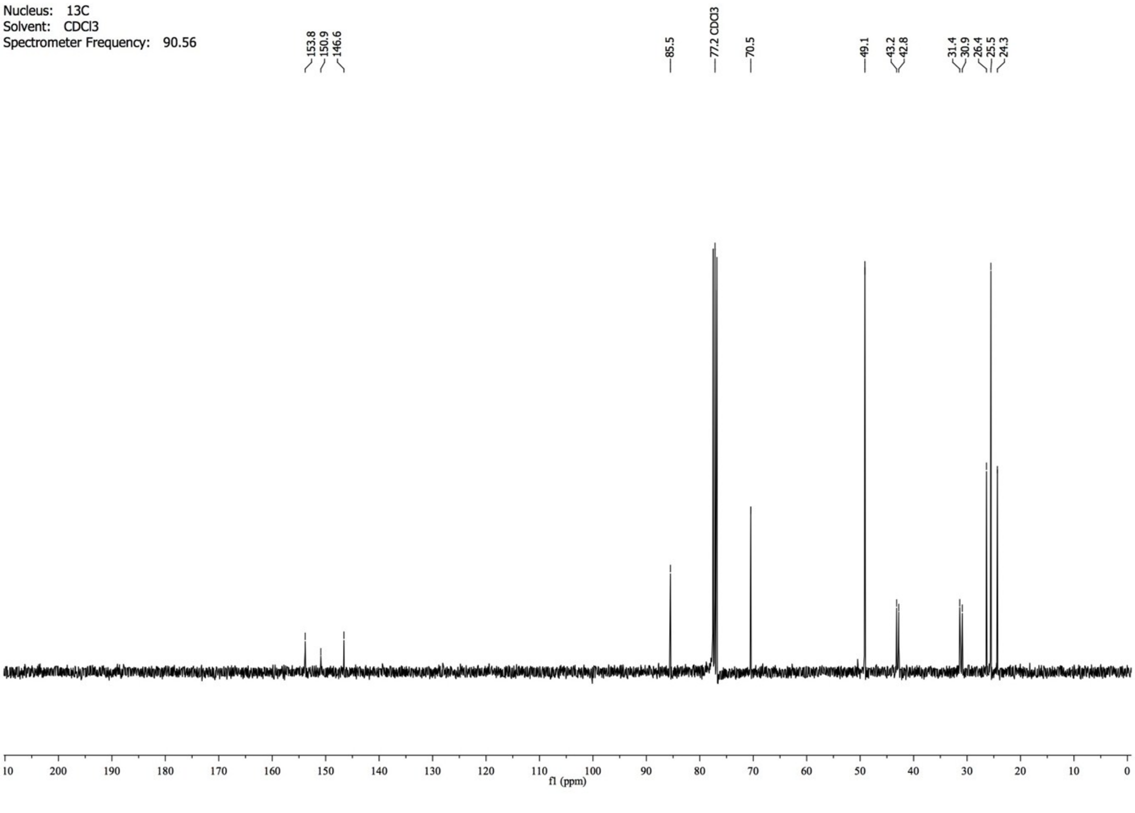
Nucleus: 13C
Solvent: CDCl3
Spectrometer Frequency: 90.56
153.8
150.9
146.6
85.5
77.2 CDCl3
70.5
49.1
43.2
42.8
31.4
30.9
26.4
25.5
24.3
10
200
190
180
170
160
150
140
130
120
110
100
90
80
70
60
50
40
30
20
10
0
f1 (ppm)

2.2. Minimal inhibitory concentration (MIC) determination

Compound-mediated growth inhibition was carried out using 96-well plates. A culture of stationary phase growing bacteria was diluted to a final $OD_{600} = 0.001$ in fresh media. 100 µL of diluted bacteria was added to 100 µL of two fold inhibitory concentration of compound to be tested and diluted two fold in each well. 96-well plates were incubated at 37 °C under a water impermeable membrane. To determine the growth of mycobacteria 100 µL of a 0.02 % resazurin solution was added 7 days for *M. tuberculosis*. A color change from purple to pink within 2 to 4 days indicated viable cells while purple colored wells suggested no bacterial growth.

2.3. FICI determination

Determination synergistic drug effects were calculated using fractional inhibitory concentration index (FICI):

$$FICI = \frac{MIC\ A+B}{MIC\ A} + \frac{MIC\ B+A}{MIC\ B}$$

MIC A+B – MIC of drug A when combined with drug B

MIC B+A – MIC of drug B when combined with drug A

Results were evaluated as follows: synergism: ≤ 0.5, indifference: > 0.5 – 4, antagonism > 4.[3]

For the combination of La-0 and Vancomycin were following values obtained:

MIC La-0 = 50 µM

MIC La-0 + Vanc. (0.4 µM) = 12.5 µM

MIC Vanc. = 6.3 µM

MIC Vanc. + La-0 (12.5 µM) = 0.4 µM

$FICI_{La\text{-}0/Vanc} \approx 0.31$

2.4 *Mycobacterium tuberculosis* Growth Analysis

GFP-expressing *Mycobacterium tuberculosis* H37Rv [4] was generated using the plasmid 32362:pMN437 (Addgene), kindly provided by M. Niederweis (University of Alabama, Birmingham, AL) [5]. $1x10^6$ bacteria were cultured in 7H9 medium supplemented with oleic acid-albumin-dextrose-catalase (OADC) (10%), Tween 80 (0.05%), and glycerol (0.2%) in a total volume of 100 µl in a black 96 well plate with clear bottom (Corning Inc, Corning, NY) sealed with an air-permeable membrane (Porvair Sciences, Dunn Labortechnik, Asbach, Germany). Growth was as measured as RLU at 528 nm after excitation at 485 nm in a fluorescence microplate reader (Synergy 2, Biotek, Winooski, VT) at indicated time points.

2.5 Analysis of *M. tuberculosis* growth in human macrophages

Mononuclear cells were isolated from peripheral blood (PBMC) of healthy volunteers by density gradient centrifugation. Monocytes were separated (purity consistently >95%) by counterflow elutriation. Human monocyte-derived Macrophages (hMDM) were generated in the presence of 10 ng/ml recombinant human M-CSF from highly purified monocytes as described.[6] *M. tuberculosis* growth in human macrophages was analyzed as described.[7] In brief $2x10^5$ hMDMs were cultured in 500µl RPMI 1640 with 10% FCS and 4mM L-glutamine in 48-well flat-bottom microtiter plates (Nunc) at 37°C in a humidified atmosphere containing 5% CO_2. Macrophages were infected with *M. tuberculosis* strain H37Rv with an MOI of 1:1. Four hours post infection, non-phagocytosed bacteria were removed by washing three times with 0.5ml Hanks' balanced salt solution (HBSS; Invitrogen) at 37°C. After washing and after 3 days of cultivation, 0.5 ml media was added to the macrophage culture. At day 7 supernatants were completely removed and macrophage cultures were lysed at 4 hours and 7 days post infection by adding 10 µl 10% Saponin solution (Sigma) in HBSS at 37°C for 15 min. Lysates were serially diluted in sterile water containing 0.05% Tween 80 (Merck, Darmstadt, Germany) and plated twice on 7H10 agar containing 0.5% glycerol (Serva) and 10% heat-inactivated bovine calf serum (BioWest, France). After 3 weeks at 37°C the CFUs were counted.

2.6 Activity based protein profiling (ABPP)

M. tuberculosis H37Rv was derived from frozen stock (2.5x10^8 bacteria/ml). Homogenous bacterial suspension was prepared in 7H9 medium (50 mL) supplemented with oleic acid-albumin-dextrose-catalase (OADC) (10%), Tween 80 (0.05%), and glycerol (0.2%). 25 mL each was incubated in 30 mL square medium bottles (Nalgene) at 37°C without shaking for three days. Preculture was diluted to 450 mL and incubated for four days. Bacteria were washed with PBS and an optical density at 600 nm of 40 was adjusted. For regular ABPP experiments (probe / DMSO control) 1 mL suspension was supplemented with 30 µM lalistat-1 (La-1; lalistat probe) or DMSO as a control and incubated for 30 min, vortexed and incubated another 30 min. For competition experiments (probe / competition control) 1 mL suspension was supplemented with 60 µM lalistat (La-0) or DMSO control and incubated for 30 min, vortexed and incubated another 30 min. Both samples were now additionally supplemented with 30 µM lalistat-1 (La-1; lalistat probe), incubated for 30 min, vortexed and incubated another 30 min. For both regular and competition experiments bacteria were washed with PBS and the pellet was stored at -80°C over night. Pellet was suspended in 1 mL PBS supplemented with 80 µL protease inhibitor (stock: 1 tablet solved in 2 ml dH_2O). Samples were sonicated (duty cycle: 50; output 10 (100%)) at 4°C for 20 min each, centrifuged (15 000 xG, 4°C, 30 min) and the supernatant was centrifuged over 0.22 µm Spin-X Centrifuge tube filter (Costar) (15 000 xG, 4°C, 15 min). Samples were stored at -80°C.

Two identical samples each derived from 1 mL OD_{600}=40 cultures were combined and treated with 120 µL gel-free ABPP Mix (40 µL Biotin-PEG_3-N_3 (Jena Bioscience, CLK-AZ104P4-100; 10 mM in DMSO), 20 µL fresh TCEP (50 mM in ddH_2O), 60 µL TBTA Ligand (1.667 mM in 80 % tBuOH and 20 % DMSO)). The final concentrations were 233 µM Biotin-PEG_3-N_3, 581 µM TCEP and 58.2 µM TBTA Ligand. The lysates were mixed by vortexing and 20 µL $CuSO_4$ solution (50 mM in ddH_2O) were added. The lysates were mixed by vortexing again and incubated for 1h at RT in the dark. After the click-reaction the lysates were transferred to 15 mL falcon tubes and 8 mL of cold acetone (-80°C, MS grade) were added. Proteins were precipitated ON at -80°C.

The precipitated proteins were thawed on ice, pelletized (16900 xG, 15 min, 4°C) and supernatant was disposed. Falcon tubes were stored on ice during the following washing procedure: The proteins were washed two times with 1 mL cold methanol (-80°C). Resuspension was achieved by sonication (15 sec at 10 % intensity) and proteins were pelletized via centrifugation (16900 xG, 10 min, 4°C). Only MS grade water was used for the following procedures. After two washing steps supernatant was disposed and the pellet was resuspended in 500 µL 0.2 % SDS in PBS at RT by sonication (15 sec at 10 % intensity). Avidin beads were thawed on ice and resuspended by carefully inverting. Then 50 µL of bead suspension were transferred into Protein LoBind Eppendorf tubes using wide bore pipette tips and washed three times with 1 mL 0.2 % SDS in PBS (resuspension: carefully inverting 10 times, pelleting: 400 xG, 3 min, RT). 500 µL protein solution from the 15 mL falcon tubes were transferred to the Protein LoBind Eppendorf tubes with washed avidin beads and incubated under continuous inverting (20 rpm, 1 h, RT). Beads were washed 3 times with 1 mL 0.2 % SDS in PBS, 2 times with 1 mL 6 M urea in water and 3 times with 1 mL PBS (resuspension: carefully inverting 20 times, pelleting: 400 xG, 3 min, RT).

The beads were resuspended in 200 µl denaturation buffer (7 M urea, 2 M thiourea in 20 mM pH 7.5 HEPES buffer). Proteins were reduced through addition of dithiothreitol (DTT, 1 M, 0.2 µL), the tubes were mixed by vortexing shortly and incubated in a thermomixer (450 rpm, 45 min, RT). Then 2-iodoacetamide (IAA, 550 mM, 2 µL) was added for alkylation, the tubes were mixed by vortexing shortly and incubated in a thermomixer (450 rpm, 30 min, RT, in the dark). Remaining IAA was quenched by the addition of dithiothreitol (DTT, 1 M, 0.8 µL). The tubes were shortly mixed by vortexing and incubated in a thermomixer (450 rpm, 30 min, RT). LysC (0.5 µg/µL, Wako) was thawed on ice and 1µL was added to each microcentrifuge tube, the tubes were shortly mixed by vortexing and incubated in a thermomixer (450 rpm, 2 h, RT, in the dark). TEAB solution (600 µL, 50 mM in water) and then trypsin (1.5 µL, 0.5 µg/µL in 50 mM acetic acid, Promega) were added and tubes were shortly vortexed after each addition. The reaction was incubated in a thermomixer (450 rpm, 13-15 h, 37 °C). The digest was stopped by adding 6 µL formic acid (FA) and vortexing. After centrifugation (100 xG, 1 min, RT), the supernatant was transferred to a new Protein LoBind Eppendorf tube. FA (50 µL, aqueous 0.1 % solution) was added to the beads and after vortexing and centrifugation (100 xG, 1 min, RT) the supernatant was added to the supernatant collected before. Again FA (50 µL, aqueous 0.1 % solution) was added to the beads and after vortexing and centrifugation (16200 xG, 3 min, RT) the supernatant was transferred to the combined supernatants.

50 mg SepPak C18 columns (Waters) were equilibrated by gravity flow with 1mL acetonitrile, 1 mL elution buffer (80% ACN, 0.5% FA) and 3 mL aqueous 0.5% FA solution. Subsequently the samples were loaded by gravity flow, washed with 5 mL aqueous 0.5 % FA solution and labeled with 5 mL of the respective dimethyl labeling solution. The following solutions were used: light (L): 30 mM $NaBH_3CN$, 0.2 % CH_2O, 10 mM NaH_2PO_4, 35 mM Na_2HPO_4, pH 7.5; medium (M): 30 mM $NaBH_3CN$, 0.2 % CD_2O, 10 mM NaH_2PO_4, 35 mM Na_2HPO_4, pH 7.5; heavy (H): 30 mM $NaBHD_3CN$, 0.2 % $^{13}CD_2O$, 10 mM NaH_2PO_4, 35 mM Na_2HPO_4, pH 7.5. Labeled peptides were eluted into new 2.0 mL Protein LoBind Eppendorf tubes using two times 250 µL elution buffer. The eluates were lyophilized and stored at -20°C.

Prior to MS measurement the samples were dissolved in 30 µL 1 % FA by pipetting up and down, vortexing and sonication for 15 min (brief centrifugation after each step). Differentially labeled samples were mixed. 0.45 µm centrifugal filter units (VWR) were equilibrated with two times 500 µL water, 500 µL 0.05 N NaOH and two times 500 µL 1 % FA (centrifugation: 16200 xG, 1 min, RT). Reconstituted and mixed peptide samples were filtered through the equilibrated filters (centrifugation: 16200 xG, 2 min, RT). Samples were analyzed via HPLC-MS/MS using an UltiMate 3000 nano HPLC system (Dionex, Sunnyvale, California, USA) equipped with Acclaim C18 PepMap100 75 µm ID x 2 cm trap and Acclaim C18 PepMap RSLC, 75 µM ID x 15 cm separation columns coupled to an Orbitrap Fusion mass spectrometer (Thermo Fisher Scientific Inc., Waltham, Massachusetts, USA). Samples were loaded on the trap and washed for 10 min with 0.1 % formic acid, then transferred to the analytical column and separated using a 120 min gradient from 3 % to 25 % acetonitrile in 0.1 % formic acid and 5 % dimethyl sulfoxide (at 200 nL/min flow rate). Orbitrap Fusion was operated in a 3 second top speed data dependent mode. Full scan acquisition was performed in the orbitrap at a resolution of 120000 and an ion target of 4E5 in a scan range of 300 – 1700 m/z. Monoisotopic precursor selection as well as dynamic exclusion for 60 s were enabled. Precursors with charge states of 2 – 7 and intensities greater than 5E3 were selected for fragmentation. Isolation was performed in the quadrupole using a window of 1.6 m/z. Precursors were collected to a target of 1E2 for a maximum injection time of 250 with “inject ions for all available parallelizable time” enabled. Fragments were generated using higher-energy collisional dissociation (HCD) and detected in the ion trap at a rapid scan rate. Internal calibration was performed using the ion signal of fluoranthene cations (EASY-ETD/IC source)

Peptide and protein identifications were performed using MaxQuant 1.5.3.8 software with Andromeda as search engine using following parameters: Carbamidomethylation of cysteines as fixed and oxidation of methionine as well as acetylation of N-termini as dynamic modifications, trypsin/P as the proteolytic enzyme, 4.5 ppm for precursor mass tolerance (main search ppm) and 0.5 Da for fragment mass tolerance (ITMS MS/MS tolerance). Searches were done against the Uniprot database for *M. tuberculosis* H37Rv (taxon identifier: 83332, downloaded on 19.5.2015). Quantification was performed using dimethyl labeling with the following settings: light: DimethLys0, DimethNter0; medium: DimethLys4, DimethNter4 and heavy: DimethLys8, DimethNter8. Variable modifications were included for quantification. The I = L and requantify options were used. Identification was done with at least 2 unique peptides and quantification only with unique peptides.

Statistical analysis was performed with Perseus 1.5.1.6. Putative contaminants, reverse peptides and peptides only identified by site were omitted from further processing. Dimethyllabeling ratios were $\log_2(x)$ transformed and z-score normalized. The average values of technical replicates were calculated and $-\log_{10}$(p-values) were obtained by a two sided one sample t-test over six biological replicates for standard ABPP with DMSO control or 4 biological replicates for competition experiments.

Proteins were ranked from highest to lowest $\log_2(x)$ transformed and z-score normalized dimethyllabeling ratios. They were also ranked from highest to lowest $-\log_{10}(x)$ transformed p-values. Proteins were finally ranked according to the sum of the ranking values from dimethyllabeling ratios and $-\log_{10}$(p-value) across both experiments (regular ABPP: probe / DMSO, competition experiment: probe / competition). 2% of the identified proteins with the highest final ranking (including regular ABPP and competition experiments dimethyllabeling ratios and p-values) were considered to be hits of lalistat. This cut-off was chosen as by this analysis a visual separation of enriched vs. not enriched proteins in both regular ABPP and competition experiments could be achieved.

2.7 Recombinant expression and labelling of proteins in *E. coli*

A N-terminal His_6 affinity tagged LipR construct was cloned in a pDONR201 (Invitrogen) vector and then in a pET300 expression vector via the GATEWAY cloning system using the primers shown below and genomic DNA from *M. tuberculosis* H37Rv. Expression was induced at an OD_{600} of 0.6 by addition of Isopropyl-β-D-thiogalactopyranosid (IPTG; final concentration: 0.25 mM) and carried out 4 h at 37°C in *E. coli* BL21 cells.

Construct: N-His_6-attB1-TEV-LipR-Stop-attB2

Primer 1: ggggacaagtttgtacaaaaaagcaggctttgagaatctttattttcagggcAACCTGCGCAAAAACGTCATCC

Primer 2: ggggaccactttgtacaagaaagctgggtgTCATTTGACTACTCCCCGTGG

After centrifugation (5 min, 6200 xG, 4°C) and removal of the supernatant bacteria were resuspended in PBS to get an OD_{600} of 40. To 1 mL of this suspension in a microcentrifuge tube 30 µL of La-1 solution in DMSO (or just DMSO as a control) were added. After 30 min incubation at RT in the dark the microcentrifuge tube was again mixed by vortexing and incubated for another 30 min at RT in the dark. After centrifugation (6200 xG, 2 min, 4°C) the supernatant was removed and the pellets were stored at -80°C.

Pellets were resuspended in 1 mL PBS (4°C) and transferred to a 'Precellys Glass/Ceramic Kit SK38 2.0 mL' tube. Tubes were cooled on ice for about 5 min or longer and cells were lysed with the Precellys Homogeniser using two times lysis program 3 (5400 rpm, run number: 1, run time: 20 sec, pause: 5 sec). After each lysis run the tubes were cooled on ice for 5 min. The ball mill tubes were centrifuged (16200 xG, 10 min, 4°C) and 86 µL of supernatant were transferred to new 1.5 mL microcentrifuge tubes and treated with 10 µL gel-based ABPP Mix (2 µL RhN_3 (Tetramethylrhodamine (TAMRA) Azide (Tetramethylrhodamine 5-Carboxamido-(6-Azidohexanyl)), 5-isomer (life technologies, T10182); 5 mM in DMSO), 2 µL fresh TCEP (50 mM in ddH_2O), 6 µL TBTA Ligand (1.667 mM in 80 % tBuOH and 20 % DMSO)). The final concentrations were: 104 µM RhN_3, 1.04 mM TCEP and 104 µM TBTA Ligand. The lysates were mixed by vortexing and 2 µL $CuSO_4$ solution (50 mM in ddH_2O) were added. The lysates were again mixed by vortexing and incubated for 1h at RT in the dark. Then 80 µL 2x Laemmli Sample Buffer were added, samples were mixed in a thermomixer (300 rpm, 3 min, 96°C) and analyzed via SDS PAGE (10 % agarose gel (PEQLAB Biotechnologie GmbH, Erlangen, PerfectBlue Dual Gel System, the gel was prepared according to the manual), 3.5 h, 300 V, 8 µL fluorescent protein standard) and fluorescence imaging (GE Healthcare, ImageQuant LAS-4000). After fluorescence scanning the gel was coomassie stained.

References

1. Rosenbaum, A.I., et al., *Thiadiazole carbamates: potent inhibitors of lysosomal acid lipase and potential Niemann-Pick type C disease therapeutics.* J Med Chem, 2010. **53**(14): p. 5281-9.
2. Braisted, A.C., et al., *Discovery of a potent small molecule IL-2 inhibitor through fragment assembly.* J Am Chem Soc, 2003. **125**(13): p. 3714-5.
3. Odds, F.C., *Synergy, antagonism, and what the chequerboard puts between them.* J Antimicrob Chemother, 2003. **52**(1): p. 1.
4. Michelucci, A., et al., *Immune-responsive gene 1 protein links metabolism to immunity by catalyzing itaconic acid production.* Proc Natl Acad Sci U S A, 2013. **110**(19): p. 7820-5.
5. Song, H., et al., *Identification of outer membrane proteins of Mycobacterium tuberculosis.* Tuberculosis (Edinb), 2008. **88**(6): p. 526-44.
6. Reiling, N., et al., *Mycobacteria-induced TNF-alpha and IL-10 formation by human macrophages is differentially regulated at the level of mitogen-activated protein kinase activity.* J Immunol, 2001. **167**(6): p. 3339-45.
7. Reiling, N., et al., *Clade-specific virulence patterns of Mycobacterium tuberculosis complex strains in human primary macrophages and aerogenically infected mice.* MBio, 2013. **4**(4).

POSTER CONTRIBUTIONS

STAPHYLOCOCCUS AUREUS VIRULENCE IS REDUCED BY INHIBITION OF THE MANGANESE UPTAKE PROTEIN MNTC

Poster presented at Gordon Research Conference - Bioorganic Chemistry, Boston (USA) **2015** by Jan Vomacka and at Gordon Research Conference - High Throughput Chemistry & Chemical Biology, Boston (USA) **2015** by Stephan A. Sieber.

Authors

Jan Vomacka, Vadim S. Korotkov, Bianca Schwanhäusser, Franziska Weinandy, Martin H. Kunzmann, Joanna Krysiak, Oliver Baron, Thomas Böttcher, Katrin Lorenz-Baath and Stephan A. Sieber

Chair of Organic Chemistry II, Technische Universität München, Department of Chemistry, Lichtenbergstraße 4, 85748 Garching, Germany

AVIRU, GO-Bio-project of the Federal Ministry of Education and Research, FKZ: 031A131

Abstract

Methicillin-resistant *Staphylococcus aureus* (MRSA) strains are responsible for severe infections for which there are only few effective antibiotic therapies, and pose a significant threat to global health. To approach this challenge chemical entities with a novel and resistance-free mode of action are desperately needed. Here we introduce a new hydroxyamide compound (AV59) that inhibits the expression of devastating toxins, shows no resistance development and reduces abscess formation upon systemic treatment in a mouse model. Starting from a successful reduction of the virulence phenotype by AV59 we identified MntC as a direct protein target via an *in situ* chemical proteomics strategy using affinity based protein profiling (ABPP). MntC is the extracellular manganese binding protein of a transmembrane ABC transporter complex that shuttles Mn^{2+} inside the cell, a process that is crucial for manganese-dependent enzyme activity, especially during infection. Consistent with this mechanism we observed that the compound has a destabilizing effect on MntC and inhibits Mn^{2+} uptake in live cells.

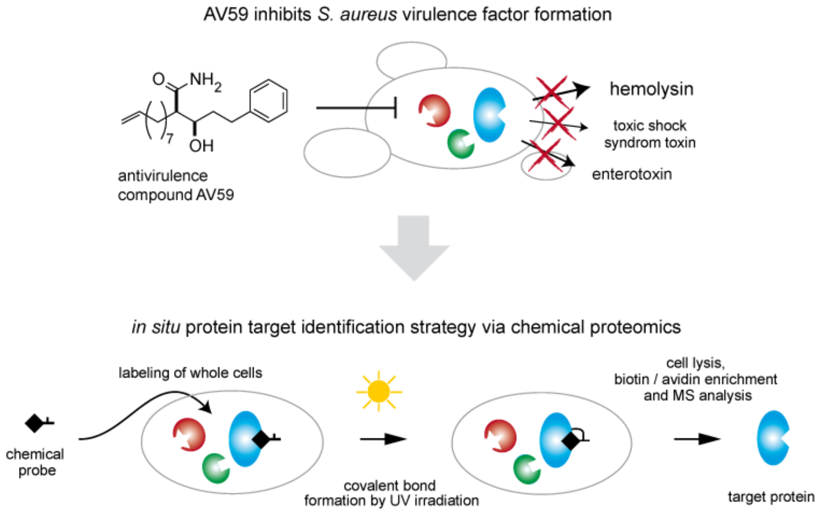
AV59 inhibits S. aureus virulence factor formation
NH2
O
7
OH
antivirulence compound AV59
hemolysin
toxic shock syndrom toxin
enterotoxin
in situ protein target identification strategy via chemical proteomics
labeling of whole cells
chemical probe
covalent bond formation by UV irradiation
cell lysis, biotin / avidin enrichment and MS analysis
target protein

Fig. 0 Overview.

Phenotype: AV59 inhibits *S. aureus* virulence

The spread of methicillin-resistant *Staphylococcus aureus* (MRSA) poses a major threat to public health. In addition to treatment with antibiotics, strategies are emerging that target the pathogenicity, i.e. the virulence, of bacteria, instead of inhibiting growth (1, 2). Bacterial virulence is determined by a diverse set of molecules, including toxins and adhesins, needed by the pathogen for infection establishment and propagation (3). Inhibition of virulence pathways disarms bacteria without directly affecting their viability, presumably thus leading to less selective pressure and slower resistance development (4-8). Hemolysin alpha (hla), a pore-forming cytotoxin causing the lysis of immune cells and erythrocytes, is one of the major staphylococcal virulence factors. AV59 inhibited hla production with an EC_{50} of 16 µM (Fig. 1A). No resistance development could be observed for this antihemolytic effect (Fig. 1B). In addition systemic treatment with the hydroxyamide showed significant reduction of abscess sizes in a MRSA mouse skin infection model (Fig. 1C).

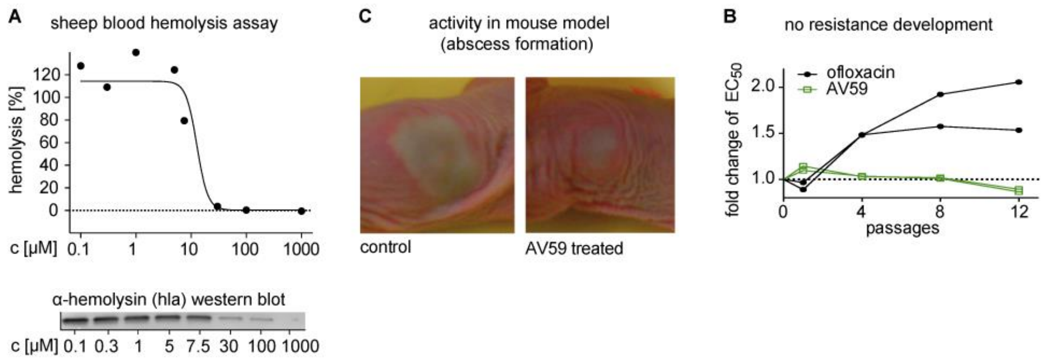

Fig. 1. AV59 inhibits *S. aureus* virulence. **A** Hemolysis inhibition with AV59 in S. aureus NCTC 8325. Confirmation by α-hemolysin (hla) western blot in a separate experiment. **B** Resistance development assay with antihemolytic compound AV59 (16 µM; sheep blood hemolysis assay) and antibiotic ofloxacin (3.5 µM; OD_{600} growth inhibition assay). Resistance development was measured by an increased EC_{50} after several passages. The curves for two biological replicates are shown. **C** Systemic treatment of skin infections with AV59 decreases the size of lesions induced by S. aureus USA 300 BAA-1717. Day 1 after infection is shown.

Protein target identification: *in situ* identification strategy via chemical proteomics

To identify direct protein target(s) of the antivirulence compound, we synthetically equipped AV59 with an alkyne handle at the terminal end of the alkyl chain, and replaced the phenyl ring by a benzophenone photocrosslinker. This functionalized photoreactive affinity based protein profiling (ABPP) probe (9) retained the antihemolytic activity of its parent molecule. Unlike the (*R**,*R**) diastereomer AV59 the corresponding (*R**,*S**) diastereomer could not inhibit hemolysis. Therefore the inactive (*R**,*S**) diastereomer and the (R*,S*) photoprobe were used as a control in target identification (Fig. 2) and validation experiments. Several proteins were found to be significantly enriched with the active (*R**,*R**) photoprobe compared to DMSO control and also to inactive (*R**,*S**) diastereomer control in S. aureus strains NCTC 8325 and USA 300. Among the hits was MntC a known virulence assotiated target. *S. aureus* transposon mutant strains lacking hit proteins (proline dehydrogenase, an esterase and FtsH) were tested for their hemolytic activity. The MntC mutant exhibited the strongest reduction of hemolytic activity compared to wild type.

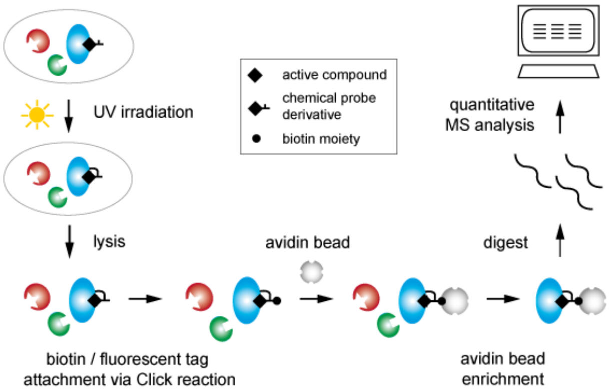
UV irradiation
active compound
chemical probe derivative
biotin moiety
quantitative MS analysis
lysis
avidin bead
digest
biotin / fluorescent tag attachment via Click reaction
avidin bead enrichment

Fig. 2. Target identification strategy: Cells are grown, labeled with a photoactivatable probe (black) and irradiated with UV light to establish a covalent binding between probe and target protein (blue). Then cells are lysed and a fluorescent and/or biotin tag is attached via Click reaction. After enrichment with avidin beads the proteins are digested, treated with dimethyl labeling reagents, mixed and analyzed via mass spectrometry.

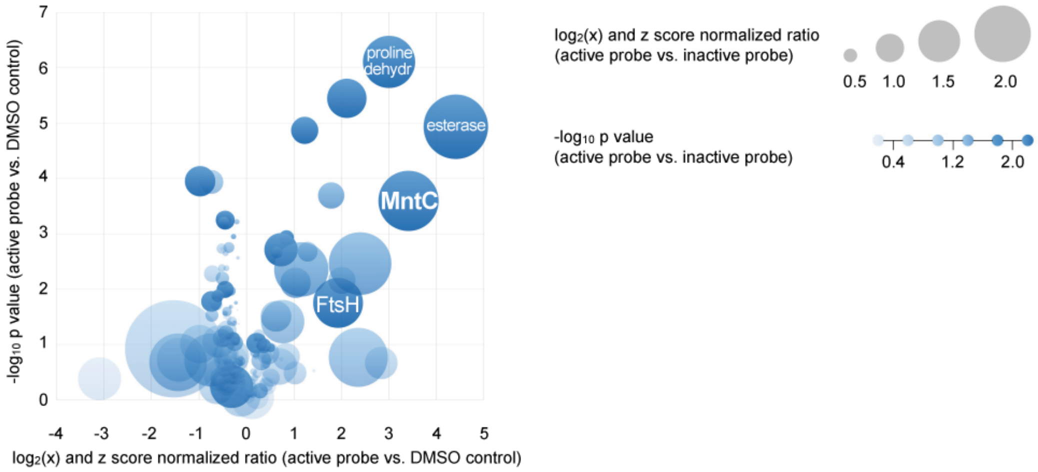

Fig. 3. Volcano plot showing p value (-$\log_{10}$) versus normalized ratio (active probe vs. DMSO control). Circles are identified proteins. Normalization was done by $\log_2(x)$ and z score (standard normal distribution) transformation. High x-axis values represent how strong proteins could be enriched by the chemical probe. High y-axis values represent proteins with enrichment factors significantly different to 0. Active vs. inactive diastereomer probe ratio is shown by size and opacity as descibed in the figure legend. The following proteins were identified as hits (uniprot accession numbers): MntC (Q2G2D8, Q2FJ07), uncharacterized protein (blast: esterase) (Q2FDX1, Q2FV90), proline dehydrogenase (Q2FFX4, Q2FXG3), ATP-dependent zinc metalloprotease FtsH (Q2FJD0, Q2G0R0).

Conclusions

The antivirulence mode of action based on MntC inhibition was further validated by a cell based manganese transport assay and a diastereomer specific destabilizing effect in a thermal shift assay with purified MntC protein. Transcriptome analysis of hydroxyamide treated *S. aureus* cells revealed parallel downregulation of common virulence associated transcriptional activators and upregulation of the virulence repressor protein SarX. MntC has previously been demonstrated to play a crucial role in *S. aureus* virulence in a murine systemic infection model (10). Due to its importance in the maintenance of stress response and virulence during infection, MntC is currently being explored as a vaccine candidate in clinical trials (11). In conclusion, AV59 and MntC are a promising drug-target pair for future studies and further pharmacological optimization.

References

1 Clatworthy, A.E., E. Pierson, and D.T. Hung, *Targeting virulence: a new paradigm for antimicrobial therapy*. Nat Chem Biol, **2007**. 3(9): p. 541-8.

2 Rasko, D.A. and V. Sperandio, *Anti-virulence strategies to combat bacteria-mediated disease*. Nat Rev Drug Discov, **2010**. 9(2): p. 117-128.

3 Ruer, S., et al., *Virulence-targeted antibacterials: concept, promise, and susceptibility to resistance mechanisms*. Chem Biol Drug Des, **2015**.

4 Hung, D.T., et al., *Small-molecule inhibitor of Vibrio cholerae virulence and intestinal colonization*. Science, **2005**. 310(5748): p. 670-4.

5 Rasko, D.A., et al., *Targeting QseC signaling and virulence for antibiotic development*. Science, **2008**. 321(5892): p. 1078-80.

6 Khodaverdian, V., et al., *Discovery of Antivirulence Agents against Methicillin-Resistant Staphylococcus aureus. Antimicrobial Agents and Chemotherapy*, **2013**. 57(8): p. 3645-3652.

7 Tang, F., et al., *Puerarin Protects Against Staphylococcus aureus-Induced Injury of Human Alveolar Epithelial A549 Cells via Downregulating Alpha-Hemolysin Secretion*. Microbial Drug Resistance, **2013**. 20(4): p. 357-363.

8 Allen, R.C., et al., *Targeting virulence: can we make evolution-proof drugs?* Nat Rev Microbiol, **2014**. 12(4): p. 300-8.

9 Evans, M.J. and B.F. Cravatt, *Mechanism-Based Profiling of Enzyme Families*. Chemical Reviews, **2006**. 106(8): p. 3279-3301.

10 Diep, B.A., et al., *Identifying Potential Therapeutic Targets of Methicillin-resistant Staphylococcus aureus Through in Vivo Proteomic Analysis*. Journal of Infectious Diseases, **2014**. 209(10): p. 1533-1541.

11 Anderson, A.S., et al., *Development of a multicomponent Staphylococcus aureus vaccine designed to counter multiple bacterial virulence factors*. Hum Vaccin Immunother, **2012**. 8(11): p. 1585-94.

STAPHYLOCOCCUS AUREUS AND LISTERIA MONOCYTOGENES VIRULENCE IS REDUCED BY THE SMALL MOLECULE INHIBITOR AV73

Poster presented at the 26th Congress of the European Society of Clinical Microbiology and Infectious Diseases, Amsterdam (the Netherlands) **2016** by Jan Vomacka.

Authors

Jan Vomacka,[1] Vadim S. Korotkov,[1] Megan C. Jennings,[2] Matthias Stahl,[1] William M. Wuest,[2] Katrin Lorenz-Baath[1] and Stephan A. Sieber[1]

[1] Technische Universität München, Department of Chemistry, Lichtenbergstraße 4, 85748 Garching, Germany

[2] Temple University, Department of Chemistry, 448 Beury Hall, Philadelphia, PA 19086, United States

Abstract

Background: Persistent bacteria forming biofilms pose a major threat in nosocomial settings. In particular in combination with multi drug resistance, toxin-secreting pathogens cause life-threatening infections.

Material / methods: We screened a library of over 200 potential anti-virulence compounds against *Staphylococcus aureus* hemolysis. The mode of action of the most potent compound was studied by quantitative proteomics experiments.

Results: One of the best compounds (AV73) from the anti-virulence screening did not only reduce hemolytic toxin α-hemolysin in *S. aureus* supernatant to less than 20% but to our surprise also impeded *in vitro* biofilm formation by *S. aureus* strain NCTC8325 to less than 25%. At the same time bacterial growth was not affected. Furthermore *Listeria monocytogenes* biofilms could be reduced by AV73. In addition, the effect on bacterial proteomes and also extracellular protein levels was analyzed. Subsequent proteomics experiments will provide a direct target profile via chemical probe based target identification / deconvolution in whole bacterial cells.

Conclusions: The simple small molecule AV73 is a potential anti-virulence (anti-biofilm and anti-hemolysis) agent addressing *S. aureus* and *L. monocytogenes* in an *in vitro* setting. A lack of growth inhibition implies low selective pressure and therefore presumably low resistance development in *S. aureus*.

Results

The spread of antibiotic resistant bacteria poses a major threat to public health. In addition to treatment with antibiotics, strategies are emerging that target the pathogenicity, i.e. the virulence, of bacteria, instead of inhibiting growth (1, 2). Bacterial virulence is determined by a diverse set of molecules, including toxins and adhesins, needed by the pathogen for infection establishment and propagation (3). Inhibition of virulence pathways disarms bacteria without directly affecting their viability, presumably thus leading to less selective pressure and slower resistance development (4-8).

Searching for potent virulence inhibitors we screened a library of over 200 potential anti-virulence compounds against *S. aureus* hemolysis. As one of the best hits we obtained AV73, a simple small molecule with a diol core structure (Fig. 1). In our recently published work we show, that a close derivative of AV73 exhibits a broad inhibition of *S. aureus* virulence (9). We therefore anticipated an effect of AV73 also on other virulence phenotypes such as biofilm formation. Indeed we could measure a clear effect on *S. aureus* but also on *L. monocytogenes* biofilms. However the desired retention of growth was not observed with *L. monocytogenes*. Here AV73 treated cultures reduced growth to 60% of DMSO control which implies a higher risk for resistance development.

To explain the phenotypic effect of AV73 on a protein level, we performed quantitative (dimethyl-labeling) mass spectrometric analysis of cellular but also extracellular proteins. For those proteomic experiments bacteria were cultured under the same conditions as in the hemolysis and biofilm assays. A strong down-regulation of hemolysins and fibriniogen-binding proteins was observed in *S. aureus* supernatants which corresponds to the anti-hemolytic and anti-biofilm formation activity of AV73. A GO term analysis of the most down-regulated proteins in *S. aureus* supernatant, grown under hemolysis assay conditions, demonstrates a clear cluster of virulence related terms like ‚pathogenesis‘, ‚cytolysis‘ and ‚cell killing‘ (Fig. 2). Future studies will include the synthesis of a photoactivatable chemical tool compound that can be used to further deconvolute the protein target spectrum and elucidate the cellular mechanisms that lead to the desired anti-virulence effect.

In conclusion, AV73 has the potential to guide efforts towards a better understanding of bacterial virulence mechanisms. This knowledge will enable the development of evolution-proof drugs (8), that address hemolysis, biofilm formation and other virulence phenotypes.

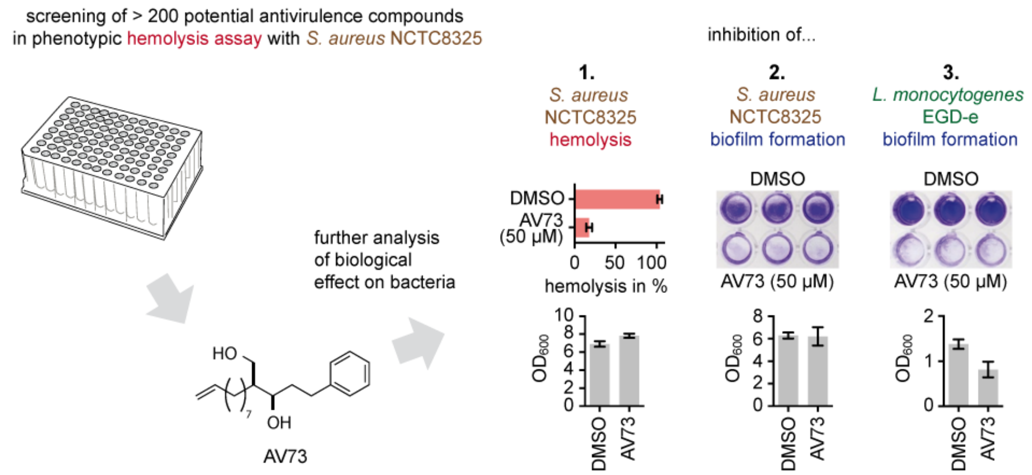

Fig. 1. Hemolysis assay was performed with a suspension of sheep erythrocytes in PBS added to bacterial supernatants. Biofilms of bacteria grown under static conditions in 96-well plates were stained with crystal violet.

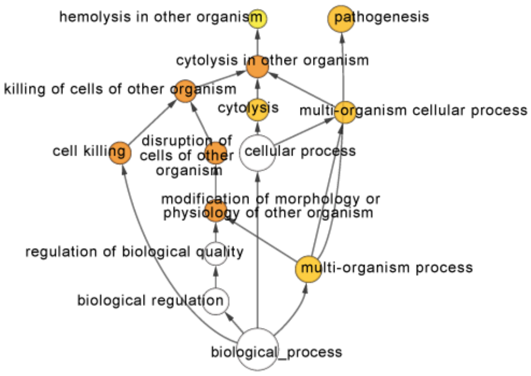
hemolysis in other organism
pathogenesis
cytolysis in other organism
killing of cells of other organism
cytolysis
multi-organism cellular process
cell killing
disruption of cells of other organism
cellular process
modification of morphology or physiology of other organism
regulation of biological quality
multi-organism process
biological regulation
biological_process

Fig. 2. GO term hierarchical network analysis of 5% most down-regulated proteins in S. aureus supernatant, grown under hemolysis assay growth conditions, treated with 50 µM AV73. Network generation with the BiNGO plugin for Cytoscape.

References

1 Clatworthy, A.E., et al., Nat Chem Biol, **2007**. 3(9): p. 541-8.

2 Rasko, D.A., et al., Nat Rev Drug Discov, **2010**. 9(2): p. 117-28.

3 Ruer, S., et al., Chem Biol Drug Des, **2015**. 86(4): p. 379-399.

4 Hung, D.T., et al., Science, **2005**. 310(5748): p. 670-4.

5 Rasko, D.A., et al., Science, **2008**. 321(5892): p. 1078-80.

6 Khodaverdian, V., et al., **2013**. 57(8): p. 3645-52.

7 Tang, F., et al., Microbial Drug Resistance, **2013**. 20(4): p. 357-63.

8 Allen, R.C., et al., Nat Rev Microbiol, **2014**. 12(4): p. 300-8.

9 Vomacka, J., et al., Chem Eur J, **2016**. 22(5): p. 1622-30.